

BUILDING ENERGY META MODELS



RESEARCH REPORT.

**Predicting
building
energy
performance
at city-scale.**

BY EMILY LENARDUZZI 6002730

MENTORED BY DR. CHARALAMPOS
ANDRIOTIS AND DR. MARTÍN
MOSTEIRO ROMERO AS PART OF THE
SUSTAINABLE DESIGN GRADUATION
STUDIO OF BUILDING TECHNOLOGY AT
TU DELFT. 2025

RESEARCH TEAM

STUDENT

Emily Lenarduzzi

MENTORS

Main mentor: Charalampos Andriotis

Second mentor: Martín Mosteiro Romero

SUPPORTING RESEARCHERS

Anna Maria Koniari

Pablo Morato

ADVISORY BOARD

Alexandra den Heijer

ACKNOWLEDGEMENTS

A sincere thank you to my mentors Charalampos Andriotis and Martín Mosteiro Romero. Thank you for all your guidance throughout this project and providing insights on topics that I was newly exploring.

Anna Maria Koniari and Pablo Morato were instrumental in getting me to this point. I am highly appreciative of the many meetings we had, for your generous time and support.

I am incredibly grateful for the friends that I've made within these past two years, whom it feels like we've known each other for much longer. To everyone who has supported me in one way or another throughout this year – thank you.

Thank you to my long-time friends at home in Canada, who have celebrated many milestones since I moved to the Netherlands, and who have been cheering me on the entire way.

Lastly, to my amazing family, Mom, Dad, Andrew, Daniel, and Angelina. Thank you for continuously supporting my journeys, I would not be here without you.

ABSTRACT

This study investigates the application of machine learning (ML) for predicting building energy performance at city scale, with a focus on reducing heating and cooling demands under current and future climate scenarios. A two-part methodology was adopted, involving: (i) large-scale building energy simulation and (ii) ML model development. Using Rotterdam, Netherlands as a case study, a computational workflow was created to automate data collection, processing, and energy simulation for 20,000 residential buildings under both the present and two projected climate conditions. Results highlight the influence of building layout, envelope thermal properties, and air tightness on reducing energy demand across a diverse range of building archetypes. An artificial neural network (ANN) was subsequently developed to enable rapid prediction of energy demands for both existing building conditions and retrofit scenarios. The analysis demonstrates that a shallow ANN is an effective ML model in terms of time efficiency, usability, and accuracy, particularly for predicting heating demands. The study highlights both the strengths and limitations of ML-based approaches relative to traditional energy modelling, offering valuable insights for energy planning and targeted retrofit decision-making at city-scale.

Keywords: Building energy modelling, Machine learning, Energy demand, Building retrofits, City-scale

CONTENTS

RESEARCH TEAM	ii
ACKNOWLEDGEMENTS.....	iii
ABSTRACT.....	iv
1. RESEARCH FRAMEWORK	2
CONTEXT	2
PROBLEM STATEMENT	3
MAIN PROBLEM.....	3
SUB-PROBLEMS.....	3
OBJECTIVE.....	3
RESEARCH QUESTIONS.....	4
MAIN QUESTION	4
SUB-QUESTIONS	4
RESEARCH METHODOLOGY	5
2. LITERATURE STUDY.....	7
BUILDING ENERGY DEMAND.....	7
ENERGY FLOWS	8
BUILDING RETROFITS.....	15
DUTCH CONTEXT	18
FUTURE CLIMATE.....	24
BUILDING ENERGY MODELLING.....	26
BUILDING LEVEL.....	26
MODELLING CHALLENGES	31
URBAN SCALE	31
CASE STUDIES.....	32
MACHINE LEARNING	35
APPROACHES	35
DEEP LEARNING (DL).....	39
CASE STUDIES.....	40
PERFORMANCE METRICS.....	46
3. METHODOLOGY.....	49
DESIGN ASSIGNMENT.....	49

METHODS.....	51
DATA COLLECTION	52
DATA GENERATION.....	53
DEMAND ANALYSIS	55
DATA STRUCTURE.....	56
ML DEVELOPMENT.....	57
PERFORMANCE EVALUATION	58
4. DATA COLLECTION	60
GEOMETRIC	60
BUILDING DATASET (Pand IDs)	60
PRE-PROCESS SELECT BUILDINGS	62
WEATHER.....	64
CURRENT.....	64
FUTURE.....	64
CONSTRUCTION	65
5. DATA GENERATION.....	69
BUILDING DATA.....	69
COLLECT 3DBAG GEOMETRY	69
PROCESSING FOR IDF	76
ENERGY SIMULATIONS.....	81
GENERATING THE IDF FILE.....	81
RHINO/ GRASSHOPPER/ HONEYBEE.....	81
PYTHON / EPPY	83
BATCH RUN SIMULATIONS.....	86
PROCESS DEMANDS.....	87
6. DEMAND ANALYSIS	89
CURRENT CLIMATE.....	89
DETACHED HOUSE / VRIJSTAANDE WONING.....	90
TERRACED CORNER / HOEKWONING.....	91
TERRACED INTERMEDIATE / TUSSENWONING.....	93
FUTURE CLIMATE.....	95
VALIDATION	98
7. DATA STRUCTURE.....	101

WORFKLOW.....	101
VERTEX DATA.....	102
FEATURE SET.....	103
8. ML DEVELOPMENT.....	106
ARCHITECTURE.....	106
INPUT LAYER.....	107
HIDDEN LAYER.....	107
OUTPUT LAYER.....	107
PHASE 1.....	107
PHASE 2.....	110
PHASE 3.....	111
FEATURE SET A.....	111
FEATURE SET B.....	112
FEATURE SET C.....	113
FEATURE SET D.....	114
9. PERFORMANCE.....	117
ARCHITECTURE.....	117
PREDICTION RESULTS.....	118
HEATING PREDICTIONS.....	118
COOLING PREDICTIONS.....	122
10. CONCLUSIONS.....	128
RESEARCH QUESTIONS.....	128
MAIN QUESTION.....	128
SUB-QUESTIONS.....	128
NEXT STEPS.....	130
11. REFLECTION.....	132
GRADUATION PROCESS.....	132
SOCIETAL IMPACT.....	134
12. REFERENCES.....	138
APPENDIX A.....	143
GITHUB.....	143
APPENDIX B.....	145
MATERIAL ID TABLE.....	145

APPENDIX C.....	150
DEMAND ANALYSIS.....	150
DETACHED HOUSE / Vrijstaande woning.....	150
TERRACED CORNER / Hoekwoning.....	152
TERRACED INTERMEDIATE / Tussenwoning.....	153
ML DEVELOPMENT.....	155
PHASE 2.....	155
PERFORMANCE.....	159
HEATING PREDICTIONS.....	159
COOLING PREDICTIONS.....	162

1

RESEARCH FRAMEWORK

CONTEXT

PROBLEM STATEMENT

RESEARCH QUESTIONS

RESEARCH METHODOLOGY

1. RESEARCH FRAMEWORK

CONTEXT

The built environment accounts for a significant share of the global energy consumption and greenhouse gas emissions, contributing to issues such as the depletion of non-renewable resources, global warming, and release of environmental air pollutants such as smog (Van Bueren et al., n.d.).

Urban areas play a significant role in addressing these climate challenges, with cities contributing between 70-76% of global CO₂ emissions and between 60-80% of global energy consumption (Aruta et al., 2024). The increasing size of the global urban area increases per capita energy use and places a further strain on energy resources (González et al.).

Within urban areas, energy use is divided between the residential, commercial and public service sectors. Energy use in buildings is the largest share of energy consumed within these sectors, with residential buildings accounting for the largest share of usage at 72%, compared to 28% for non-residential buildings (González et al.). Global energy trends show that since 2000, energy consumption within buildings has been increasing at an average rate of 1.2% per year, attributed in part to increased urbanization and the transition to electricity as the primary energy source (González et al.).

In the Netherlands, climate targets include a 49% reduction in greenhouse gas emissions by 2030 compared to the 1990 levels (European Commission, 2021). A key focus of achieving this goal is to transition the existing housing stock away from fossil fuels and reduce energy consumption by systematically retrofitting existing houses at neighbourhood, district, and eventually city scales.

To understand strategies for reducing building energy consumption it is necessary to analyze the current building energy demand. However, predicting building energy demand is complex as it depends on multiple factors, including environmental data, building characteristics, and occupant behaviour (Olu-Ajayi et al., 2021). Traditional modelling approaches, using energy simulation tools require an extensive amount of detailed input data, often unavailable or time-intensive to collect (Olu-Ajayi et al., 2021). And simulation processing times can be excessively long, making such tools impractical for large, city-scale applications.

Machine learning (ML) has emerged as an effective alternative to traditional building energy simulation tools. Such data-driven models can generate accurate energy demand predictions, often with fewer input requirements (Fathi et al., 2020a). However, the use of ML models, and specifically deep learning (DL) approaches for city-scale energy predictions remains an underexplored area (Li et al., 2023). Particularly in addressing retrofit interventions for diverse building typologies and considering future weather scenarios predicted by climate change (Li et al., 2023).

PROBLEM STATEMENT

MAIN PROBLEM

Predicting building energy demand at city-scale is a significant challenge due to the distinct environmental, building, and occupant characteristics, across thousands of diverse buildings, as well as the computational limitations of traditional energy simulation tools in handling such large-scale data complexity.

SUB-PROBLEMS

- Accurately predicting the impact of energy-saving retrofit interventions across a wide variety of building typologies, accounting for the diversity in building geometry and construction.
- Overcoming the lack of readily available, building-specific energy demand data for thousands of buildings that is necessary for city-scale modelling.
- Applying machine learning, particularly deep learning approaches for large-scale building energy demand prediction, considering diverse building characteristics and future climate scenarios.

OBJECTIVE

This research project aims to develop a scalable computational workflow, leveraging machine learning, to accurately predict the energy demand for residential buildings at city-scale and investigate the energy demand across diverse building typologies. As well, this research aims to assess the impact of energy-saving retrofit interventions, considering both current and future climate conditions. By combining computational and machine learning methods, this project aims to overcome data availability challenges and speed up the energy modelling process, ultimately enabling targeted building retrofit interventions across the Dutch housing stock to maximize energy savings.

RESEARCH QUESTIONS

MAIN QUESTION

The main question this research project intends to answer is:

How can machine learning be used to predict energy performance for residential buildings at city-scale to reduce heating and cooling demands, considering future weather scenarios from climate change?

SUB-QUESTIONS

The main research question is divided into a series of sub-questions, that investigate energy-saving **retrofit interventions**, at **city-scale**, using **machine learning** methods.

RETROFIT INTERVENTIONS

- How can ML be used to assess the impact of retrofit interventions across different building typologies?

CITY-SCALE

- How can computational methods be leveraged for energy modelling at city-scale?

MACHINE LEARNING

- How can ML models improve the efficiency of building energy modelling?
- What is an effective ML model, in terms of time efficiency and useability, for predicting building energy performance?
- What are the limitations of ML models compared to traditional energy modelling?

RESEARCH METHODOLOGY

The research started with a literature study to define the research framework and identify scientific gaps, such as the limited exploration of ML models for energy prediction at urban scale, or the lack of studies accounting for future climate scenarios.

The study, described in chapter 2. LITERATURE STUDY identifies relevant case studies and existing research related to building energy demand and retrofit interventions – particularly in the context of the Netherlands, as well as building energy modelling, and ML prediction models.

Findings from the literature study helped to inform the next stages of the research methodology, that is further described in chapter 3. METHODOLOGY.

2

LITERATURE STUDY

BUILDING ENERGY DEMAND

BUILDING RETROFITS

DUTCH CONTEXT

FUTURE CLIMATE

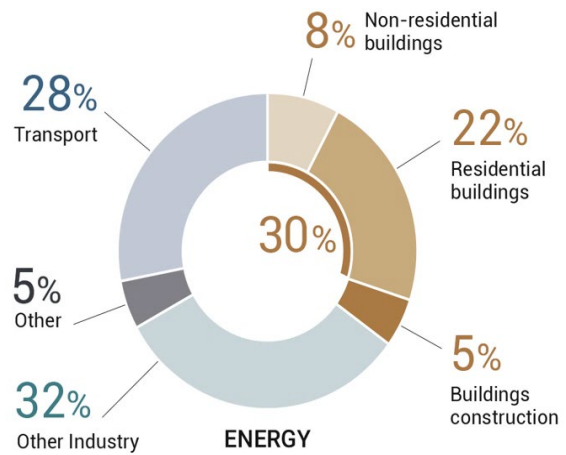
BUILDING ENERGY MODELLING

MACHINE LEARNING

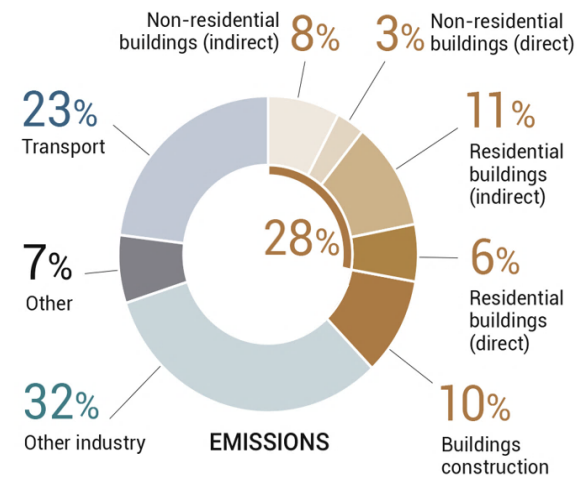
2. LITERATURE STUDY

BUILDING ENERGY DEMAND

Building energy use accounts for a significant share of global energy consumption and CO₂ emissions. González et al. reports that building operations are responsible for approximately 30% of global energy use and 28% of global energy-related CO₂ emissions, shown in Figure 1. The residential building sector consumes 22% of total energy, and contributes to almost 15% of CO₂ emissions, highlighting a target area with significant potential for lowering energy consumption and CO₂ emissions.



The Buildings Climate Tracker (BCT) index is a measure of the global progress towards decarbonizing the building sector, tracking indicators such as energy efficiency investments, renewable energy use, and CO₂ emissions, shown in Figure 2.



The BCT index highlights a widening gap between current efforts and the trajectory needed to achieve a zero-carbon building stock by 2050, underlining the urgent need for coordinated action across the building sector to reduce energy use and CO₂ emissions.

Figure 1: Contribution of building operational energy use to global energy consumption and share of CO₂ emissions (Global Alliance for Buildings and Construction et al., 2020).

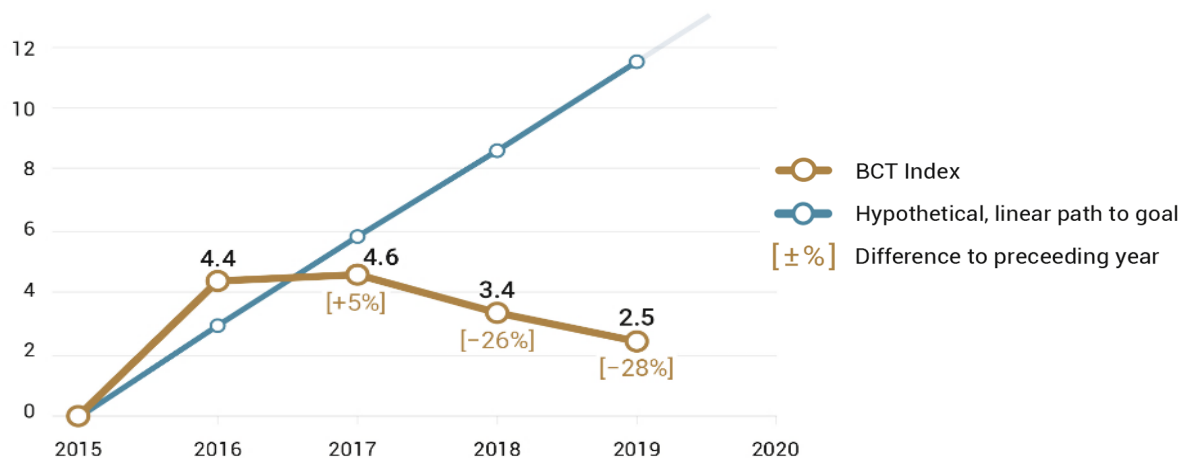


Figure 2: Buildings Climate Tracker (BCT) index, measuring global progress towards decarbonizing the building sector (Global Alliance for Buildings and Construction et al., 2020).

The building energy demand refers to the amount of energy required for heating, cooling, electricity, and other functions. The building energy demand is governed by the outdoor climate conditions, building design characteristics – such as the surface area of the building envelope, amount of insulation, and size of windows – the building occupancy and desired thermal comfort of occupants, and the use of electrical appliances (Van Bueren et al., n.d.). The factors related to the building energy demand are shown within the building energy chain in Figure 3.

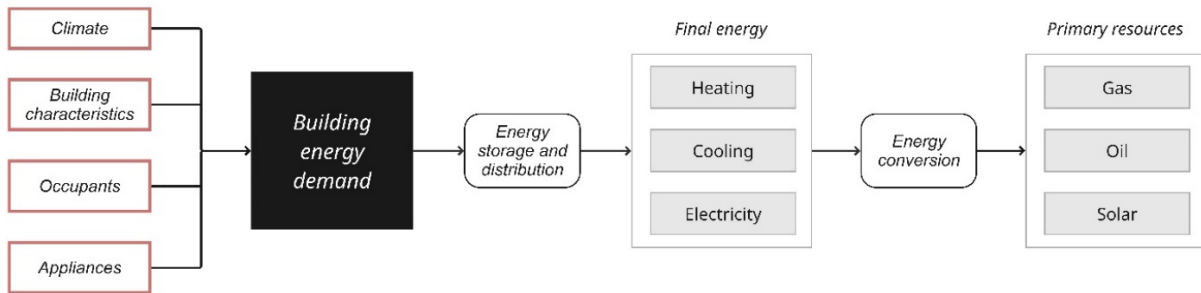


Figure 3: Energy chain within buildings (Adapted from Van Bueren et al., n.d.).

For countries, including the Netherlands, within the Organized Economic Cooperation and Development (OECD) region, a significant share of the building energy demand is attributed to space heating demands, as shown in Figure 4.

Considering the energy chain for buildings, Van Bueren et al. (n.d.) proposes a three-step strategy for reducing energy consumption, starting with reducing the energy demand, prioritizing renewables for primary energy use, and implementing efficient energy conversion measures when non-renewable resources are used, shown in Figure 5.

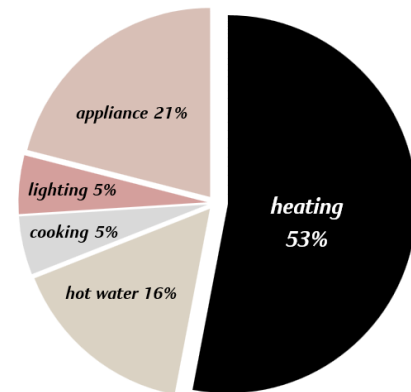


Figure 4: Share of residential final energy consumption within 19 OECD countries (Adapted from Van Bueren et al., n.d.).

ENERGY FLOWS

Summing the energy flows within a building, also known as a thermal energy balance, is necessary to determine the heating and cooling demands. When the summation of energy flows into and out of the building is negative, the building does not receive enough heat, thus there is a heating demand. Conversely, when the flows are positive, the building receives excess heat and there is a cooling demand.

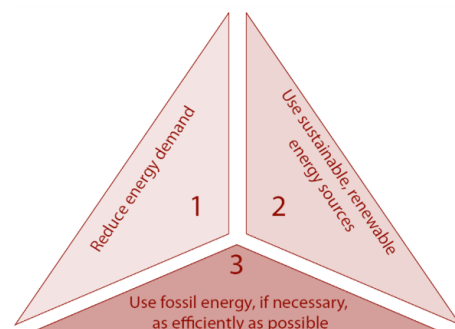


Figure 5: Strategies for reducing energy consumption (Konstantinou, 2014).

Equation 1: Thermal energy balance.

$$\sum \text{energy gains} + \text{energy losses}$$

$$\sum \text{transmission} + \text{infiltration} + \text{ventilation} + \text{solar} + \text{internal}$$

The thermal energy balance is comprised of energy gains and losses determined by transmission, infiltration, ventilation, solar, and internal heat flows. Analyzing the thermal energy balance is a critical step to determine the building's potential energy savings (Van Bueren et al., n.d.).

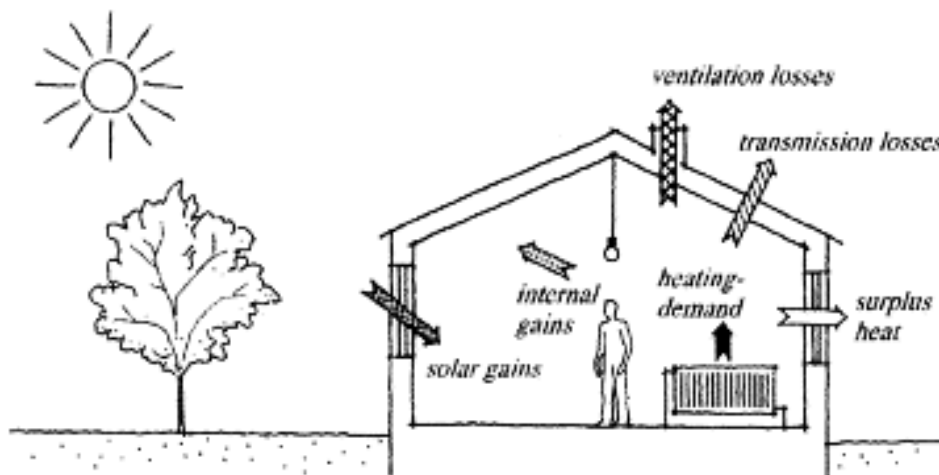


Figure 6: Building energy flows (Wittchen & Aggerholm, 2000).

TRANSMISSION

Transmission losses represent losses via the building envelope surfaces, including the roof, walls, windows, and ground floor.

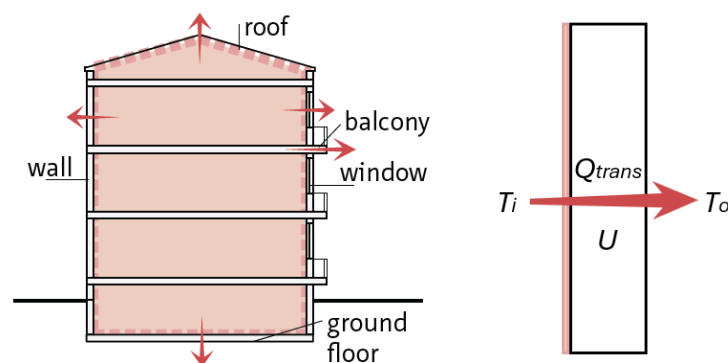


Figure 7: Transmission losses via the building envelope, when temperature indoor (T_i) is less than temperature outdoor (T_o) (Adapted from Konstantinou, 2014).

Heat losses via transmission occur through a surface area, A , as a function of the difference between indoor temperature (T_i) and outdoor temperature (T_o), and overall heat transfer coefficient, U . The heat transfer coefficient is related to the combined heat transfer coefficient for convection and radiation at the indoor side, α_i , and outdoor side, α_o , and the thermal resistance, of the surface, R_c .

Equation 2: Transmission losses.

$$Q_{trans} = UA(T_o - T_i)$$

$$U = \frac{1}{\frac{1}{\alpha_i} + R_c + \frac{1}{\alpha_o}}$$

In older buildings, the heating demand is largely governed by transmission losses. Transmission losses can be significantly reduced by improved insulation, as shown in Figure 8. Improved insulation increases the thermal resistance of the building elements (R_c -value), thus lowering the thermal transmittance (U -value), effectively reducing heat loss.

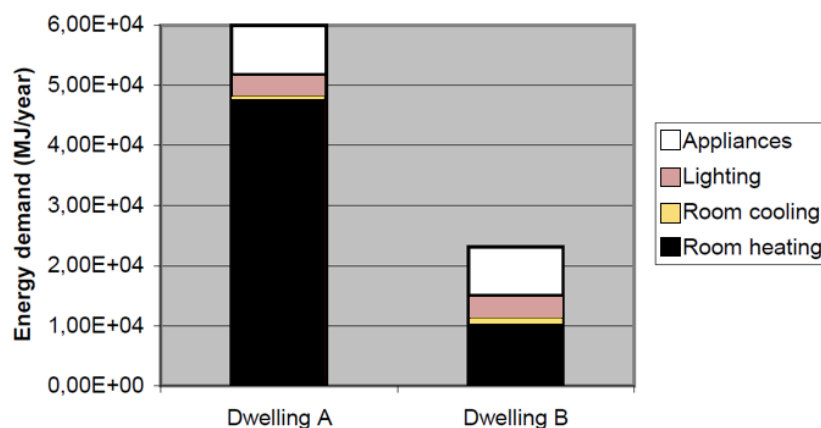


Figure 8: Average energy demands for typical Dutch pre-war, poorly insulated (Dwelling A) and modern, well-insulated (Dwelling B) buildings (Adapted from Van Bueren et al., n.d.).

INFILTRATION

Infiltration describes the uncontrolled air leakage into a building via cracks in the construction, especially at junctions like the wall and window frame, or between the roof and walls. Infiltration is driven by the difference between indoor and outdoor temperatures and the outdoor air flow through the envelope.

Equation 3: Infiltration losses.

$$Q_{inf} = (1 - \eta)m_{inf} C_p(T_o - T_i)$$

Infiltration, Q_{inf} is typically measured in $m^3/\text{second}/m^2$ of envelope area and is calculated from the mass flow rate of air, m_{inf} , heating capacity of air, C_p , the differential between outdoor and

indoor temperatures, and ventilation system efficiency, η . Where lower values of Q_{inf} result in lower infiltration losses. Areas prone to air infiltration are shown in Figure 9.

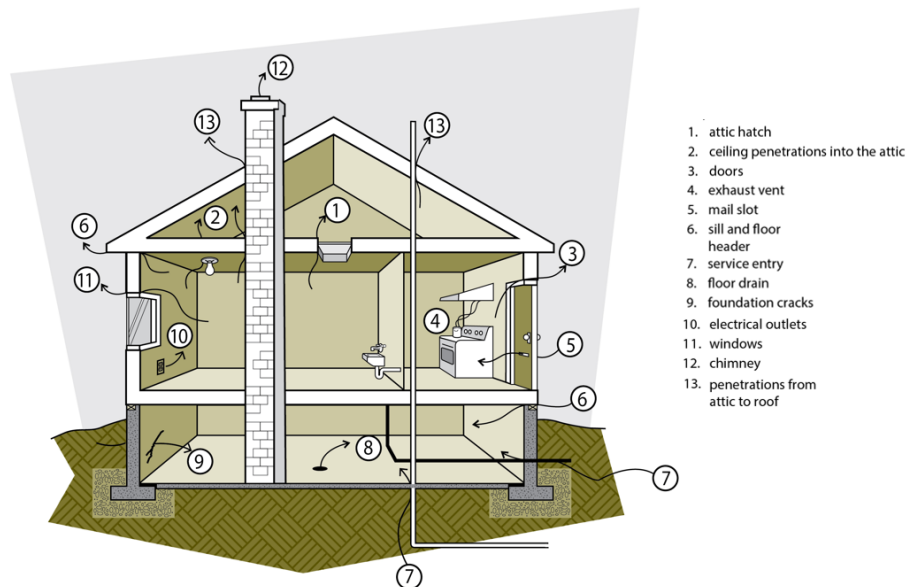


Figure 9: Typical building locations prone to infiltration (Canada, 2025).

VENTILATION

Outdoor air also enters and exits the building via window openings, grilles, and/or mechanical ventilation systems. Ventilation losses have a similar expression to that described by infiltration, but where the mass flow rate of air is for ventilation, m_{vent} .

Equation 4: Ventilation losses.

$$Q_{vent} = (1 - \eta)m_{vent} C_p(T_o - T_i)$$

Building ventilation can be described by four main systems:

1. Natural ventilation via window openings and grilles, where no mechanical ventilator is used.
2. Mechanical exhaust ventilation.
3. Mechanical supply ventilation.
4. Balanced ventilation, with mechanical supply and exhaust ventilation, and with heat recovery.

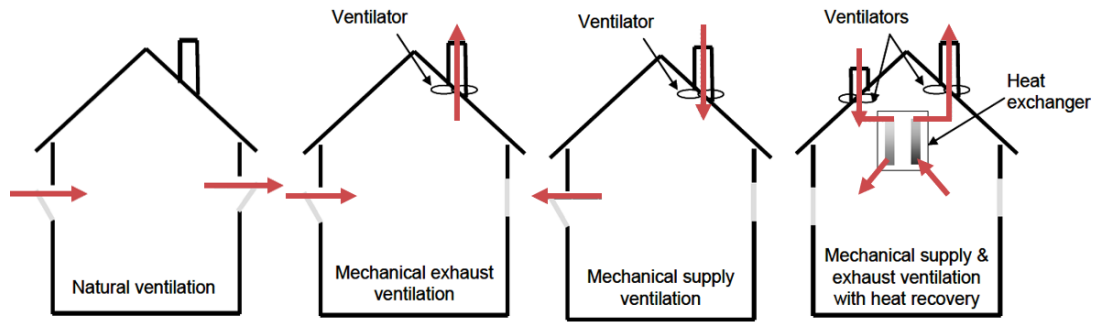


Figure 10: Main types of building ventilation systems (Adapted from Van Bueren et al., n.d.).

The type of ventilation system impacts how much heat is lost as air flows into and out of the building. Natural ventilation and basic mechanical systems (with exhaust or supply only) lead to higher, uncontrolled ventilation losses since they do not recover heat from the outgoing air. In contrast, balanced systems, reduce heat losses by using a heat exchanger to transfer heat from warm exhaust air to cool the incoming supply air, thus significantly reducing heat losses (Van Bueren et al., n.d.).

SOLAR GAINS

Solar gains occur via solar radiation entering the building through windows, and the outer surface of walls and the roof. The heat is stored by the building construction and later released to the indoor environment. Solar heat gains depend on the thermal mass of the building, building orientation, shading measures, and the orientation, type, and size of the building's windows (Richards Partington Architects, 2012).

Thermal mass is related to a material's ability to absorb, store, and release heat. During the day, incident solar radiation is absorbed by the building construction, shown in Figure 11 (left). At night, as the indoor temperature drops, the construction gradually releases the stored heat back into the space, shown in Figure 11 (right). Materials with high thermal mass, such as concrete, brick, or masonry can absorb more heat than lightweight materials such as timber due to their high specific heat capacity and density (Zero Carbon Hub, 2015).

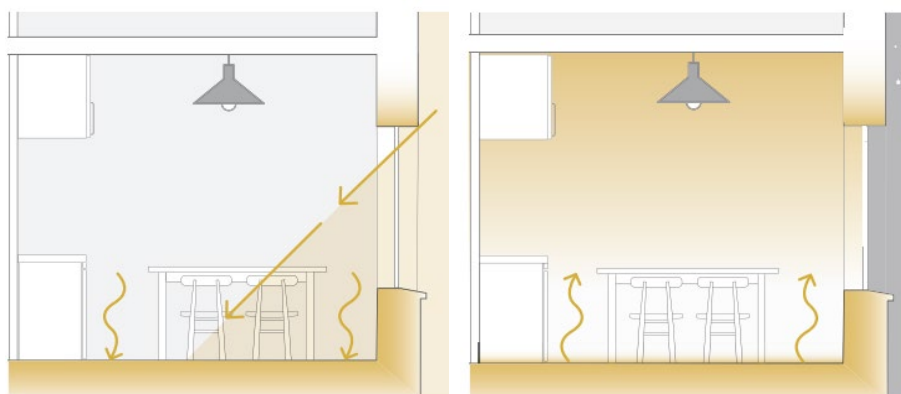


Figure 11: Solar radiation absorption in the building construction during the day (left) and heat release during the night (right) (Richards Partington Architects, 2012).

External solar gains are strongly influenced by the building's orientation. Thus, identical building designs can have very different energy demands if oriented differently. West and southwest-facing elevations receive strong afternoon sun, which can help to reduce heating demands in winter but may significantly increase cooling demands in summer months.



Figure 12: Solar exposure for different building orientations (Richards Partington Architects, 2012).

Solar gains can be effectively reduced via external shading devices, that reduce incident solar radiation. Again, as shown in Figure 13, the reduction in solar radiation is strongly influenced by the building orientation.

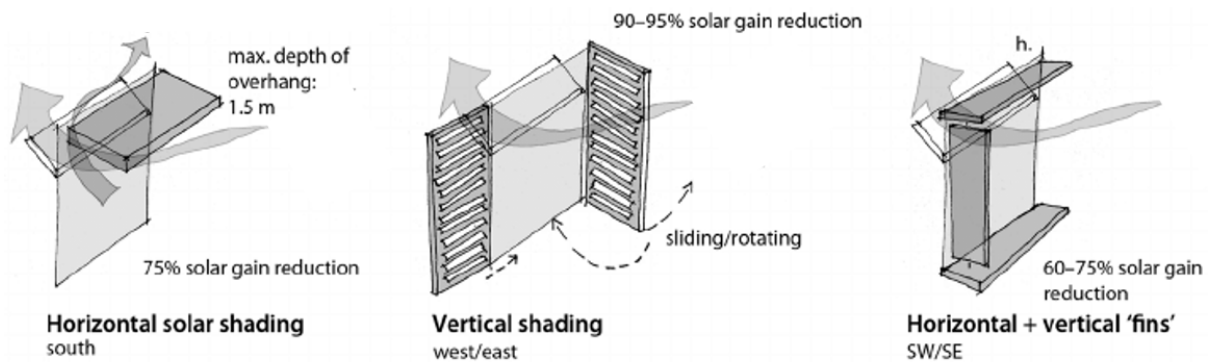


Figure 13: External shading devices and corresponding reductions in solar gains (Alabdullatif et al., 2016).

Static solar gains can be approximated by the solar heat gain coefficient for windows and shades, g_{glass} and g_{shade} , the window area, A_{window} , and the total incident solar radiation, P_{sol} .

Equation 5: Solar gains.

$$\sum g_{glass} A_{window} g_{shade} P_{sol}$$

Note, this expression does not take into account the dynamic effects related to the building's thermal mass and heat release over time.

INTERNAL GAINS

Internal heat gains occur from lighting, electrical appliances such as fridges, laptops, TVs, and the building occupants, shown in Figure 14.

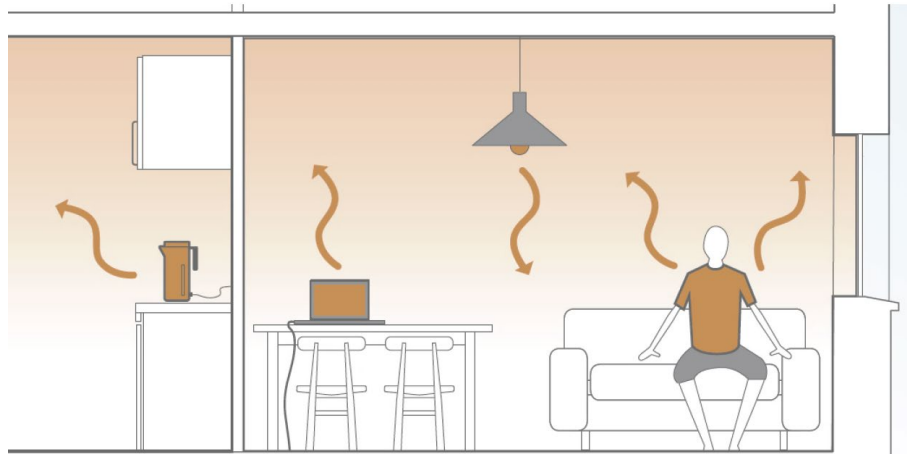


Figure 14: Sources of internal heat gains (Richards Partington Architects, 2012).

Approximations can be made for each of the internal heat gains. For lighting, $P_{int,light}$ is calculated from the fraction of heat released to the room, ζ_{light} , percentage of building floor area where the light is on, β_{floor} , total building floor area, A_{floor} , and the lighting's electrical power, P_{light} .

Equation 6: Internal gains due to lighting.

$$P_{int,light} = \zeta_{light} * \beta_{floor} * A_{floor} * P_{light}$$

For appliances, internal gains are estimated from the total power of all appliances (excluding lighting), P_{app} , per building floor area, A_{floor} .

Equation 7: Internal gains due to appliances.

$$P_{int,app} = A_{floor} * P_{app}$$

For building occupants, P_{int} , is calculated using the number of people in the building, n_{people} , and the metabolic heat generation, P_M .

Equation 8: Internal gains due to occupants.

$$P_{int} = n_{people} * P_M$$

BUILDING RETROFITS

The building envelope is the physical boundary that separates the conditioned indoor space from the unconditioned outdoor environment (SIGA, n.d.). The main building envelope layers, shown in Figure 15, function to:

1. Protect the indoor space from environmental effects including wind, rain, snow, and solar radiation.
2. Provide thermal insulation to minimize heat transfer across the envelope.
3. Provide an airtight seal to reduce the heat and moisture transfer through the structure.

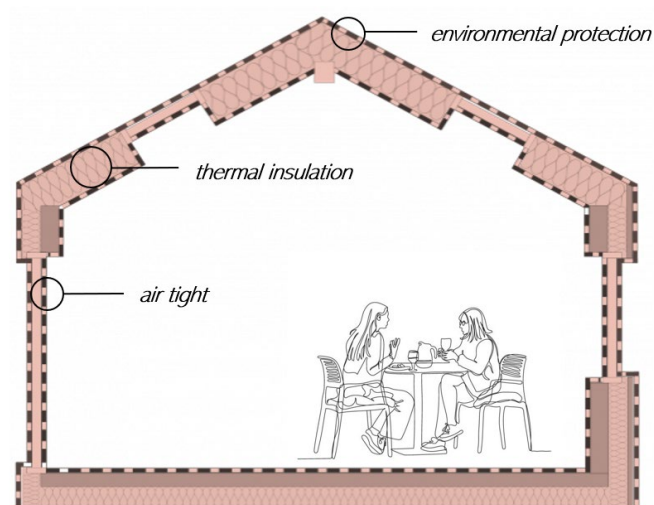


Figure 15: Key functions of the building envelope (Adapted from SIGA, n.d.)

The building envelope is the most critical component of the building's energy performance and thus, represents the primary target for building retrofits aimed at reducing energy demand. Key parameters influencing envelope performance include the thermal transmittance of exterior walls, roofs, ground floors, windows, and the size and orientation of openings, shown in Figure 16.

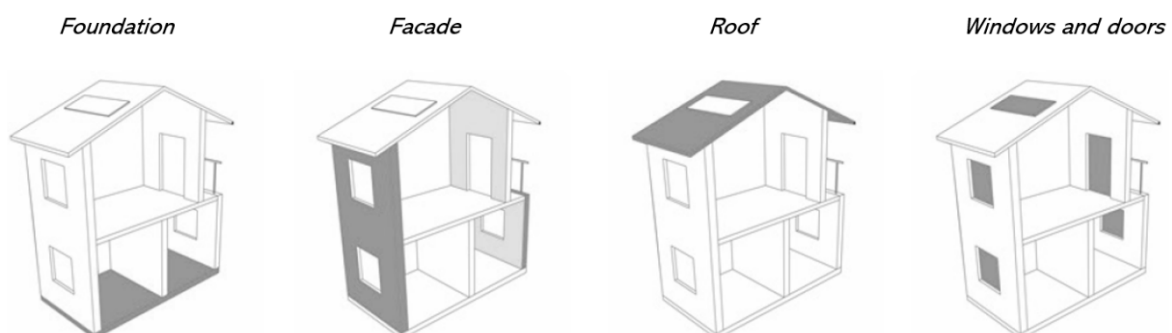


Figure 16: Building envelope components (Adapted from Wahi, 2020).

Older buildings often exhibit poor building envelope performance due to physical degradation of the structure (for example, cracks in the façade), high air infiltration, and insufficient thermal insulation, which significantly increases energy demand (Konstantinou, 2014).

Specifically, houses constructed between the 1920s and 1970s are typically constructed with uninsulated cavity walls, where the air gap provides limited resistance to heat transfer. Adding insulation to the cavity is an effective retrofit strategy to significantly improve the thermal transmittance of the facade and thus lower the heating demand without major renovation (Koh et al., 2022).

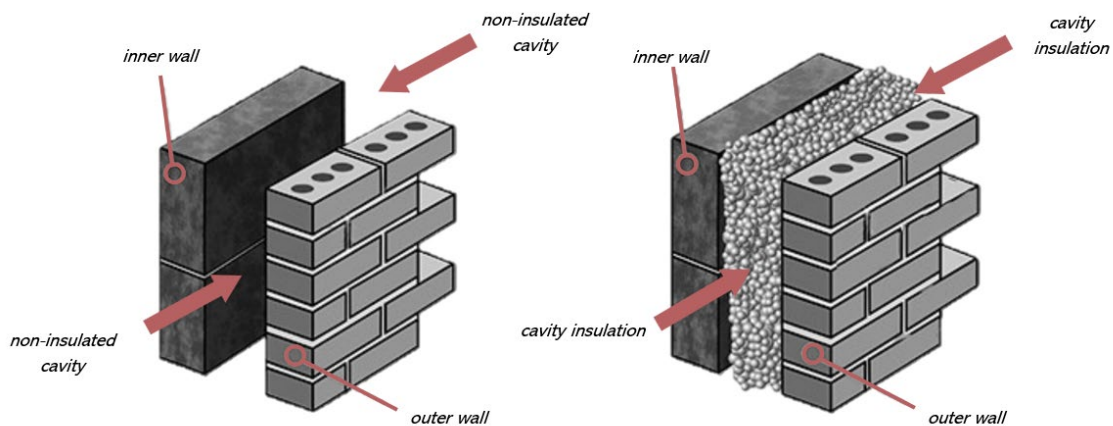


Figure 17: Before (left) and after (right) installation of cavity wall insulation (Adapted from *Everything You Should Know About Cavity Wall Insulation*, 2022).

In addition to cavity wall insulation, improving airtightness and upgrading other envelope components such as windows are critical measures to reduce energy demand. Building airtightness refers to how well the building envelope resists the uncontrolled air leakage into or out of the building. While no building is completely airtight, minimizing uncontrolled airflow, through sealing gaps, at key areas, such as behind window or door trim, as shown in Figure 18, is essential for reducing heat losses and lowering energy demand (Canada, 2025).

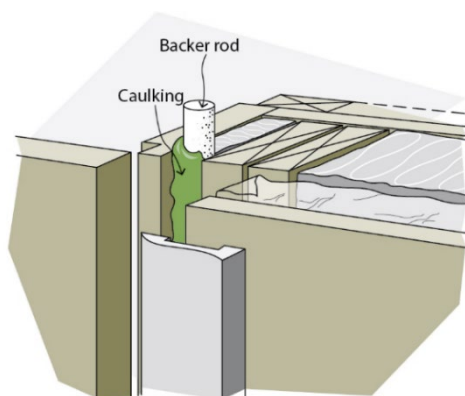


Figure 19: Sealing (caulking) behind window or door trim (Canada, 2025).

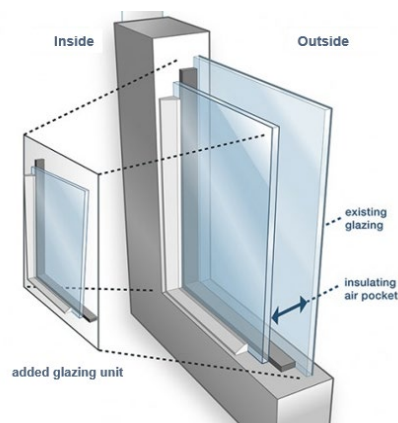


Figure 19: Retrofitting window from single to double pane (Adapted from *ecoGlaze® Retrofit Double Glazing* | Green Magazine, 2015).

Windows typically exhibit the poorest thermal performance of all components and thus can contribute significantly to heat loss and solar gains (Konstantinou, 2014). Upgrading single-glazed windows to double or triple-glazed units with low-E coatings and insulated frames significantly improves the thermal resistance (lower U-value), minimizing heat losses. As well, retrofitting strategies that optimize the ratio of window openings to solid building surface, otherwise known as the window-to-wall ratio (WWR) are an effective way to reduce energy demands (Konstantinou, 2014).

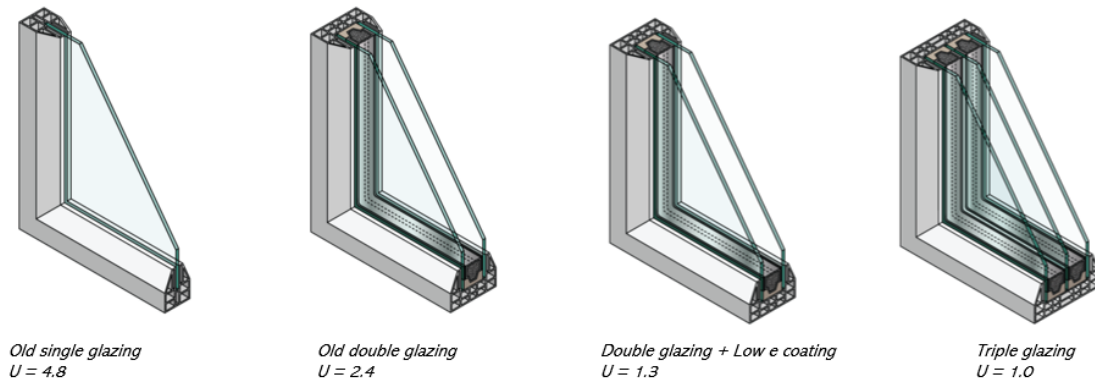


Figure 20: Reductions in U-value for different glazing units (Adapted from Types and Parts: Glazing, 2024).

DUTCH CONTEXT

The RVO (Rijksdienst voor Ondernemend) assessed the distribution of houses in the Netherlands to characterize the energy performance of different housing types in the “Voorbeeldwoningen Bestaande Bouw” (Example Homes Existing Construction) guide.

From approximately 8 million existing houses, terraced or row houses represent the largest share of the housing stock, at 41% considering both intermediate and corner houses, as shown in Figure 21.

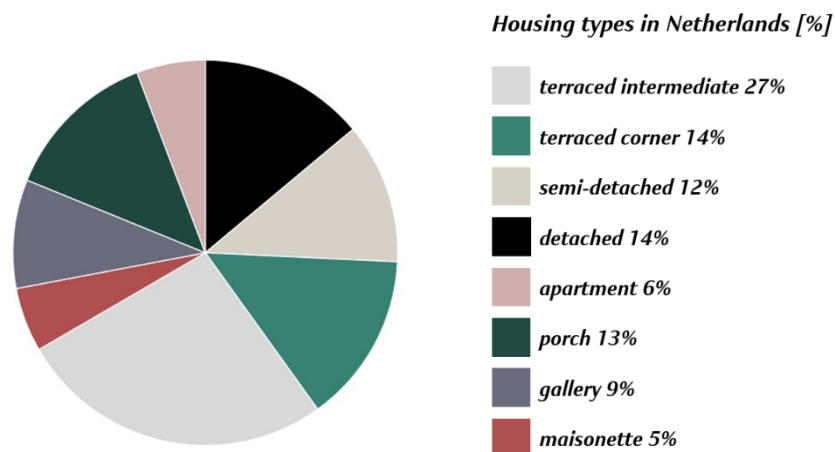


Figure 21: Distribution of housing types in the Netherlands, considering all construction periods (Adapted from Ministry of the Interior and Kingdom Relations, 2022).

The guide uses data from the WoON2018 survey (Woon Onderzoek Nederland 2018) – a housing survey in the Netherlands that provides insights on Dutch housing characteristics and energy performance. The energy module of the survey assessed approximately 4,500 existing houses throughout the Netherlands, collecting data on:

- **Housing characteristics:** building geometries and insulation levels.
- **Energy systems:** HVAC system types, efficiencies, and the presence of renewable energy installations.
- **Occupants:** energy use patterns, and preferences.



terraced intermediate



terraced corner



semi-detached



detached



apartment



porch



gallery



maisonette

Figure 22: Housing types in the Netherlands (Ministry of the Interior and Kingdom Relations, 2022).

For each house type, the heating demand and energy performance are calculated at five different energy consumption levels:

- Current:** current energy consumption based on the characteristics from the Woon2018 residential survey (median values).
- Original:** energy consumption in accordance with the building construction and installations of the building's original construction year (without any insulation improvements or energy-related retrofits).
- Retrofit 1:** after retrofit with mechanical air exhaust ventilation and gas heating.
- Retrofit 2:** after retrofit with mechanical air exhaust ventilation and installation of an electric heat pump (ground water source).
- Retrofit 3:** after retrofit with balanced ventilation and installation of an electric heat pump (ground water source).

For example, for the archetype “Terraced house built between 1946 – 1964”, the thermal characteristics and installations, shown in Table 1, are used to calculate the heating demand.



Figure 23: Terraced house built between 1946 – 1964 (Ministry of the Interior and Kingdom Relations, 2022).

At each energy level, the demand is compared to the “Standard for Home Insulation”. The standard ensures houses are sufficiently insulated to enable the transition from natural gas to low-temperature heating systems (such as an electric heat pump).

Insulations, R_c are in units $m^2 K/W$, thermal transmittance U in units W/m^2K , and infiltration q_v in units $dm^3/s/m^2$.

Table 1: Characteristics used to calculate the heat demand and energy performance (Adapted from Ministry of the Interior and Kingdom Relations, 2022).

Terraced house between 1946 – 1964					
Architectural					
	Surface Area [m^2]	Current	Retrofit 1	Retrofit 2	Retrofit 3
Ground floor	44.21	$R_c = 0.15$	$R_c = 3.50$	$R_c = 3.50$	$R_c = 3.50$
Façade	39.78	$R_c = 0.35$	$R_c = 1.70$	$R_c = 1.70$	$R_c = 1.70$
Sloped roof	48.00	$R_c = 0.72$	$R_c = 3.50$	$R_c = 3.50$	$R_c = 3.50$
Flat roof	0.00	$R_c = 0.72$	$R_c = 3.50$	$R_c = 3.50$	$R_c = 3.50$
Window	19.86	$U = 2.90$	$U = 1.40$	$U = 1.40$	$U = 1.40$
Door	4.82	$U = 3.40$	$U = 1.40$	$U = 1.40$	$U = 1.40$
Infiltration		Standard rate	$q_v = 0.7$	$q_v = 0.7$	$q_v = 0.4$
Installations					
Ventilation		Natural	Natural supply, mechanical exhaust	Natural supply, mechanical exhaust	Balanced
Heat recovery		No	No	No	Yes
Space heating		Gas boiler	Gas boiler	Electric heat pump	Electric heat pump
Hot tap water		Gas boiler	Gas boiler	Hybrid heat pump	Hybrid heat pump
PV panels (m^2)		0.00	0.00	0.00	0.00
Energy performance					
Standard for Home Insulation (kWh/m^2)		61.6	61.6	61.6	61.6
Heating demand (kWh/m^2)		162.5	53.6	53.6	37.2

The brochure provides a structured approach for calculating the heating demand across the Dutch housing stock, using the NTA8800 standard for calculations, and highlighting the influence of different retrofit measures. However, the use of the NTA8800 calculation standard introduces uncertainty about the energy consumption results. NTA8800 calculations are based on standardized assumptions for weather, occupant behaviour, and do not depict actual use cases or climate variations (Van Den Brom et al., 2022). Also, the calculation provides an overestimation of the energy consumption for older houses (especially pre-1946), where the archetype tends to use overly conservative values for insulation levels that are not representative of the actual (Van Den Brom et al., 2022).

(Nieman et al., 2021) broadly categorized the Dutch housing characteristics based on four construction periods, summarized in Table 2.

Table 2: Dutch housing characteristics from pre-1945 to 1995 and beyond (Nieman et al., 2021).

	PRE-1945	1945-1975	1975-1995	POST-1995
CAVITY WALLS	Pre-1920 single brick wall construction. Post-1920 cavity walls constructed were narrow and uninsulated.	Uninsulated cavity walls.	Cavity walls with moderate insulation.	Well insulated cavity walls.
WALLS/ROOF	Uninsulated.	Uninsulated or minimal insulation used.	Minimum thermal insulation Rc value of 1.3 m ² K/W.	Minimum thermal insulation value of 2.50 m ² K/W.
FLOORS	Wooden ground floors.	Wooden floors gradually replaced by non-insulated concrete floors.	Prefabricated concrete floors. Limited insulation.	Prefabricated concrete floors. Minimum thermal insulation value of 2.50 m ² K/W
WINDOWS	Single glazing in wooden or steel frames.	Single glazing predominated, particularly on upper floors, double glazing emerged on ground floors.	Double glazing became mandatory in living rooms (1979).	Double glazing mandated for entire building.
VENTILATION, INFILTRATION	Uncontrolled infiltration due to minimal attention to airtightness. Natural ventilation through leaks, cracks, windows.	Natural ventilation via windows, wall vents, and basic exhaust ducts.	Reduced uncontrolled infiltration. Natural air supply via grilles or windows, combined with mechanical exhaust.	Significant airtightness improvement. Balanced ventilation systems with heat recovery.
HEATING	Heating localized, using coal, gas, or oil stoves.	Individual gas heaters or stoves.	High temperature central heating standard.	High temperature central heating with improved efficiency.

Based on the four building periods, (Nieman et al., 2021) considers a retrofit framework considering three different retrofit levels:

- Level 2:** insulation improvements of limited thickness and quality.
- Level 3:** high-quality insulation improvements.
- Level 4:** high-cost retrofit measures such as a new roof, adding exterior wall insulation, and/or implementing a balanced ventilation system with heat recovery.

Nieman highlights that houses constructed before 1945 have significantly higher heat demands due to poor insulation and airtightness. After implementing Level 4 retrofits, houses are often compatible with medium-temperature and low temperature heating systems without major adjustment to the heat delivery system. Findings suggest that the heat demand is strongly influenced by compactness, and year of construction, which has an implication on the structure's thermal quality, and airtightness (Nieman et al., 2021).

FUTURE CLIMATE

Koninklijk Nederlands Meteorologisch Instituut (KNMI) is the national advisory group on climate change in the Netherlands. In 2023, the KNMI published a report on climate change scenarios in the Netherlands, representing the most current findings on climate change from the Intergovernmental Panel on Climate Change (IPCC) and for the Netherlands (The Royal Netherlands Meteorological Institute, n.d.).

Weather projections are provided for key climate variables – temperature, precipitation, radiation, relative humidity, and wind speed by comparing mean data from the reference period of 1991–2020 to future years 2033, 2050, 2100, and 2150.

The KNMI scenarios are based on the IPCC's global framework of Shared Socioeconomic Pathways, (SSPs), which result in different global greenhouse gas trajectories and temperature increases. The points represented in Figure 24 correspond to the temperature increase expected for each of the KNMI scenarios and the range of uncertainty based on both the emissions and the way in which the climate responds.

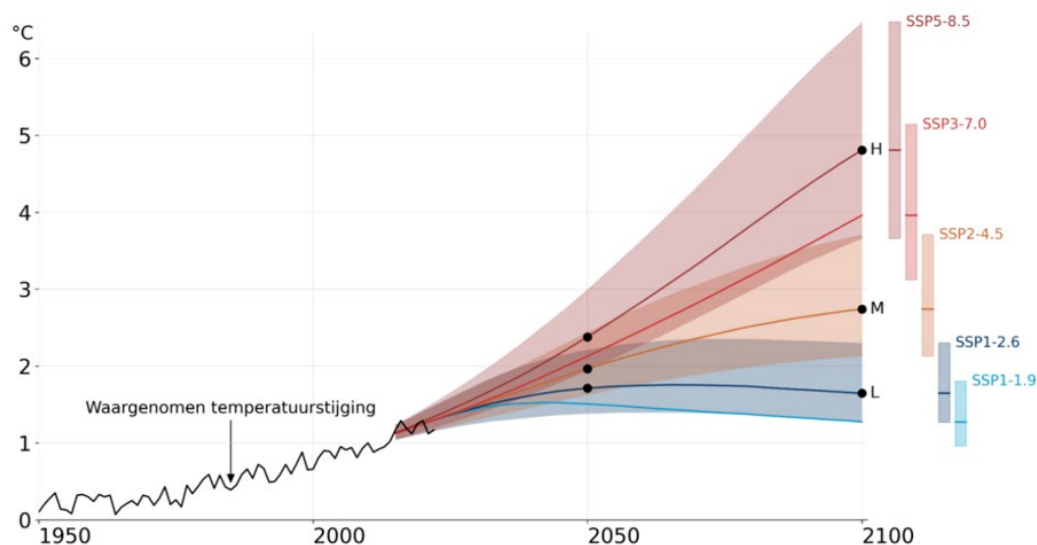


Figure 24: Observed global temperature increase compared to the reference period of 1850-1900 (black line). Predicted temperature increase for each SSP (black points). Range in uncertainty for each SSP (coloured bars). (KNMI *Klimaatscenario's*, n.d.).

Projections are provided for two emissions scenarios, based on high (H) and low (L) CO₂ emissions. And two air moisture scenarios of dry (D) and wet (N) climates, producing the matrix of four climate scenarios for the Netherlands, shown in Figure 25.

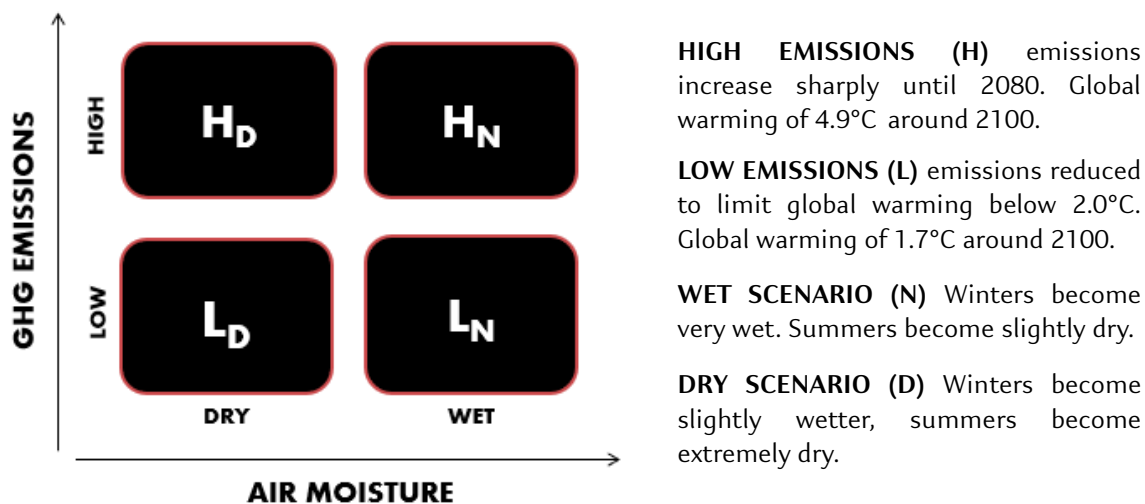


Figure 25: Matrix of climate scenarios in the Netherlands. Adapted from (KNMI Klimaatscenario's, n.d.).

In all scenarios, the following changes are expected when compared to the 1991-2020 reference period:

- Increase in average temperature
- Increase in solar radiation
- Increase in droughts
- Wetter winters
- Increase in extreme summer downpours
- Little change in wind speed and direction

EPWshiftr is an open-source software tool that enables users to generate future weather files – used for energy modelling – for any location worldwide (Epwshiftr, 2021). The tool statistically shifts baseline weather data by using the projected differences for each key climate variable – such as mean temperature increases, shown in Figure 26.

Season	Variable	Indicator	2100 Ld	2100 Ln	2100 HD	2100 Hn
Global temperature increase compared to 1991-2020			0.8°C	0.8°C	4.0°C	4.0°C
Global temperature increase compared to 1850-1900			1.7°C	1.7°C	4.9°C	4.9°C
Year	Temperature	average	+0.9°C	+0.9°C	+4.4°C	+4.1°C
		average daily maximum	+1.0°C	+0.9°C	+4.3°C	+3.9°C
		average daily minimum	+0.8°C	+0.8°C	+4.5°C	+4.5°C

Figure 26: Future climate scenarios for De Bilt, NL (KNMI Klimaatscenario's, n.d.)

By inputting the future climate variables, EPWshiftr can be used to generate local, future weather files that reflect climate change in the Netherlands.

BUILDING ENERGY MODELLING

BUILDING LEVEL

To understand the thermal behaviour of a building, an accurate model is required, with a detailed description of the building geometry, construction, installations, and internal loads. Often this data is not readily available, resulting in assumptions being made or standard values being used for model inputs. Due to these limitations, energy models often vary from the building's true energy use (Fathi et al., 2020a). Developing more representative building energy models is an important step to understand effective retrofit strategies to reduce energy use (Fathi et al., 2020a).

MODEL TYPES

Building energy modelling (BEM) can be categorized as either physics-based or data-driven (Li et al., 2023).

Physics-based

Simulation-based model. The building energy use is predicted from heat and mass balance equations based on detailed physical building characteristics. Simulations using software such as DOE-2, EnergyPlus and TRNSYS, often require a large number of detailed inputs about the building and environment, including:

- HVAC (Heating, Ventilation and Air Conditioning) system
- Insulation thickness
- Thermal properties
- Internal occupancy loads
- Solar radiation

Simulation software such as EnergyPlus can model hourly variations in model inputs, providing a good representation of a building's energy behaviour. However, using such granular input data results in time-intensive simulations that require significant computational resources, especially when modelling energy use at city-scale (Aruta et al., 2024), (Li et al., 2023).

Data-driven

Relies on historical building energy usage data and uses mathematical models to find underlying relationships between model input and output variables. These models require substantial historical data and often do not account for detailed building properties (Li et al., 2023).

MODELLING APPROACHES

Zhang et al. (2024) describes the typical steps for a data-driven BEM study:

- Data collection: Obtaining historical data from a building management system, HVAC sensors, occupant sensors, and weather stations.

- Data preparation: Improving data quality by resolving missing values and eliminating outliers.
- Feature selection: Identifying key variables that affect the building energy consumption, for example, occupancy, weather, and building system characteristics.
- Algorithm selection and model training: Identify the most suitable algorithm based on the input dataset characteristics and study objective.

Zhang et al. (2024) expands on the primary approaches used for feature selection, including:

- Filter methods: identify optimal features by statistically evaluating the relationship between each feature in the dataset and the target variable, for example, the relationship between WWR and heating demand.
- Wrapper methods: iteratively train and evaluate model performance with different feature combinations to identify the most effective subset.
- Embedded methods: make use of algorithms that integrate feature selection within the learning process.

MODEL INPUTS

Building geometry

The LoD is a representation of a 3D building model, categorized into five representation classes, shown in Figure 27, where:

- LoD0: represents the building footprint.
- LoD1: prismatic model of the building's footprint extruded to the building height.
- LoD2: model with differentiated surfaces, walls and simplified roof structure.
- LoD3: includes detailed architectural features, windows and doors.
- LoD4: includes indoor building features, internal walls, doors.

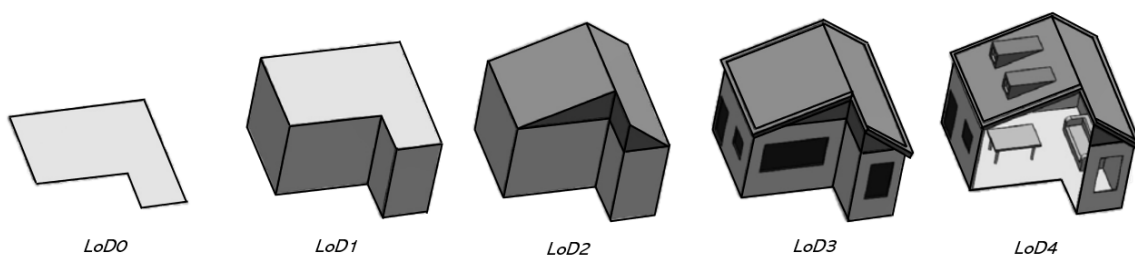


Figure 27: LoDs for 3D building models (Adapted from Li et al., 2023).

Biljecki et al. (2016), notes that different LoDs can affect thermal performance calculations. Key building features, such as roof details, wall areas, window and door locations and sizing, significantly impact the building's thermal gains, and losses, however, are not captured by lower LoDs, LoD0 and LoD1.

Biljecki et al. (2016) provides a more refined classification of LoDs based on currently available 3D building models, shown in Figure 28.

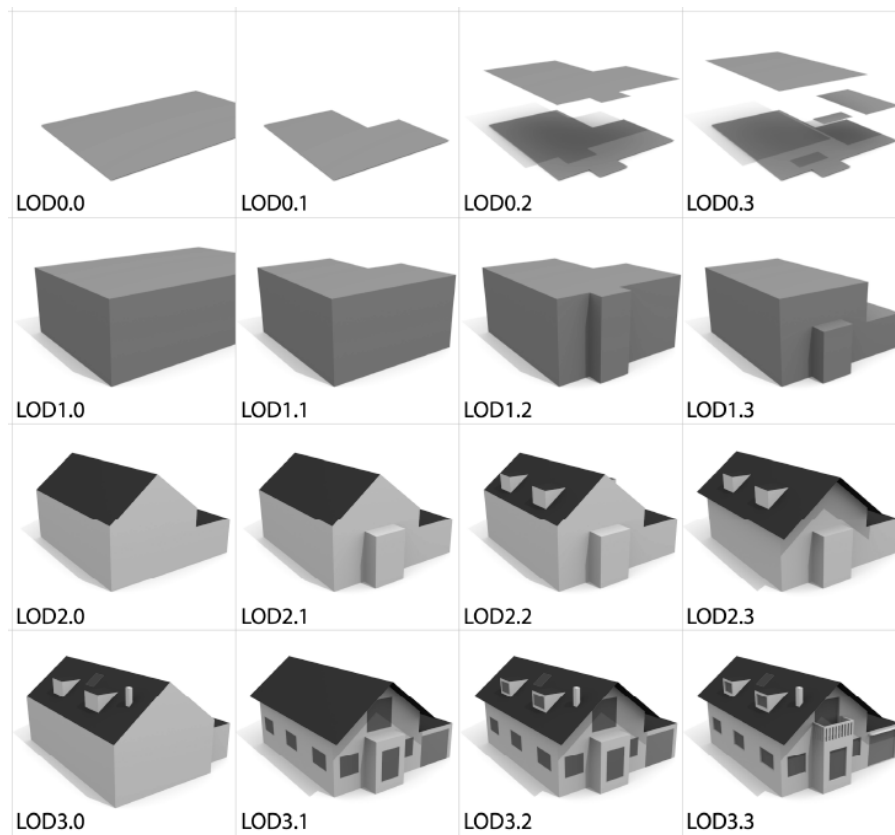


Figure 28: Refined LoD classifications for 3D building models (Biljecki et al., 2016).

Higher LoDs – such as LoD2 – can improve the reliability of energy simulations. As well in considering, the influence of different retrofit measures on energy performance, higher LoDs that provide more detailed feature representations may be required (Li et al., 2023).

Aruta et al. (2024) provides a summary of the geometric properties for BEM, shown in Figure 29. Model inputs are defined first by the characteristic dimensions, construction period, and construction type, that is then used to define the percentage of transparent to opaque building surface area, ratio of conditioned (net) floor area to gross floor area, ratio of net to gross building volume, and floor heights.

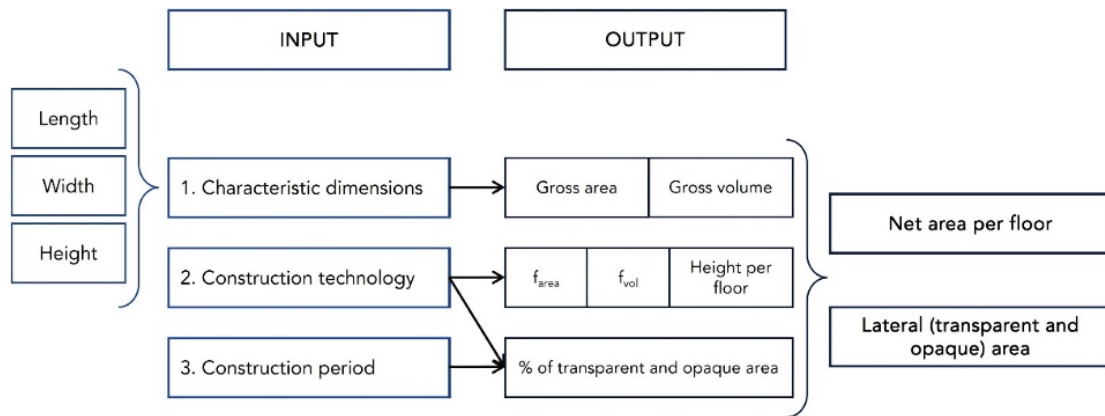


Figure 29: Example input parameters pertaining to building construction and geometry, where f_{area} is the ratio between net area and gross area, and f_{vol} is the ratio of net and gross volume (Aruta et al., 2024).

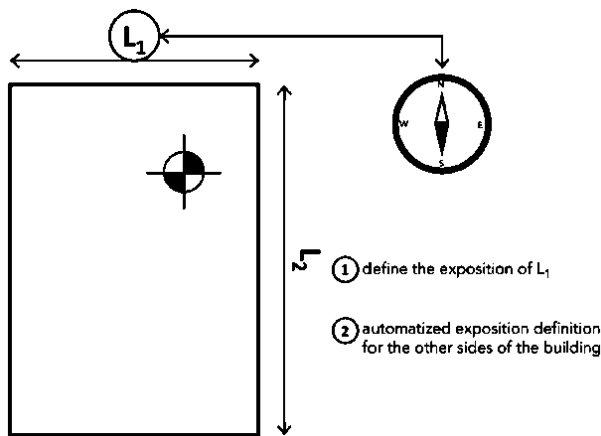


Figure 30: Logic for defining building exposures (Aruta et al., 2024).

After defining the geometry, it is necessary to orient the building according to its geospatial properties, to determine the exposures of the building's surfaces, and if there are building adjacencies. Where the building adjacencies determine the corrective coefficients to account for solar shading.

In Aruta et al. (2024), the one side of the building is defined, and the remaining building exposures are automatically oriented, shown in Figure 30.

Thermal characteristics

The thermal characteristics of the building construction impact the solar heat gains and heat gains via transmission. Thermal characteristics used for BEM are shown in Table 3.

Table 3: Example thermal characteristics for model simulation (Aruta et al., 2024).

Thermal parameters		Unit
External vertical opaque wall thermal transmittance	U_{wall}	W/m ² K
Roof thermal transmittance	U_{roof}	W/m ² K
Thermal transmittance of horizontal opaque structures	U_{ground}	W/m ² K
Thermal transmittance of windows	U_{window}	W/m ² K
Thermal transmittance of vertical and horizontal opaque separation structures between adjacent building units	U_v	W/m ² K
Solar transmission factor for windows	g_{total}	-
Distribution efficiency	N_d	-
Production yield	N_p	-
Transmission coefficient	H_T	W/K

Where the transmittance coefficients, U_{wall} , U_{roof} , U_{ground} , U_{window} define how much heat is transferred through the building envelope under temperature differences, influencing both heating and cooling loads. The transmission coefficient, H_T combines the thermal transmittance coefficients, into a single value for the overall thermal performance of the building envelope. The solar transmission factor, g_{total} impacts the amount of solar radiation transmitted through windows, leading to solar heat gains.

HVAC system

The following HVAC system parameters can be represented in a BEM (Aruta et al., 2024):

- Heating generator typology: type of heat source, for example, gas boiler, heat pump, electric heater. Impacting the efficiency of heat generation.
- Heating terminal: type of terminal units, for example radiators, or in-floor heating. Influencing evenly heat is distributed within the building.
- Regulation system: thermostats and sensors, improving the heat supply by adjusting based on internal temperatures.
- Distribution system: how heat is distributed, for example, via ductwork or pipes. Where losses can occur in the distribution process, if the system is poorly insulated.
- Space volume: how much heating or cooling energy is required to maintain the desired comfort, where larger volumes require more energy as they have greater exposure to heat transfer via walls, roofs, and windows.
- Nominal power or average power: determines if the heating or cooling system is oversized or undersized and if it can meet the heating and cooling needs of the space system. Where oversized systems lead to an uneven heat transfer. Undersized systems struggle to meet heating or cooling demands.
- Ventilation system and type: govern heat transfer through air exchange, either increasing heat losses (from uncontrolled infiltration) or reducing heat losses (via controlled ventilation with heat recovery).
- Age of cooling system: impacts the cooling efficiency – the building's ability to maintain thermal comfort throughout heat gains.

Meteorological data

Typical meteorological data included in BEM studies, influencing heating and cooling demands include (Fathi et al., 2020a), (Olu-Ajayi et al., 2021), (Carpino et al., 2022):

- Outdoor air temperatures
- Solar radiation
- Wind speed and direction
- Humidity
- Dew point temperatures
- Atmospheric pressure

For modelling the heating demand, an example workflow of model inputs and calculated outputs is shown in Figure 31.

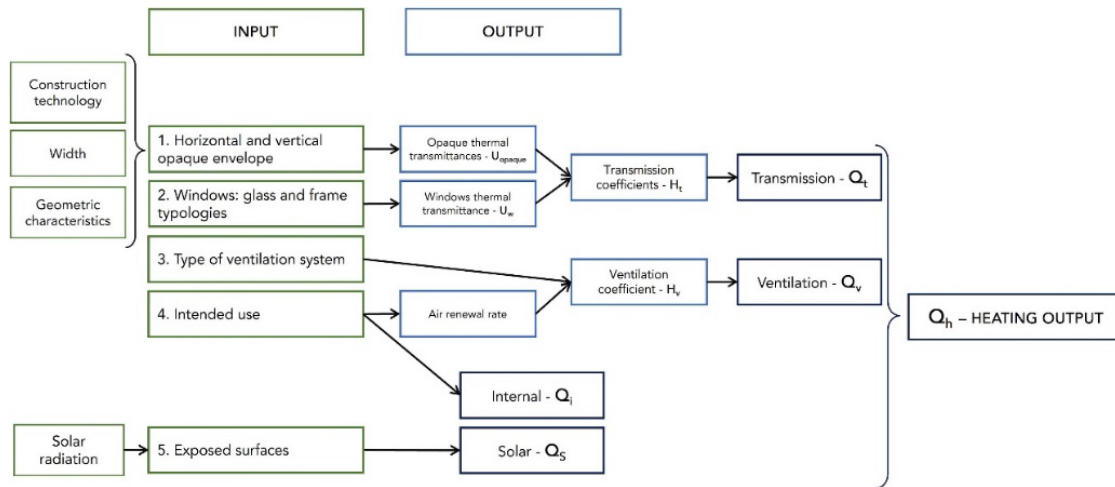


Figure 31: Definition of model inputs and outputs for calculating the heating demand (Aruta et al., 2024).

MODELLING CHALLENGES

Zhang et al. (2024) identifies the key challenges involved in BEM:

- Data quality and availability: historical energy consumption data may be incomplete or noisy, or unavailable for the study area of interest, increasing prediction errors and uncertainty, and making validation challenging.
- Energy uses: lack of information on whether gas consumption is from heating or direct hot water, and whether electricity consumption is from cooling or lighting needs (Aruta et al., 2024).
- Complexity of prediction scenarios: energy consumption is impacted by multiple factors, such as weather, building characteristics, and occupant behaviour. These interactions add complexity to the model. Advanced algorithms, such as deep learning, may be required to effectively capture non-linearity.
- Model scalability: improving model generalization – the model’s ability to extract useful information from similar buildings and make suitable adjustments based on the target building’s characteristics. Especially challenging when data is limited or unavailable for the target area.

URBAN SCALE

In the presence of building energy performance certifications, such as LEED, there is a focus on developing accurate energy models for individual buildings. However, to achieve the desired carbon reductions and environmental targets there is a need to evaluate building energy performance at urban scale (Fathi et al., 2020a).

Urban building energy modelling (UBEM) identifies the seasonal or annual energy demand of buildings across a city, considering the interdependency of buildings and the influence of the urban environment on building energy performance. Physics-based UBEM models simulate energy use from the building characteristics, including building geometry, HVAC systems, and occupancy patterns (Li et al., 2023).

Where BEM focusing solely on modelling the energy performance of individual buildings, UBEM considers surrounding effects, for example the radiation exchange between buildings and the environment, impacted by the height and density of the building network (Li et al., 2023). UBEM is considerably more challenging compared to BEM, due to data acquisition, data scale, and processing time.

MODEL TYPES

UBEM is categorized into two main types: top-down, and bottom-up models.

Top-down

- Relies on aggregate energy data, does not model individual buildings.
- Simple modelling approach and greater availability of required data.
- Not suitable for conducting detailed analysis and informing building-level energy conservation measures.

Bottom-up

- Calculates energy demand of each building then scales up to the entire city.
- Requires substantial computational resources.
- Incorporates detailed building characteristics and urban environmental features.

Due to the detailed nature of bottom-up models, they can present a notable advantage over top-down models, supporting decision-makers to understand building-level energy conservation strategies and identify retrofit opportunities. However, a challenge lies in scaling-up bottom-up models to a large city-level study, and balancing prediction accuracy with simulation time intensity (Li et al., 2023).

CASE STUDIES

ADDRESSING LIMITATIONS OF BUILDING ARCHETYPES

Thrampoulidis et al. (2023) notes that bottom-up approaches often use building archetypes – building definitions that represent a group of buildings with similar properties – to perform large-scale analysis with reasonable computational time and cost. The disadvantage of using building archetypes in a bottom-up retrofit approach is that the unique properties of each building are not captured, and thus individual building results may deviate significantly from reality.

Wahi et al. (2024) aimed to address the limitations of archetype-based energy modelling approaches by employing a sampling-based methodology to capture housing variability across terraced and apartment buildings in the Netherlands. The study assessed the readiness of these housing types for low temperature heating (LTH) supplied by district heating (DH).

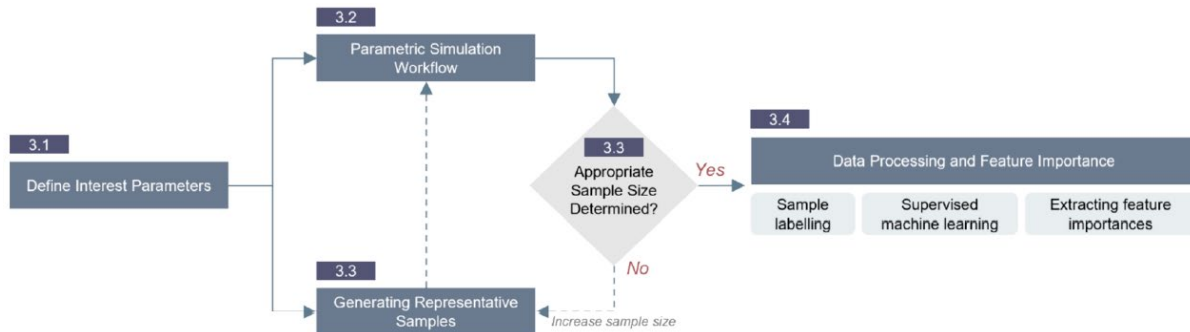


Figure 32: Sampling based methodology (Wahi et al., 2024).

The approach generated representative samples of housing types using Latin Hypercube Sampling (LHS) to reflect variations in geometry, insulation, heating systems, and occupant behaviour. For each housing type a sample size of 1,300 was determined to adequately represent the variability.

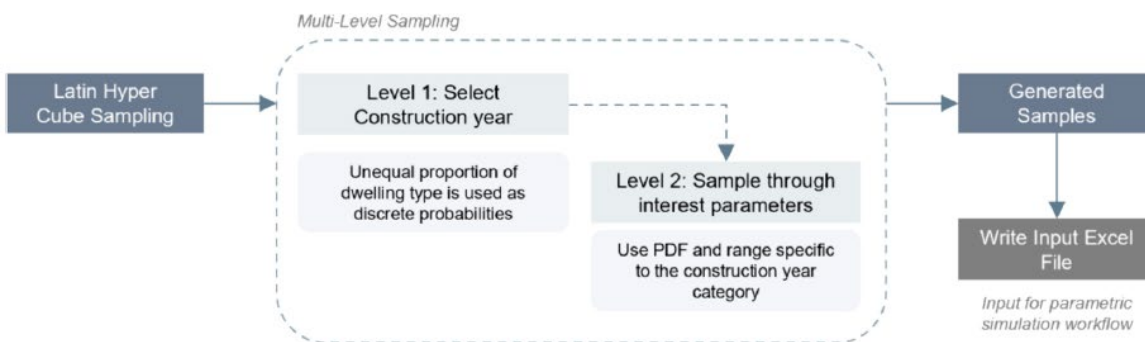


Figure 33: Latin hypercube sampling methodology (Wahi et al., 2024).

Simulations were conducted using dynamic energy modelling tools (Ladybug and Honeybee) to evaluate the annual heating demand and thermal comfort under high-, medium-, and low-temperature heating conditions. Inputs included insulation levels, airtightness, heating setpoints, ventilation types, and radiator capacity.

Machine learning approaches including Random Forest (RF) were used to predict LTH readiness and identify the key input variables. From the sensitivity analysis, the most influential parameters for predicting LTH readiness were:

1. Heating setpoints (occupant behaviour).
2. Ventilation-related parameters (system type and infiltration rates).
3. Building envelope characteristics (roof, glazing, and wall insulation).
4. Radiator sizing.

This approach provided an effective methodology for analyzing large building stocks and capturing housing variability. The approach could be expanded to consider other housing types, considering more than terraced (intermediate) and apartments, as well as other climatic conditions.

REFINED BUILDING ARCHETYPE APPROACH

Aruta et al. (2024) used a refined building archetype approach – by modelling buildings with the true geometric, orientation, location, and building adjacency properties, but with thermal parameters corresponding to an energy performance reference standard. This approach is more representative than the typical archetype-based approach – that generalizes building geometric data based on broad building periods and housing types.

The study modelled the energy demands using building geometric data, thermal properties of the building constructions, and HVAC system data. The complete list of input parameters is shown in Table 3.

For validation, Aruta et al. (2024), compared space heating and cooling demands to those derived from EnergyPlus. Through comparative analysis, the goal was to identify where the model required adjustment to better depict temporal variations or complex interactions.

Comparison between the prediction tool and EnergyPlus simulations showed a deviation of +5% to -4% for heating and cooling seasons.

Limitations include the reliance on high-quality input data that was unavailable at the time of study. As well as the potential inaccuracies resulting from applying an archetype-based approach at large scale (Aruta et al., 2024).

Table 4: Definition of model inputs and outputs for calculating the heating demand (Aruta et al., 2024).

Model Inputs
Geometry
Construction technology
Construction year
Building intended use
Building length L ₁
Building width L ₂
Number of floors
L ₁ exposure (N, E, S, W)
If isolated building (Y, N)
If taller buildings nearby (Y, N)
Shared building surfaces
Roof solar exposure
Walls solar exposure
Thermal
Vertical wall typology
Vertical wall thickness
First floor slab typology
First floor slab thickness
Roof typology
Roof thickness
Window glass type
Window frame type
Type of screening
Systems
Heating generator typology
Heating terminal
Regulation system
Distribution system
Volume
Nominal power
Ventilation system type
Age of cooling system

MACHINE LEARNING

APPROACHES

ML describes techniques used to detect patterns in a dataset to predict future data or conduct other decision-making processes. The three main ML types are:

1. Supervised learning (predictive): Produce mapping from inputs to outputs given a labelled dataset of inputs and corresponding outputs.
2. Unsupervised learning (descriptive): Detect patterns in dataset from given inputs.
3. Reinforcement learning: Learning performance from reward or penalty signals.

Common ML methods used for building energy modelling include:

- Classification: map inputs to output classes.
- Regression: map inputs to continuous output variables.
- Clustering: assign similar data points to distinct clusters.
- Dimension reduction: reducing random variables via feature selection or extraction.

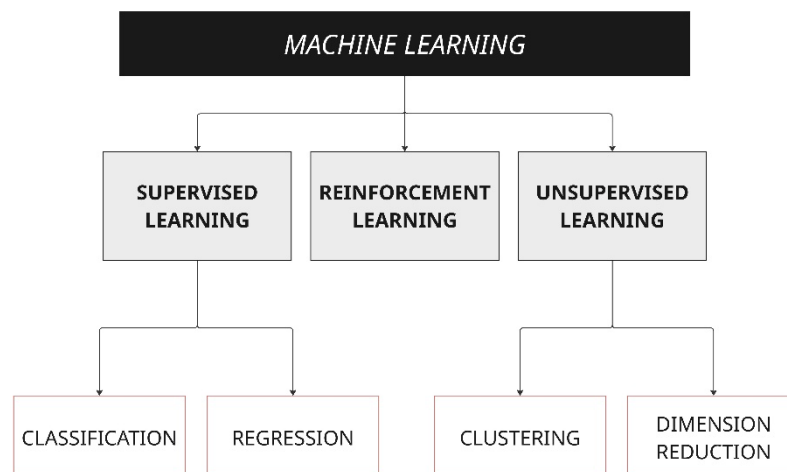


Figure 34: Machine learning methods common for building energy modelling (Adapted from Fathi et al., 2020a).

Due to the complexity of factors involved in BEM, models often rely on data-driven approaches using historical energy consumption data, to predict future energy demands, otherwise known as building energy performance forecasting (BEPF). Implementing machine learning methods within BEPF can improve the efficiency of mapping and classifying building energy use, requiring less detailed thermal-physical characteristics compared to typical physics-based forward models (Fathi et al., 2020a).

The key steps for implementing machine learning within BEPF are shown in Figure 35.

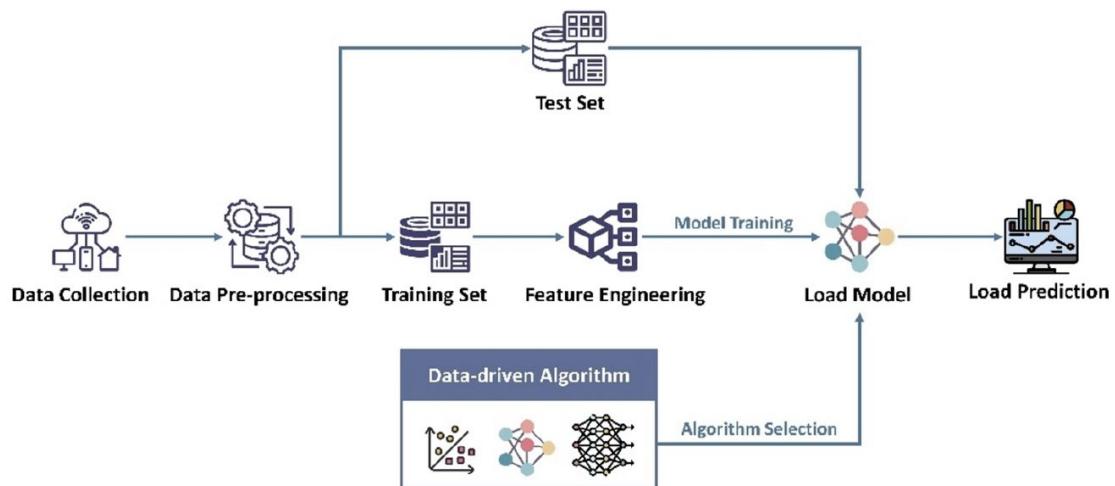


Figure 35: Data-driven framework for predicting building energy demands (Zhang et al., 2024).

Typical machine learning methods within BEPF are shown in Figure 36.

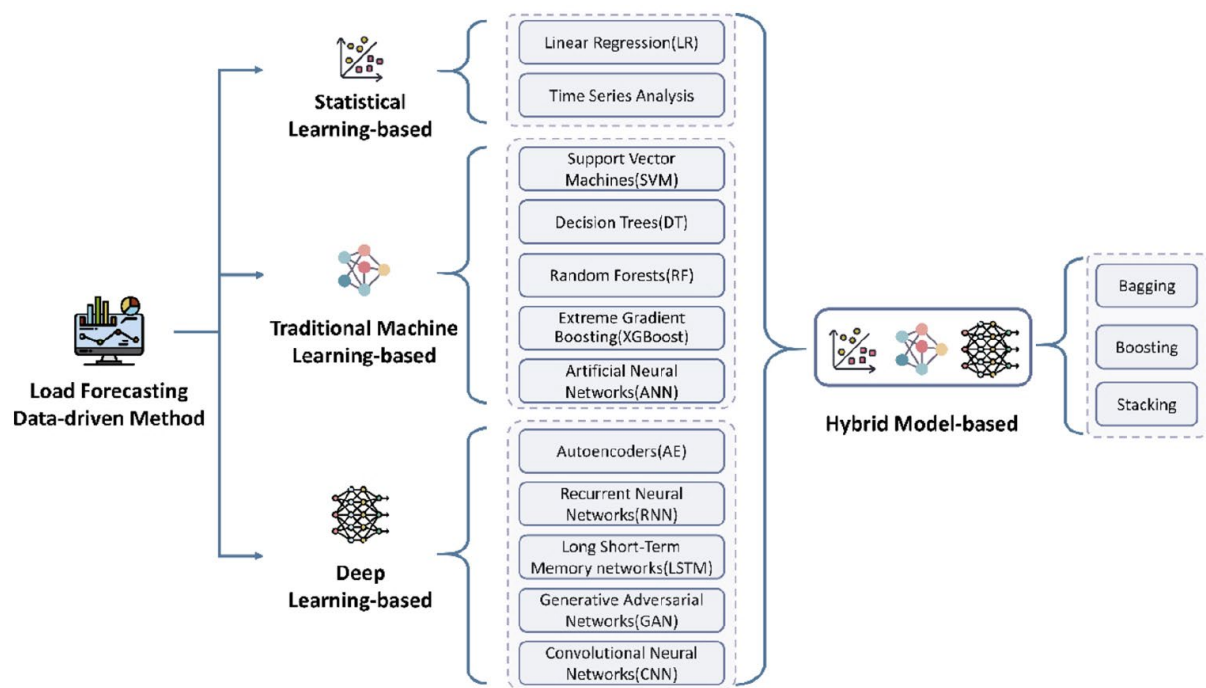


Figure 36: Overview of data-driven load prediction models (Zhang et al., 2024).

Fathi et al. (2020a) reviewed existing BEPF studies at individual and urban scales (including neighbourhoods, districts and cities). The share of BEPF studies were 61% for individual building level and 39% for urban level. Where, a lack of data is the main reason for the lower number of urban scale studies.

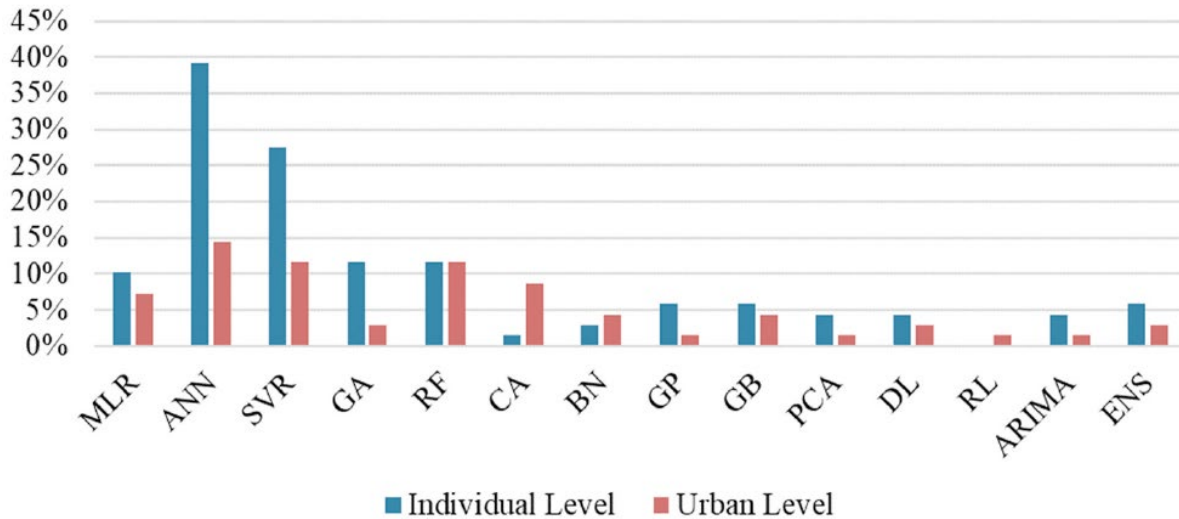


Figure 37: Machine learning methods in BEPF at individual and urban levels (Fathi et al., 2020a).

The following machine learning methods, shown in Table 5 were found throughout BEM and UBEM studies.

Artificial neural network (ANN), support vector regression (SVR) and random forest (RF) are used more frequently than reinforcement learning (RL) or autoregressive integrated moving average (ARIMA), mainly, due to their ability to capture more useful information in time series data (Fathi et al., 2020a).

From the studies reviewed, there was only one urban scale study that used RL, and no studies at the individual building level. This is likely due to the complexity of RL and the requirement of extensive building energy input data (Fathi et al., 2020a).

Table 5: Machine learning methods common in BEM and UBEM studies (Fathi et al., 2020a).

ML methods
Artificial Neural Networks (ANN) *
Support Vector Regression (SVR) *
Multiple Linear Regression (MLR)
Genetic Algorithms (GA)
Random Forests (RF)
Cluster Analysis (CA) **
Bayesian Networks (BN) **
Gaussian Processes (GP)
Gradient Boosting (GB)
Principal Component Analysis (PCA)
Deep Learning (DL)
Reinforcement Learning (RL)
Auto-Regressive Integrated Moving Average (ARIMA)
Ensemble Prediction (ENS)

* ML methods used more frequently at individual building level.

** ML methods used more frequently at urban level.

Fathi et al. (2020a), explored the building types, energy types, input data, and time scales studied at urban and individual building levels.

Table 6: Number of studies using the various energy types (Fathi et al., 2020a).

Energy Type	All Study Levels		Individual Level		Urban Level	
	Count	Percentage	Count	Percentage	Count	Percentage
EL	31	45%	23	33%	8	12%
H&C	27	39%	18	26%	9	13%
NG	2	3%	0	0%	2	3%
TBE	20	29%	7	10%	13	19%

Majority of studies focus on predicting electricity (44%), next to heating and cooling demands (39%).

There is not a universally optimal combination of criteria for achieving the most accurate ML-based BEPF model. The accuracy of the ML model is highly dependent on the data characteristics and study objective (Fathi et al., 2020a).

Time scales studied are shown in Figure 40. Notably urban scale studies are typically performed at annual time scales, likely due to the challenges involved in simulating hourly data at urban scale.

There were no studies in the review that used future weather scenarios to investigate the effects of climate change. Also, none of the studies explored the impact of retrofit strategies on future building energy performance (Fathi et al., 2020a).

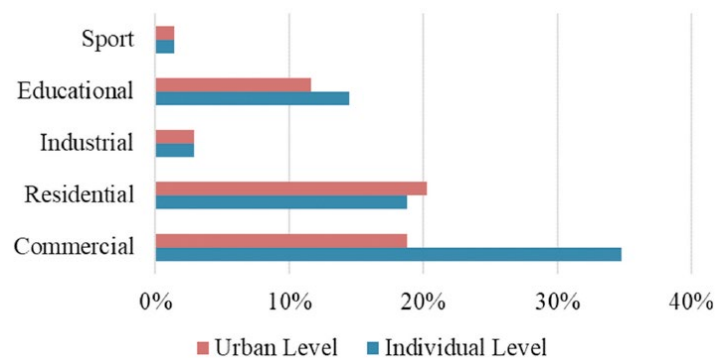


Figure 38: Building types studied at urban and individual levels (Fathi et al., 2020a).

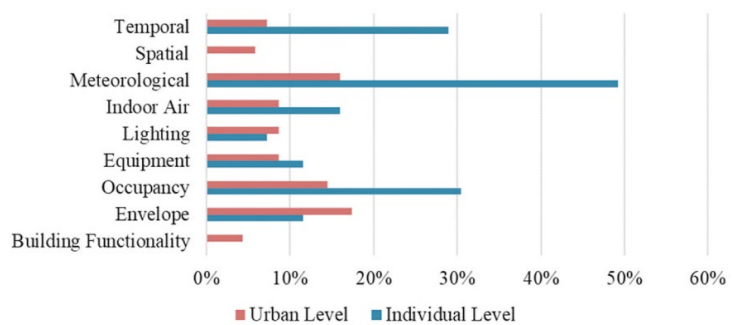


Figure 39: Input data used in building energy performance studies (Fathi et al., 2020a).

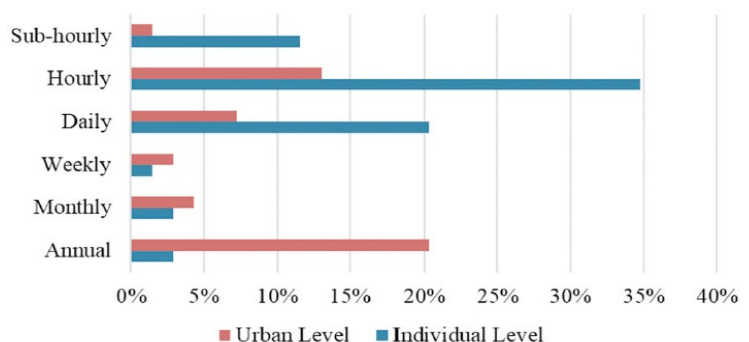


Figure 40: Time scales used in building energy performance studies (Fathi et al., 2020a).

DEEP LEARNING (DL)

Several limitations are present when developing a physics-based UDEM, mainly the time-consuming nature and inability to handle a massive, heterogeneous dataset representing the building and surrounding environment at urban scale. To address these limitations DL techniques have recently been employed (Li et al., 2023).

DL is a ML method based on artificial neural networks that simulate the connections and information processing used by neurons in the human brain to automatically learn, identify complex patterns, and detect features from large datasets. DL offers the ability to process unstructured heterogeneous data, for example extracting relevant urban features from satellite imagery (Li et al., 2023).

Li et al. (2023), provides a comprehensive review of bottom-up physics-based UDEM studies published between 2017-2022 and existing DL techniques used in UDEM workflows. From the reviewed literature the following DL approaches were most frequently used:

1. Autoencoder: extracts essential features from the input data and then reconstructs these features back into the input data.
2. Artificial neural network (ANN): multiple inter-connected basic units (neurons), that simulate interactions between neurons in human brain, creating information transmission.
3. Convolutional neural network (CNN): extracts distinctive features from input data and performs classification or regression, often used for processing image data.
4. Recurrent neural network (RNN): introduces a recurrent structure to the network, often used to process sequential data, such as time-series data. Ability to capture temporal dependencies in the input sequence and use previous data to predict the next outputs.
5. Graph neural network (GNN): most often used for processing graph structured data, ability to identify the relationships between nodes in a graph to complete classification and regressions tasks.

From the review, CNN was the most used algorithm. Almost all studies that used CNN were processing images, which is logical based on CNN's strong ability to extract important features from image data (Li et al., 2023).

A comparison between physical simulations and deep learning approaches is shown in Table 7.

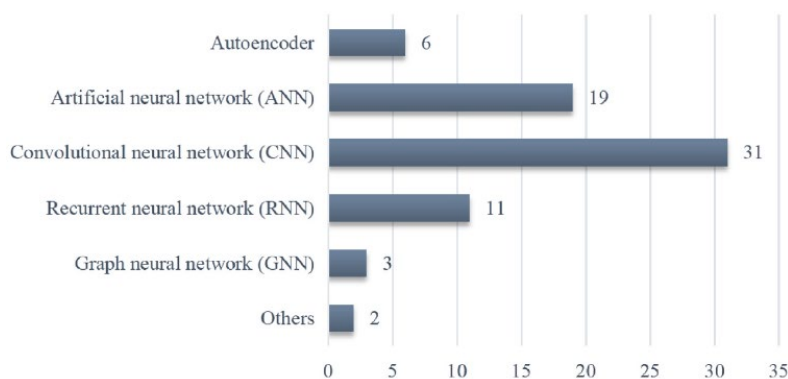


Figure 41: Deep learning algorithms used in the reviewed literature (Li et al., 2023).

Table 7: Comparison of physical simulations and deep learning approaches (Li et al., 2023).

Category	Representative methods	Advantages	Limitations
Physical simulation	EnergyPlus [80], TRNSYS [81], DOE-2 [82], CitySim [83].	The parameters inputs are relatively explainable. The parameters can be readily adjusted. There is no need for historical building energy data.	Inputting building details and parameters necessitates extensive work. The cost of computation is really high. It requires prior knowledge of software and thermal dynamics.
Deep learning approaches	ANN, CNN, RNN, GNN.	Strong nonlinear fitting capability for simulating real-world situations. Higher performance of energy estimation. Fast computation speed.	It is a black-box model and hard to explain. To train high-performance models, a large amount of data is required.

CASE STUDIES

COMPARATIVE ANALYSIS OF ML MODELS

Olu-Ajayi et al. (2021) explored building energy prediction using ML as well as DL approaches, with the aim of developing a model to enable designers to input key building features to predict the annual average energy consumption using a large residential building dataset. The study evaluates the performance of nine ML models to compare the computational efficiency in terms of training times as well as the algorithm’s predictive accuracy, using:

1. Artificial Neural Network (ANN)
2. Gradient Boosting (GB)
3. Deep Neural Network (DNN)
4. Random Forest (RF)
5. Stacking, K Nearest Neighbour (KNN)
6. Support Vector Machine (SVM)
7. Decision tree (DT)
8. Linear Regression (LR)

The study explores the impact of building archetypes (including detached houses and apartments) on feature selection and model performance. And the impact of dataset size on the model’s accuracy, across all nine models.

RF was used to rank the input features by importance. The most impactful variables included total floor area, roof characteristics, number of heated rooms, and weather conditions, shown in Figure 42.

The study found that the building archetype did not significantly affect feature selection or model performance. Algorithms were evaluated using coefficient of determination, R^2 , mean absolute error (MAE), mean squared error (MSE), and root mean squared error (RMSE) performance metrics. DNN achieved the highest accuracy, outperforming all other models. ANN and GB followed with slight reductions in accuracy compared to DNN. Notably, DT had the shortest training time but showed lower accuracy. Larger datasets significantly improved model accuracy for all algorithms, highlighting the importance of the dataset size in model predictions (Olu-Ajayi et al., 2021).

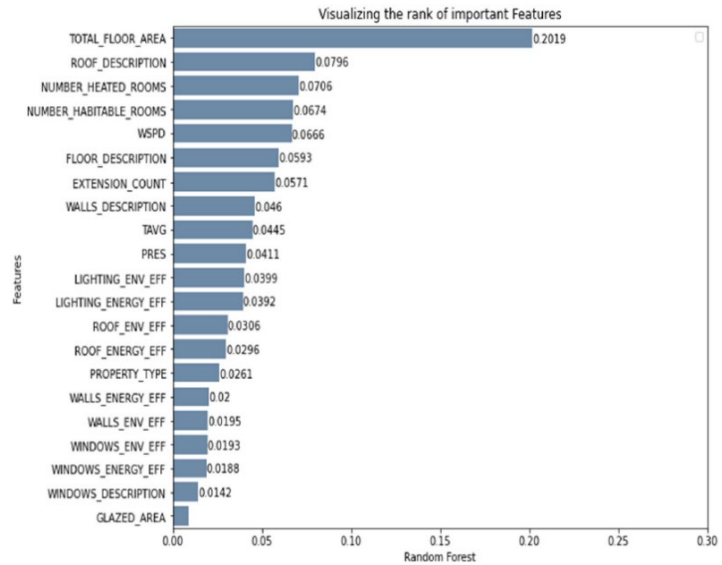


Figure 42: Feature selection using RF (Olu-Ajayi et al., 2021).

The study highlights the potential of machine learning, particularly deep learning, in energy prediction tasks, and the importance of algorithm selection, data quantity, and data quality.

EVALUATING PERFORMANCE

Geysen et al. (2017) explored the prediction of thermal load in district heating by combining multiple ML approaches into an expert advice system that identifies the best performing model. The model was trained with 20 months of hourly thermal load data, outdoor temperatures, and control signals from a district heating system in Sweden. The following models were used:

- Linear regression
- Artificial neural network
- Support vector machine
- Extremely randomized (extra) tree regressors

The methodology works with a predictor, and forecaster. The predictor refers to the individual models and the forecaster aggregates the predictions by adjusting the weights to determine the most accurate predictor at each stage.

Predictions from the individual models are combined by dynamically assigning weights to the best-performing models based on past performance. Methods used fixed share and polynomials weighted average in order to optimize the model weights. Model performance was evaluated using MAPE, showing that the ANN was the best-performing model, with the extremely randomized tree regressor and SVM next. The linear regression model performed the worst based on its limited ability to predict non-linear relationships (Geysen et al., 2017).

HYBRID STATISTICAL + ML APPROACH

Fathi et al. (2020b) explored the use of statistical and machine learning approaches to predict campus energy use, considering effects of climate change. Historical data was collected from 12 university buildings in Florida, including the following inputs:

- Electricity and natural gas use over a three-year period.
- Outdoor temperature, relative humidity, and solar radiation for both historical and future climate scenarios (2041, 2057, 2063) using North American Regional Climate Change Assessment Program (NARCCAP) weather files.
- Wall and window thermal transmittance (U-values), solar heat gain coefficient, and lighting and equipment loads.
- Building space functionalities, grouped by gross square footage percentages.

The study utilized the following models:

- Clustering: K-means was used to create building archetypes based on thermophysical and space functionality characteristics, reducing model complexity.
- Feature Selection: Principal component analysis (PCA) was used to identify the most influential variables for prediction.
- Prediction: ARIMA and long short-term memory models (LSTM) were used to predict monthly and hourly energy use.

The model results were compared to the building’s actual energy use and RMSE was used to evaluate the performance. The model showed +/- 15% error, considered acceptable within the ASHRAE-14 guidelines (Fathi et al., 2020b).

LSTM used the average outdoor temperature, relative humidity, solar radiation, and the hour of the day as the predictor variables to forecast the energy use for three future climate scenarios in years 2041, 2057, and 2063, where energy was projected to be up to 20% higher (Fathi et al., 2020b).

The model then forecasted the energy use for these future climate scenarios, considering the implementation of different building envelope variations, as shown in Table 8.

Table 8: Envelope properties for different retrofit interventions (Fathi et al., 2020b).

Envelope Scenario	Envelope Properties	Future Climate Scenario		
		2041	2063	2057
		Coldest	Median	Hottest
1	Wall U-Value (W/m ² °C)	0.24	0.18	0.19
2	Roof U-Value (W/m ² °C)	1.99	1.99	1.99
3	Windows U-Value (W/m ² °C)	4.26	4.26	4.26
4	Windows SHGC	0.2	0.2	0.2
5	1 to 4 Combined	All Above	All Above	All Above

The model showed that Envelope Scenario 5, considering implementing all retrofit interventions, had the greatest impact on reducing energy consumption under the future weather scenarios, shown in Table 9. It would be valuable to understand the cost implications of

implementing scenarios 1 versus 5, considering the scale of intervention and minimal difference in energy savings from the baseline.

Table 9: Energy use forecasted with different retrofit interventions for future weather scenarios (Fathi et al., 2020b).

Envelope Scenario	CEUP for Future Climate Scenario (MWh)					
	2041	Difference with 2018 Baseline (%)	2063	Difference with 2018 Baseline (%)	2057	Difference with 2018 Baseline (%)
	Coldest		Median		Hottest	
1	775.36	3.64	833.19	11.37	896.33	19.81
2	770.42	2.98	830.57	11.02	887.87	18.68
3	768.85	2.77	829.74	10.91	884.51	18.23
4	775.36	3.64	833.19	11.37	896.33	19.81
5	758.52	1.39	821.14	9.76	871.19	16.45

This study shows the importance of considering future climate scenarios for energy prediction. However, is limited by the number of buildings considered in the study, and the limited number of retrofit interventions applied.

AUTOMATING ENERGYPLUS INPUT DATA

Zhang et al. (2024) aimed to overcome challenges of data scarcity, feature extraction, and poor model generalization often faced in data-driven building energy prediction models. And suggested a novel framework for generating the input data files (IDF) needed for EnergyPlus models using retrieval augmented generation (RAG) and spatiotemporal graph neural networks (STGNN) to increase the correlation between the generated EnergyPlus model and real model.

The IDF files were generated based on HVAC design standards and the EnergyPlus model library. The process includes:

- Input building design specifications including energy efficiency standards, building type and location, and features such as WWR.
- Use natural language processing (NLP) methods to analyze the language input and extract key parameters.
- Implement text mining methods to extract HVAC parameters from design standards, such as minimum energy efficiency standards and maximum allowable WWRs.
- Search the existing EnergyPlus model library for IDF files that are similar to the target building, such as buildings with the same location or similar use patterns and extract relevant parameters.
- Generate the IDF file, designing a template for a LLM prompt that combines the parameters obtained from the design standards and EnergyPlus model library.

The model's accuracy, in terms of predicting annual heating, cooling and total energy consumption was validated with reference EnergyPlus files generated from the same building specifications or with actual measured data, depending on the building case. Validation used RMSE and MAPE. The model showed alignment to the reference EnergyPlus model with a <5% MAPE (Zhang et al., 2024).

BUILDING RETROFIT DECISION MAKING

Carpino et al. (2022) introduces a methodology to reduce possible risks and improve the decision-making process associated with implementing energy-saving retrofits. The study uses Uncertainty Analysis and Sensitivity Analysis (UA/SA) to verify the probability of meeting the performance target after implementing some retrofit strategy.

- **Uncertainty analysis:** determines the range of variability in model outputs due to the range of uncertainty in input variables.
- **Sensitivity analysis:** identifies significant parameters that affect the output variable.

Retrofitting measures include improving thermal insulation, replacing windows, improving HVAC systems, and installing renewable energy systems. Input data for key variables identified from the SA were then refined to increase the chance of meeting the performance target.

The following uncertain parameters, particularly impacted the output energy performance:

1. Efficiency of cooling system
2. Cooling set-point temperature
3. Heating set-point temperature

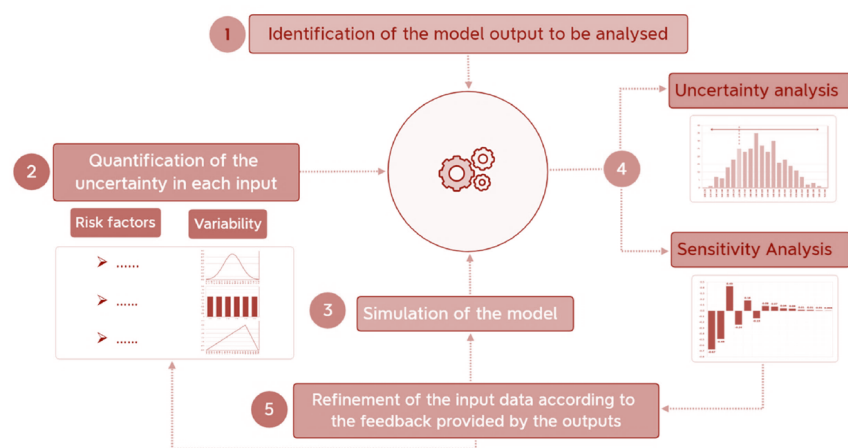


Figure 43: UA/SA workflow Carpino et al. (2022).

Through applying UA/SA methods, the probability of meeting the energy performance target after retrofit was increased to 82%, as well as achieving a significant reduction in the primary energy demand (Carpino et al., 2022).

Thrampoulidis et al. (2023) developed a building-level surrogate model using artificial neural networks (ANNs) to approximate optimal retrofit solutions. The model was applied to a municipality in Geneva with approximately 36,000 residential buildings and trained using building archetypes, representative of 92-99% of the residential building stock. Optimization models were used to find retrofit packages that minimized total cost and CO₂ emissions. The building level retrofit strategies include:

1. Adding insulation to the roof, façade or ground floor
2. Replacing windows with those of higher U-values
3. Energy system replacements including heating and cooling systems, and installing renewable technologies

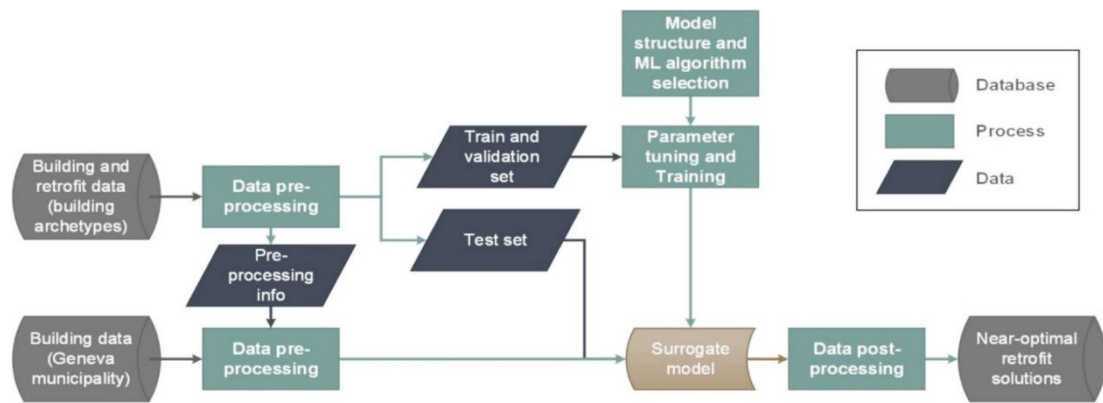


Figure 44: Methodology for training, testing and validating the surrogate retrofit model (Thrampoulidis et al., 2023).

For each building, a set of ten optimal building retrofit solutions were generated based on nine retrofit dimensions:

- A. Cost of retrofit intervention (regression)
- B. CO₂ emissions (regression)
- C. Selection of energy system (classification)
- D. Sizing / capacity of energy system (regression)
- E. Selection of renewables (classification)
- F. Sizing of renewables (regression)
- G. Selection of storage system (classification)
- H. Sizing of storage system (regression)
- I. Selection of building envelope intervention (classification)

The surrogate model performed well for predicting the cost and emissions but poorly for predicting the size of renewables (PV capacity). The model showed significant advantages to traditional energy optimization models, generating predictions for over 36,000 buildings within 9 minutes compared to what would be 90 days for traditional models (Thrampoulidis et al., 2023).

The study highlights that building retrofits, especially large-scale retrofits, are considered of highest importance to reduce the overall share of energy consumption and GHG emissions of the building sector. And that surrogate models are an effective method for reducing the time intensity of energy modelling at large-scale.

PERFORMANCE METRICS

Several performance metrics can be used to assess the prediction ability of an ML model. BEM studies typically include:

MEAN SQUARED ERROR (MSE)

The MSE measures the squared difference between the predicted values and the true values. An error value closer to zero is an indication of a good prediction model. The MSE is shown in Equation 9.

Equation 9: MSE

$$MSE = \frac{1}{n} \sum_{i=1}^n (\hat{y}_i - y_i)^2$$

ROOT MEAN SQUARED ERROR (RMSE)

The RMSE also measures the difference between the predicted values and the true values and is calculated from the square root of the MSE, shown in Equation 10.

Equation 10: RMSE

$$RMSE = \sqrt{\sum_{i=1}^n \frac{(\hat{y}_i - y_i)^2}{n}}$$

For reporting test set performance, RMSE can be applied because it penalizes larger errors more significantly, offering an interpretable metric in the original units of heating and cooling demand. However, RMSE is sensitive to outliers, and a poor prediction can disproportionately influence the result (Olu-Ajayi et al., 2021).

MEAN ABSOLUTE ERROR (MAE) / MEAN ABSOLUTE PERCENTAGE ERROR (MAPE)

The MAE measures the average absolute difference between the predicted values and the true values, shown in Equation 11. Unlike with the MSE and RMSE metrics, the errors are not squared when using MAE, so an equal weighting is given to all errors. Meaning also that it is less sensitive to extreme values in the dataset (Olu-Ajayi et al., 2021).

Equation 11: MAE

$$MAE = \frac{1}{n} \sum_{i=1}^n |\hat{y}_i - y_i|$$

The MAE provides an interpretable indication of errors, since the units of the error are the same as for the prediction values. MAE is also typically used to calculate the mean absolute percentage error (MAPE), from Equation 12.

Equation 12: MAPE.

$$MAPE = MAE * 100\%$$

The MAPE provides a clear indication of the magnitude of error between the predicted and true values.

R-SQUARED / COEFFICIENT OF DETERMINATION (R²)

The R² is a measure of how well the prediction model fits the data, assessing the proportion of variance in the dependent variable that can be explained by the independent variable, or how predictable the dependent variable is from the set of independent variables (Olu-Ajayi et al., 2021). An R² closer to one means the model better fits the dataset, with a value of one indicating a perfect fit. The R² is calculated from Equation 13.

Equation 13: R²

$$R^2 = 1 - \frac{\sum_{i=1}^n (\hat{y}_i - \bar{y})^2}{\sum_{i=1}^n (y_i - \bar{y})^2}$$

Although a high R² indicates a strong model fit to the dataset, it is not necessarily an indication of the model's ability to accurately predict new, unseen targets. Thus, the R² is typically used in combination with the other performance metrics to assess both prediction ability and model fit (Olu-Ajayi et al., 2021).

3

METHODOLOGY

DESIGN ASSIGNMENT

METHODS

3. METHODOLOGY

DESIGN ASSIGNMENT

Through large-scale energy simulations and machine learning techniques, this study investigates the influence of climate and building characteristics on heating and cooling demands across multiple building typologies. The areas of focus within the building energy chain are highlighted in Figure 45.

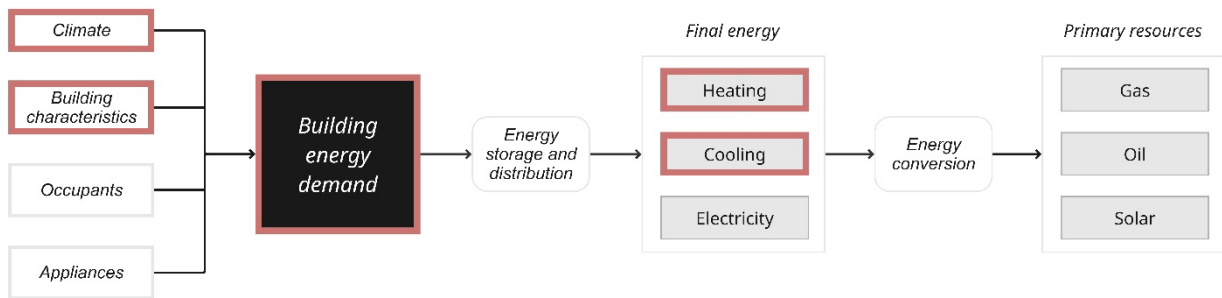


Figure 45: Focus areas within the building energy chain (Adapted from Van Bueren et al., n.d.).

And line with the hierarchy of strategies for reducing energy consumption, this study explores retrofit strategies that reduce energy demand, via improved building envelope performance, highlighted in Figure 46.

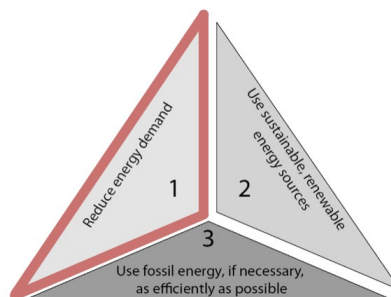


Figure 46: Focus area within the hierarchy of strategies for reducing energy consumption (Konstantinou, 2014).

The key project deliverables are shown in Table 10.

Table 10: Design assignment, deliverables, and tools.

Deliverables	Tools
COMPUTATIONAL WORKFLOW	
Automated workflow for data collection, processing, simulation, and ML training and evaluation, adaptable to various datasets.	<ul style="list-style-type: none"> ▪ Scripting using Visual Studio, Python ▪ Data handling using Excel, JSON

ENERGY DEMAND DATASET

Dataset of simulated heating and cooling demands for thousands of residential buildings in Rotterdam, reflecting a range of typologies, geometries, and retrofit interventions.

- Energy simulation using EnergyPlus
- Automated data generation using Python

ENERGY ANALYSIS

Analysis of building energy demands under current and future climate conditions and assessment of retrofit impacts across different building typologies.

- Analysis and data visualization using Excel, Python, Matplotlib

MACHINE LEARNING MODEL

ML predictive model for building energy demand and evaluation of prediction accuracy from the generated dataset.

- Model development and evaluation within Visual Studio, using Python, PyTorch, Scikit-learn

METHODS

A two-part methodology was adopted, focused on modelling the heating and cooling demands for residential buildings in the Netherlands, involving: (i) large-scale building energy simulations and (ii) ML development. The methodology is structured in the following stages:

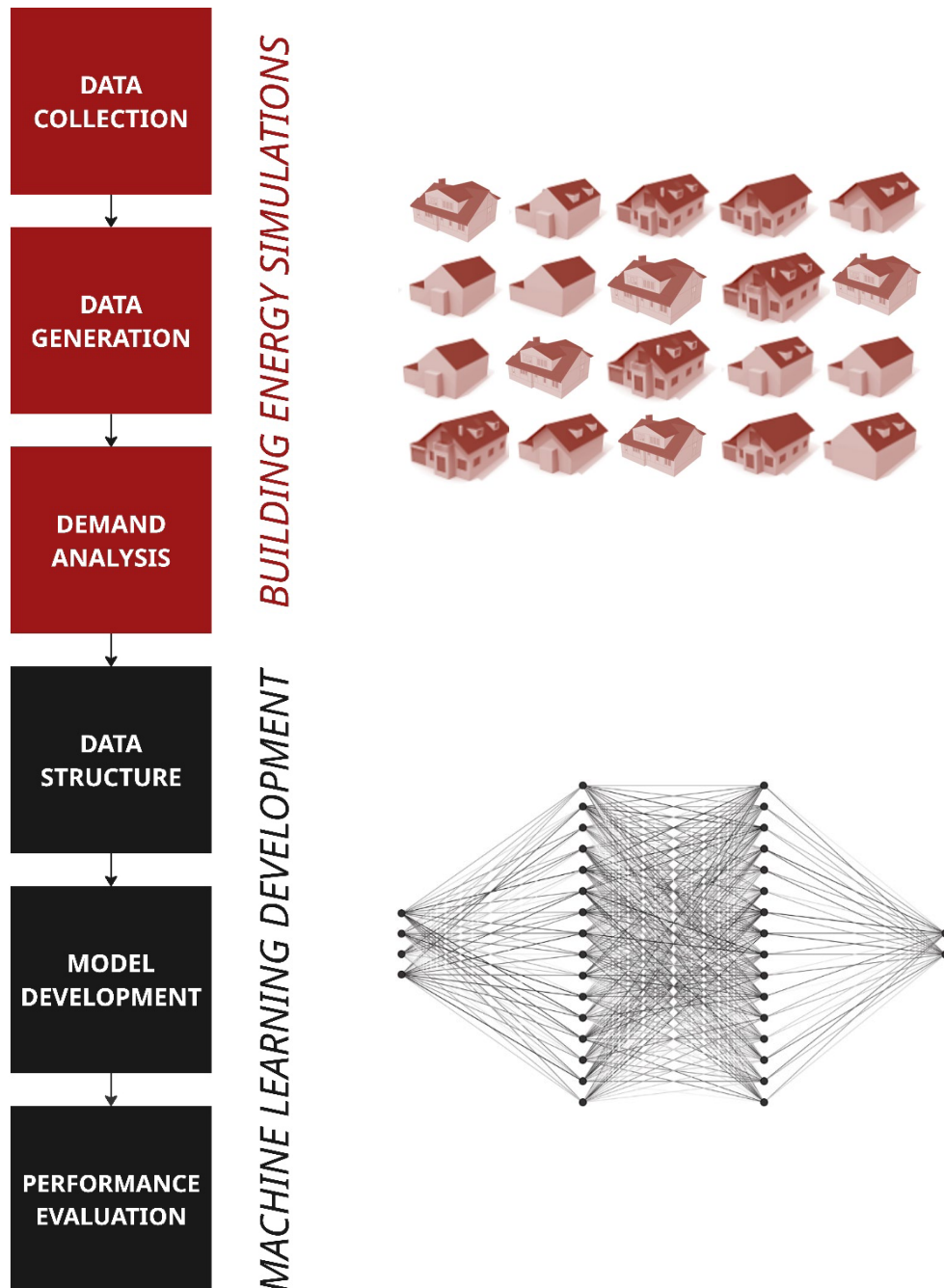


Figure 47: Project methodology.

Each stage of the methodology is summarized below. For further detail, see the corresponding chapters.

- **LITERATURE STUDY** [chapter 2]
- **DATA COLLECTION** [chapter 4]
- **DATA GENERATION** [chapter 5]
- **DEMAND ANALYSIS** [chapter 6]
- **DATA STRUCTURE** [chapter 7]
- **ML DEVELOPMENT** [chapter 8]
- **PERFORMANCE** [chapter 9]

DATA COLLECTION

The data collection phase involves collection of geometric, weather, and thermal parameters pertaining to the building construction. The objective was to connect the building geometries to their respective archetypes and associated thermal properties. These parameters were used to run energy simulations for the current, and future weather conditions in 2050 and 2080. The data collections are shown in Figure 48.

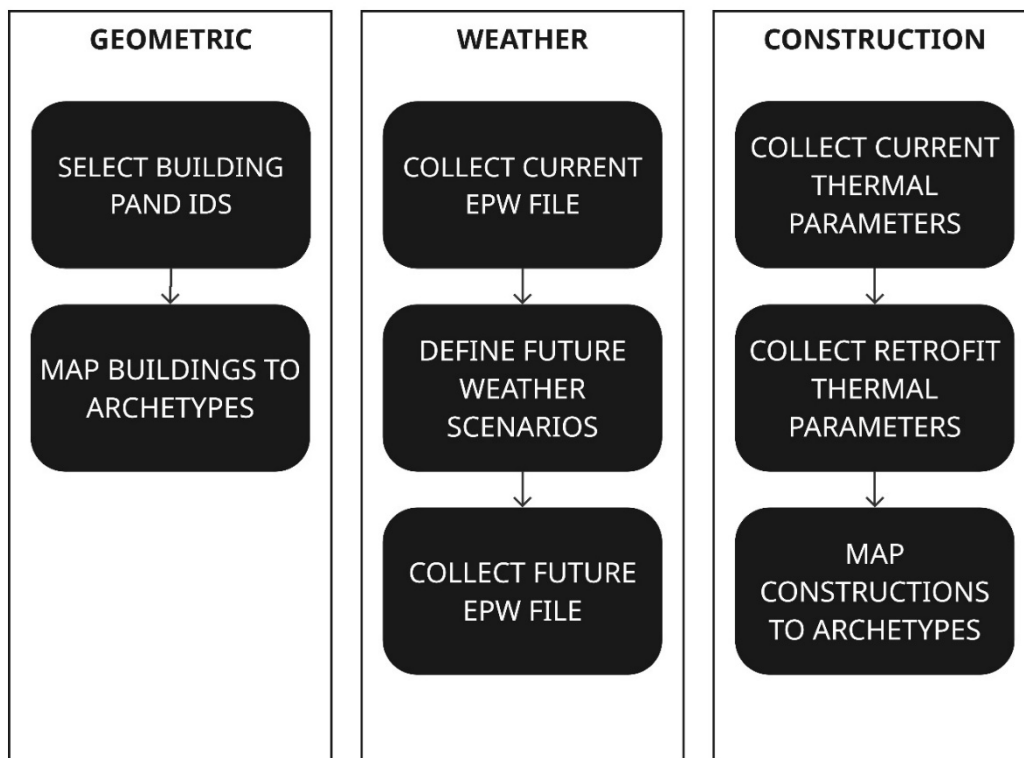


Figure 48: Data collection steps.

DATA GENERATION

Data generation involved producing the dataset of 3DBAG building data, as well as the EnergyPlus simulations for each building. The methodology for generating building data and EnergyPlus simulations are shown in Figure 49.

EnergyPlus simulations (one of the most prominent energy simulation tools) were generated to understand the heating and cooling demand for each individual building within the study.

The thermal properties of the construction elements, including floors, windows, walls, and roofs were derived from the archetypes. The two simulation scenarios are:

- **Current archetype (A):** with thermal parameters in accordance with the building construction and installations of its current construction year.
- **Retrofit archetype (B):** with thermal parameters corresponding to a retrofit intervention package, i.e. improved insulation, and reduced infiltration.

In both scenarios, the heating and cooling demands are evaluated at the current weather state, **2020**, and with projections for future weather scenarios, **2050**, and **2080**, producing the simulation matrix in Figure 50.

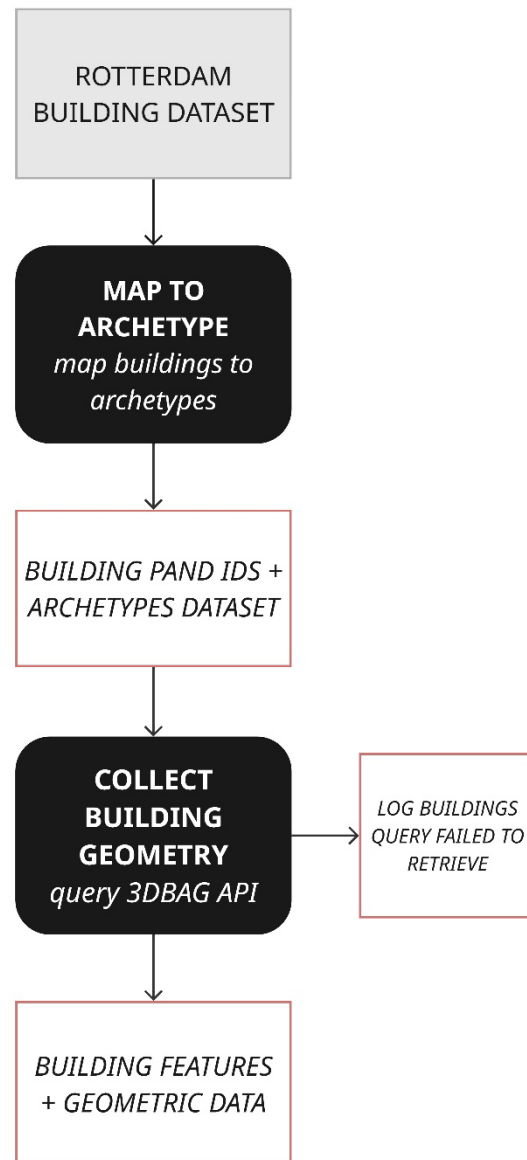


Figure 49: Data generation workflow for building geometry.

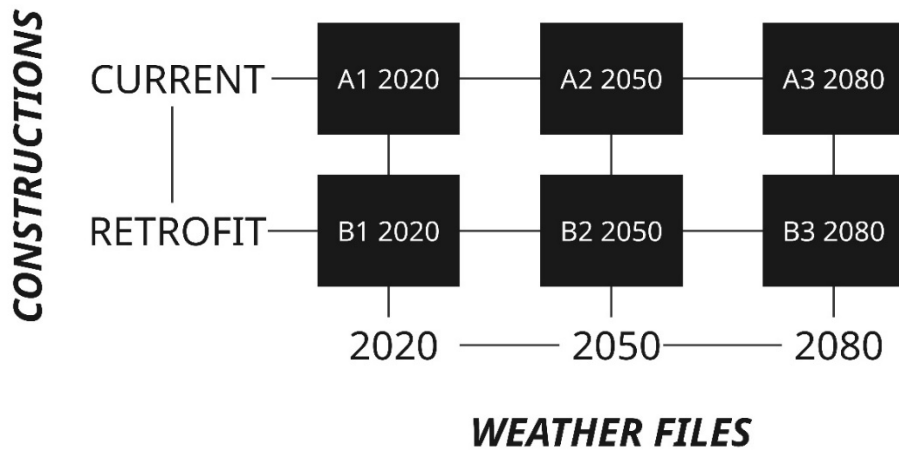


Figure 50: Matrix of EnergyPlus simulations for the study.

Considering the matrix of simulation options, and working with a large-scale database, it was necessary to automate the EnergyPlus simulation process. Using a Python script to:

- Format data: for each individual building, format building geometry for simulation.
- Map inputs: map inputs to each archetype in a structured format.
- Create IDF: generate the input data file per building for EnergyPlus simulations.
- Run: execute simulations.
- Collect data: collect simulation results for heating and cooling demands for later processing.

The data generation workflow is shown below in Figure 51.

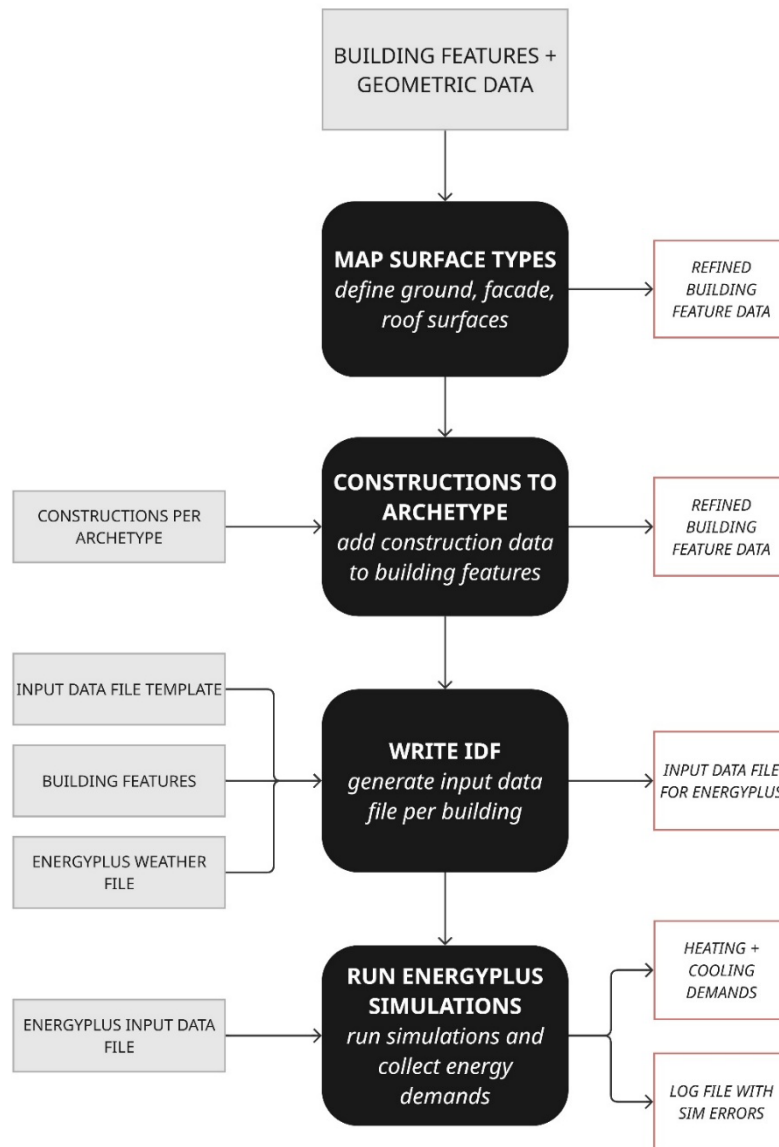


Figure 51: Data generation workflow for producing EnergyPlus simulations.

DEMAND ANALYSIS

After collecting the simulation results from EnergyPlus, the demand analysis involves analyzing the heating and cooling energy demands per archetype, assessing the differences between housing type, and construction period. As well as investigating how the demands change across archetypes under future weather scenarios.

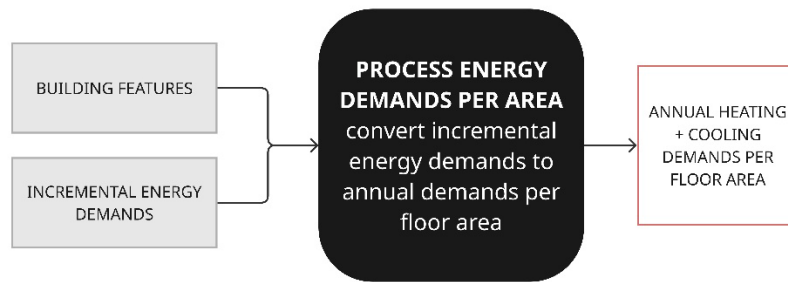


Figure 52: Demand analysis workflow.

To achieve this, the EnergyPlus simulation files are merged with the building features to determine the energy demands per floor area, that could be used for further analysis. Demands are analyzed for the full simulation matrix, considering current and retrofit demands for current and future weather scenarios.

DATA STRUCTURE

Data structuring is required to prepare the input features and energy simulation results for ML. This involves flattening the inputs and outputs to a tabular format and merging geometric, weather, and thermal construction features to a single dataset. This stage also involves addressing missing values, checking for outliers, and eliminating extremes where required. The structured feature set can then be implemented to the ML model. The methodology was conducted using energy simulations for the current weather, A1, and B1, shown below in Figure 53.

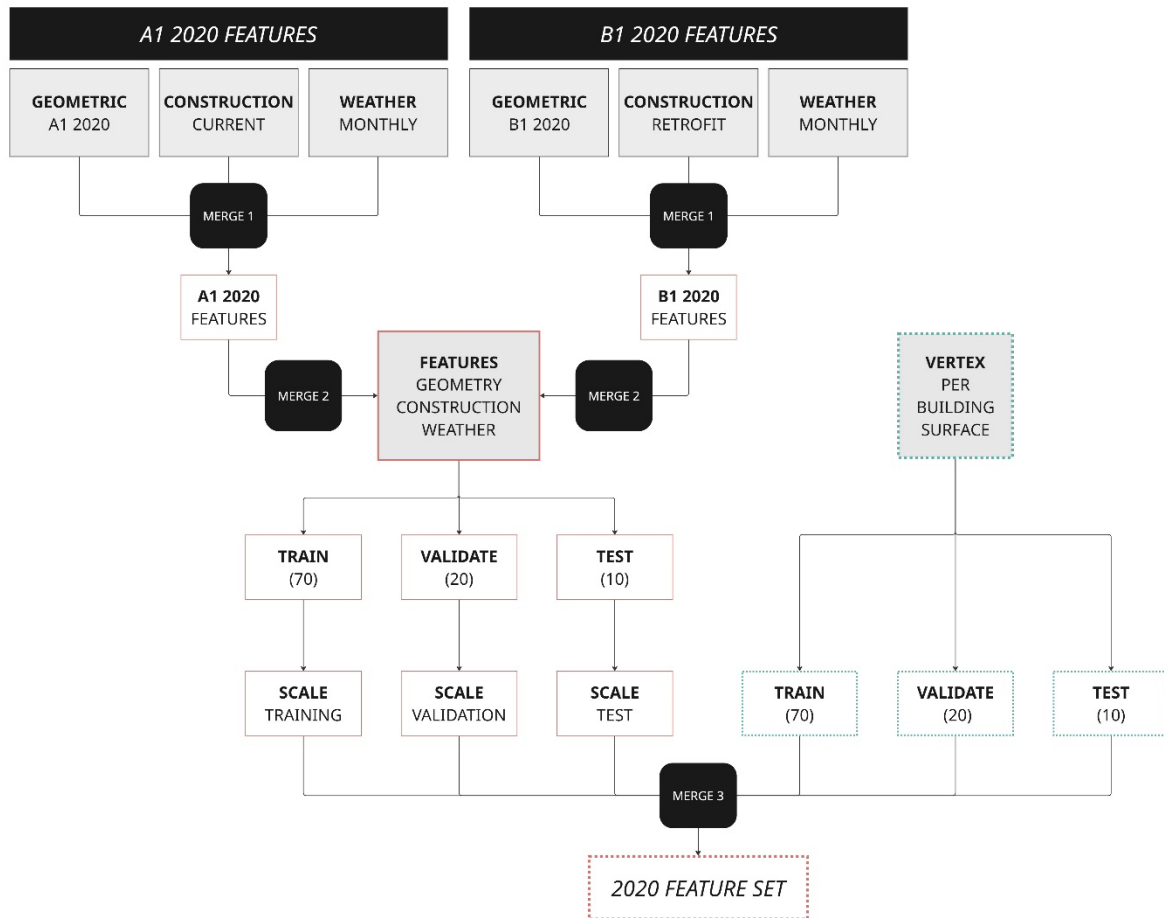


Figure 53: Data structuring workflow.

The same data structuring would be required for energy simulations for using future weather, at years 2050, (simulations A2, B2) and 2080 (simulations A3, B3) although this stage was not integrated within the study.

ML DEVELOPMENT

Model development involves creating a ML model to predict the energy demands for current and retrofit building constructions. The objective was for the ML model to serve as an efficient alternative to EnergyPlus, enabling rapid and accurate prediction of heating and cooling demands across large building inventories. The development stage involves several iterations of training and testing to understand the model’s prediction abilities when using different feature sets, and hyper-parameters.

The model was developed using the energy simulations at the current weather state. Future weather files were used for the demand analysis but were not integrated within the ML stage of the project.

PERFORMANCE EVALUATION

Performance evaluation involves a comparative analysis between the predicted heating and cooling demands, and the simulated energy demands from EnergyPlus.

The standard performance metrics found from the literature were used to assess the prediction ability of the ML model; MSE, RMSE, MAE, MAPE and the R^2 .



4

DATA COLLECTION

GEOMETRIC

WEATHER

CONSTRUCTION

4. DATA COLLECTION

Data was collected within the context of Rotterdam, Netherlands. The datasets used throughout the project are summarized in Table 11.

Table 11: Datasets used throughout the project.

DATASETS	
NIEMAN BUILDING TYPOLOGIES	Dataset of approximately 405,000 buildings in the Netherlands with location IDs that can be used to download the corresponding building geometry from 3DBAG.
BUILDING GEOMETRIES	3DBAG open data set of current 3D building models in the Netherlands, at multiple levels of architectural detail.
CONSTRUCTION CHARACTERISTICS	Example Homes Guide 2022 of building archetypes, (based on construction year and building type) with associated thermal transmittance values for construction (floors, walls, windows, roof).
CURRENT WEATHER FILES	EnergyPlus weather files for Rotterdam, based on current standard meteorological years.
FUTURE WEATHER FILES	EnergyPlus weather files for De Bilt, Netherlands, based on morphed meteorological data for 2050, 2080.

GEOMETRIC

BUILDING DATASET (Pand IDs)

The original Nieman Building Typologies database contained approximately 405,000 buildings, each associated to a Pand ID – a geometric identifier, for the geometry and attribute data of the building object, and Nieman Typology – the classification of a building based on the building type, and construction period. Based on Nieman’s classification there are 21 residential building typologies.

The “Example Homes Guide 2022”, of housing types representing the current housing stock in the Netherlands, was used in part to identify the typologies of interest for this study. From approximately 8 million existing houses, the distribution of each house type is shown in Figure 54 (Ministry of the Interior and Kingdom Relations, 2022).

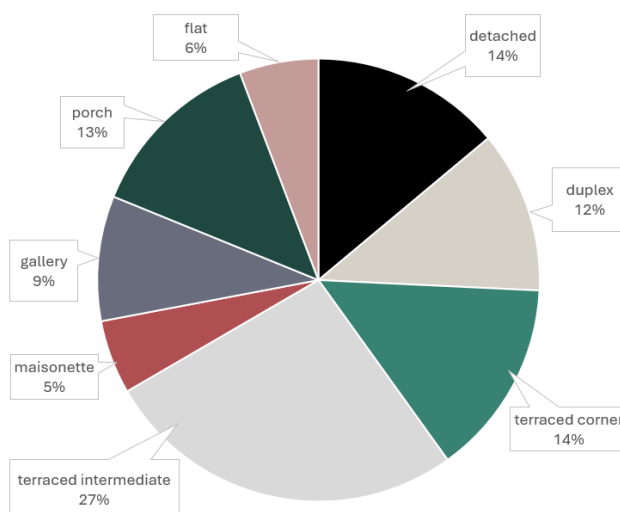


Figure 54: Distribution of housing types in Netherlands, over all construction periods.

Since dwellings constructed before 1975, prior to the adoption of the Bouwbesluit (Building Decree) thermal regulations, typically demonstrate poor energy performance (Wahi et al., 2024), the distribution of houses constructed before 1975 was also investigated, shown in Figure 55.

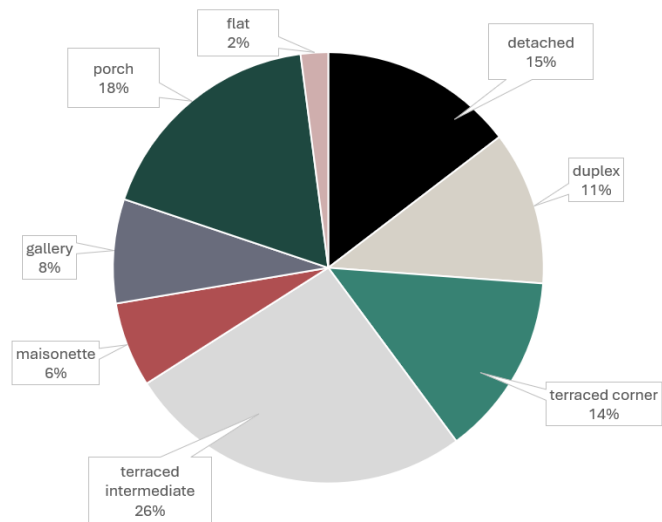


Figure 55: Distribution of housing types in Netherlands constructed prior to 1975.

The most prominent housing types from each distribution are shown in Table 12.

Table 12: Most common housing types in the Netherlands overall and constructed pre-1975.

	Overall distribution	Distribution pre-1975
1	Terraced Intermediate (27%)	Terraced Intermediate (13%)
2	Terraced Corner (14%)	Porch (9%)
3	Detached (14%)	Detached (7%)
4	Porch (13%)	Terraced Corner (7%)

Based on the distributions, the terraced intermediate, terraced corner, and detached housing types were selected for the study. And the corresponding Nieman typologies are shown in Table 13.



Figure 56: Typologies for study, Terraced Intermediate (Hulsman, 2024), Terraced Corner (Ministry of the Interior and Kingdom Relations, 2022) Detached (Street View of Ring 613 · Google Maps, n.d.).

Table 13: Selected Nieman typologies for study.

Nieman Typology	Housing type	Building period
6	Terraced Intermediate	pre-1946
7	Terraced Intermediate	1946 – 2018
8	Terraced Corner	1946 – 2018
21	Detached	1965 – 2018

PRE-PROCESS SELECT BUILDINGS

The Nieman Building Typologies database, shown in Figure 57 includes the following features:

- Building use (Gebruiksdoel): intended building function, i.e. residential or commercial.
- Surface area (Oppervlakte)
- Number of floors (Aantal Bouwlagen)
- Construction period (Bouwperiode)
- Original year of construction (Oorspronkelijk Bouwjaar)
- Type of object (Soort Object)

BAG Pand ID	Gebruiksdoel	Oppervlakte	Aantal Bouwlagen	Bouwperiode	Oorspronkelijk Bouwjaar	Soort Object	Voorbeeldwoning	Subtype	Nieman Typologie
["0599100000640838"]	["bijeekomstfunctie"]	810		< 1965	1448		overig	gemiddeld	
["0599100000641495"]	["bijeekomstfunctie"]	611		< 1965	1470		overig	gemiddeld	
["0599100000658109"]	["bijeekomstfunctie"]	81		< 1965	1609		overig	gemiddeld	
["0599100000690520"]	["kantoorfunctie"]	515		< 1965	1609		overig	gemiddeld	
["0599100000755952"]	["kantoorfunctie"]	553		< 1965	1616		overig	gemiddeld	
["0599100000658105", "0599100000755950"]	["bijeekomstfunctie"]	1077		< 1965	1616		overig	gemiddeld	
["0599100000755951"]	["bijeekomstfunctie"]	90		< 1965	1616		overig	gemiddeld	
["0599100000755950"]	["kantoorfunctie"]	927		< 1965	1616		overig	gemiddeld	
["0599100000658105", "0599100000690517"]	["bijeekomstfunctie"]	343		< 1965	1616		overig	gemiddeld	
["0599100000658105", "0599100000755950"]	["bijeekomstfunctie"]	144		< 1965	1616		overig	gemiddeld	
["0599100000702379", "0599100100015073"]	["bijeekomstfunctie"]	4036		< 1965	1640		overig	gemiddeld	
["0599100000702379", "0599100100015073"]	["kantoorfunctie"]	253		< 1965	1640		overig	gemiddeld	
["0599100000702379"]	["bijeekomstfunctie"]	3783		< 1965	1640		overig	gemiddeld	
["0599100000759798"]	["bijeekomstfunctie"]	309	5	< 1946	1870	Onzelfstandige woning	rijwoning tussen	rijwoning tussen	6
["0599100000269304"]	["industrie functie"]	480		< 1965	1678		overig	gemiddeld	
["0599100000757230", "0599100000757231"]	["logiesfunctie"]	673	4	< 1946	1871	Tussenwoning	rijwoning tussen	rijwoning tussen	6
["0599100000690517"]	["kantoorfunctie"]	460		< 1965	1707		overig	gemiddeld	
["0599100000691902"]	["logiesfunctie"]	220	3	< 1946	1872	Onzelfstandige woning	rijwoning tussen	rijwoning tussen	6
["0599100000620292"]	["industrie functie"]	41		< 1965	1712		overig	gemiddeld	
["0599100100007490"]	["industrie functie"]	883		< 1965	1712		overig	gemiddeld	
["0599100000660350"]	["industrie functie"]	91		< 1965	1712		overig	gemiddeld	
["0599100000702318"]	["kantoorfunctie"]	1117		< 1965	1723		overig	gemiddeld	
["0599100000618558"]	["kantoorfunctie"]	389	4	< 1946	1873	Onzelfstandige woning	rijwoning tussen	rijwoning tussen	6
["0599100000312693"]	["woonfunctie", "industrie functie"]	114	3		1873	Bedrijfs-/Dienstwoning			6
["0599100000702318"]	["kantoorfunctie"]	53		< 1965	1723		overig	gemiddeld	
["0599100010033222"]	["gezondheidszorgfunctie"]	640		< 1965	1723		overig	gemiddeld	

Figure 57: Nieman building dataset for processing.

The database was processed to select the typologies of interest and handle missing values. From the dataset, the steps include:

1. Filter for Nieman typology of interest (*Nieman typologie*)
2. Filter for residential building function (*Woonfunctie*).
3. Remove entries with multiple Pand IDs.
4. Remove buildings with blank entries for building period (*Bouwperiode*).
5. Filter for terraced and detached housing type (*Soort Object*, *Tussenwoning*, *Vrijstaand*).
6. Filter for intermediate and corner housing sub types (*Voorbeeldwoning*, *Tussenwoning*, *Hoekwoning*).

After filtering the dataset, the selected typologies represent approximately 75,000 houses. The ratio of each typology within the filtered dataset is shown in Figure 58.

The Nieman typologies provide a high-level grouping of building data, where a single typology combines multiple building periods. For example, looking at Table 13, Typology 7 includes all intermediate terraced houses from 1946-2018. To better represent the construction features associated with each building period, each Nieman typology was then categorized as a specific **Archetype**, based on the housing type and a more granular building period. The complete list of archetypes used for the study is shown in Table 14.

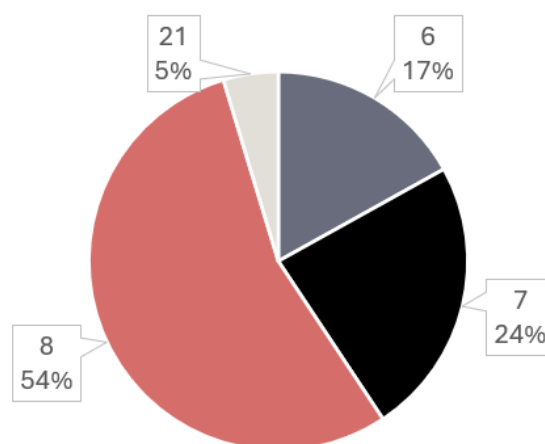


Figure 58: Distribution of selected Nieman typologies within the filtered dataset.

Table 14: Building archetypes used for study.

Nieman Typology	Archetype	Housing type	Building period
6	TI.1946	Terraced Intermediate	pre-1946
7	TI.1946-1964		1946 – 1964
	TI.1965-1974		1965 – 1974
	TI.1975-1991		1975 – 1991
	TI.1992-2005		1992 – 2005
	TI.2006-2014		2006 – 2014
	TI.2015-2018		2015 – 2018
8	TC.1946	Terraced Corner	pre-1946
	TC.1946-1964		1946 – 1964
	TC.1965-1974		1965 – 1974
	TC.1975-1991		1975 – 1991
	TC.1992-2005		1992 – 2005
	TC.2006-2014		2006 – 2014
	TC.2015-2018		2015 – 2018
21	D.1965	Detached	pre-1965
	D.1965-1974		1965 – 1974
	D.1975-1991		1975 – 1991
	D.1992-2005		1992 – 2005
	D.2006-2014		2006 – 2014
	D.2015-2018		2015 – 2018

WEATHER

CURRENT

Weather data used the EnergyPlus weather (EPW) file for Rotterdam/the Hague. The EPW file includes hourly measurements of parameters such as air temperature, relative humidity, wind speed and direction, solar radiation, atmospheric pressure, and precipitation. The EPW file used is made up of historical weather data from 2009 to 2023, based on the Typical Meteorological Year (TMYx) method, which uses representative months to create a statistically representative annual dataset (*Climate.onebuilding.org*, n.d.). The selected EPW file is thus representative of the most current climate conditions for Rotterdam and was used for the energy simulations at the current weather state.

FUTURE

Future weather scenarios for the years 2050 and 2080 were based on pre-generated EPW files for De Bilt, Netherlands. These files are part of a dataset developed by modifying observed historical weather data to represent expected climate conditions in 2050 and 2080 (Heiranipour et al., 2024).

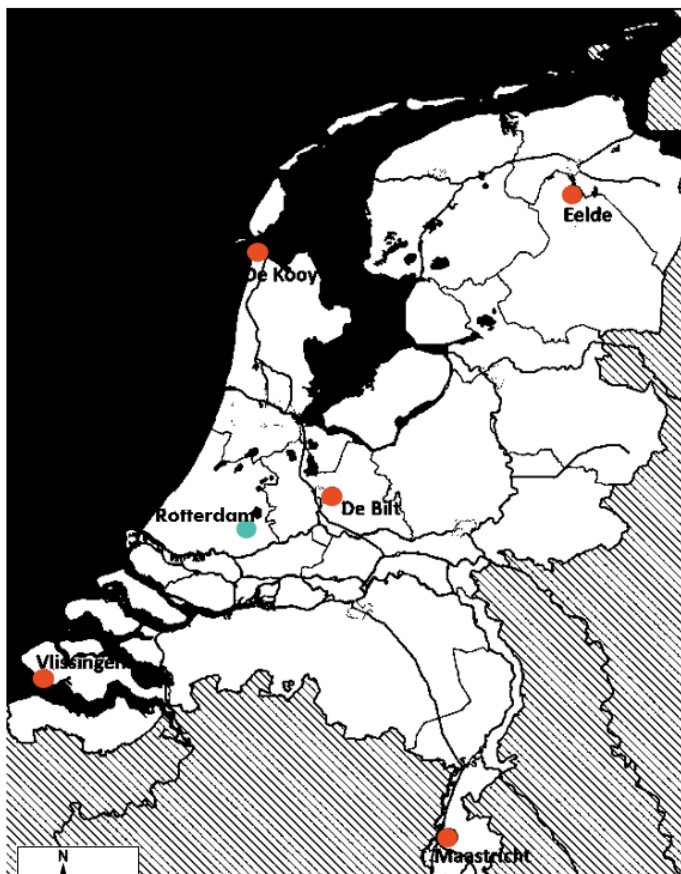


Figure 59: KNMI climate projections in the NL are based on 5 climate reference stations – De Bilt, Den Helder (De Kooy), Groningen (Eelde), Maastricht, Vlissingen, capturing distinct regional climate differences across NL. Adapted from (De Vos, 2024).

The EPW files are developed by:

- **Morphing**

This method uses historical weather data and then morphs or shifts the temperature, humidity, and other variables according to projected changes from global climate models (GCMs).

- **Dynamical Downscaling:**

Uses regional climate models (RCMs) to simulate future weather, at the Representative Concentration Pathway (RCP) 8.5 greenhouse gas emissions scenario, which is the highest-warming pathway from the IPCC.

Despite the current weather file being for Rotterdam, De Bilt was used for future weather energy simulations since De Bilt represents the nearest station with readily available, future weather data. Using the pre-generated

EPW files eliminated the need to produce a future weather file using computational tools such

as EPWshiftr (that apply the same morphing methodology but for any location), which under the time constraints of the project was advantageous.

CONSTRUCTION

Thermal parameters for building envelope components were obtained from the “Example Homes Guide 2022”, which provides construction parameters for each archetype within the Dutch residential building stock. The guide gives standardized thermal characteristics, including insulation values (R_c) for walls, roofs, and floors, and U-values for windows for both the current building state and a retrofit scenario. The R_c and U-values from the guide were obtained for each of the selected archetypes for both the current and retrofit building states. For example, for the Detached house constructed prior to 1965, the data obtained is shown in Figure 60.

Detached house pre-1965		
Architectural		
	Current	Retrofit 1
Ground floor	$R_c = 0.15$	$R_c = 3.50$
Façade	$R_c = 0.35$	$R_c = 1.70$
Sloped roof	$R_c = 2.50$	$R_c = 3.50$
Flat roof	$R_c = 0.85$	$R_c = 3.50$
Window	$U = 1.80$	$U = 1.40$
Door	$U = 3.40$	$U = 1.40$
Infiltration	Standard rate	$q_v = 0.7$

Figure 60: Example homes guide detached house < 1965 thermal properties (Ministry of the Interior and Kingdom Relations, 2022)


	<1945	1945-1975	1975-1995	>1995
Terraced houses 				
Corner houses / 2^1 semi-detached houses 				
Detached houses 				
Gallery/porch dwellings 				

Figure 61: Nieman broad archetype classification (Nieman et al., 2021).

The guide does not provide explicit infiltration rates, which are a critical feature to estimating thermal performance. From Figure 60, for the current conditions, the guide suggests a standard rate but does not provide what rate is used. Thus, infiltration parameters were taken from the Nieman report "Standard and Target Values for Existing Housing" (2021), which defines

standard energy demands for the Dutch housing stock for several retrofit scenarios. The Nieman report classifies houses according to broader typologies than used in this study, based on the construction period and housing type, shown in Figure 61.

Despite the broader typology classification, the reported infiltrations were mapped to the archetypes for this study and used for simulating current and retrofit states. The mapping of thermal parameters to each archetype for this study is further discussed in Chapter 5.

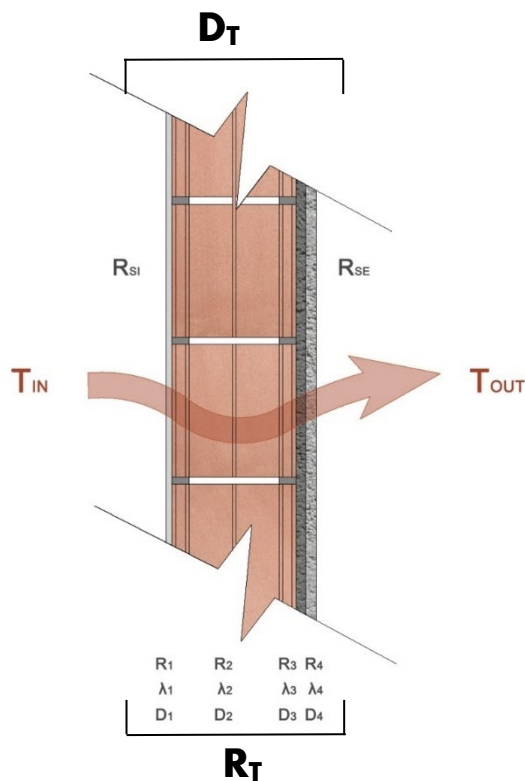


Figure 62: Simplified building envelope section, showing assembly thickness (D_t) overall insulation (R_c), indoor temperature (T_i), outdoor temperature (T_o). Adapted from (Franco, 2023).

Each archetype was assigned a simplified definition of envelope layers, using the overall assembly thickness, D_t , and overall insulation R_c , used to calculate the conductivity, shown in Equation 14.

Equation 14: Conductivity.

$$\lambda_T = \frac{D_t}{R_t}$$

This simplification was used to address the lack of detailed layer-by-layer assembly data for floors, walls and roofs. The “Example Homes Guide 2022” provides only aggregate R_c values for each building element and archetype, rather than specifying R_c or conductivity for individual materials within the assembly. As a result, it was not feasible to define each construction in terms of its true material build-up. Also, specifying detailed assemblies for every archetype would add significant simulation time without improving the reliability of the model inputs, given the lack of available data.

Thus, for the main thermal envelope elements, assumptions had to be made for the thickness of the element, density, and specific heat capacity (based on the requirements of the EnergyPlus simulation). Assumptions for main envelope elements were informed by the Nieman report, "Standard and Target Values for Existing Housing" based on the following materials:

- Roof: Lightweight concrete, roof screed
- Façade: Solid clay-brick masonry
- Window: Single or double-glazed unit
- Floor: Softwood/timber floor

For each archetype, two discrete material scenarios were defined per element:

- **CURRENT CONDITION:** Reflects the existing envelope build-up, using lower insulation values and higher conductivities.
- **RETROFIT CONDITION:** Applies a single retrofit upgrade per archetype, reducing conductivity for all main elements, and improving window U-values.

This resulted in a material ID table that describes the parameters of the main thermal elements for each archetype, that are used to run the EnergyPlus simulations. The material ID table is attached in APPENDIX B.

Note, only one retrofit scenario per archetype was studied, yielding two discrete R_c values per element. In future work, a continuous range of R_c values should be generated to simulate a wider spectrum of retrofit possibilities.



5

DATA GENERATION

**BUILDING DATA
ENERGY SIMULATIONS**

5. DATA GENERATION

BUILDING DATA

COLLECT 3DBAG GEOMETRY

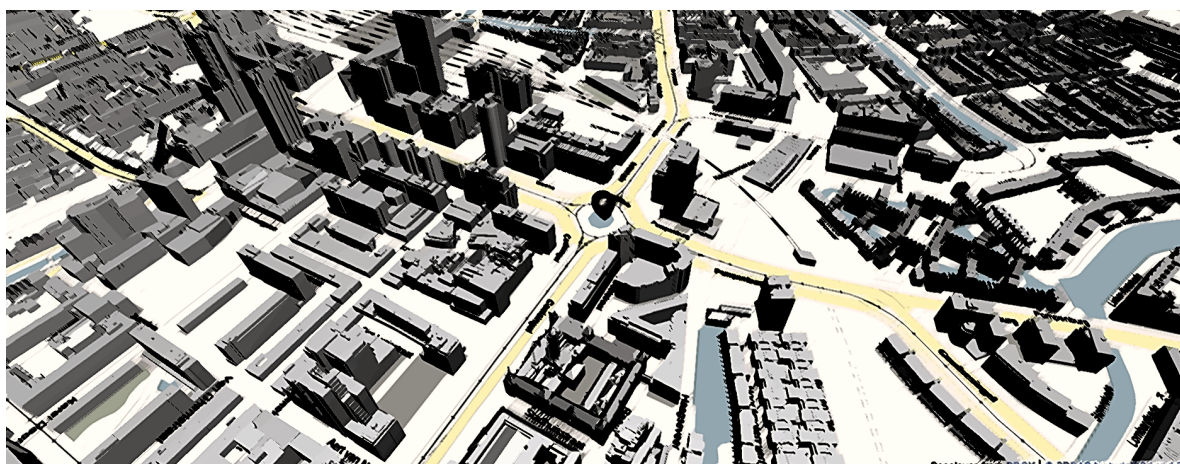


Figure 63: Rotterdam perspective, visualized in 3DBAG (3DBAG Viewer, 2024).

The 3DBAG, is an open-access platform that provides detailed 3D data of buildings in the Netherlands (3D geoinformation research group, 2023). The 3DBAG reconstructs building geometry using:

- The Basic Registration of Addresses and Buildings (BAG) – an openly available data set, containing building data for all addresses in the Netherlands, including location, building function, year of construction, and geometric properties (3D geoinformation research group, 2023).
- BAG geometries are obtained from aerial photos and terrestrial measurements and are represented as 2D polygons, showing the outline of the building as projected from above.
- Actueel Hoogtebestand Nederland (AHN) – provides detailed elevation data from LiDAR measurements – represented as point clouds – for all buildings and topography across the Netherlands.

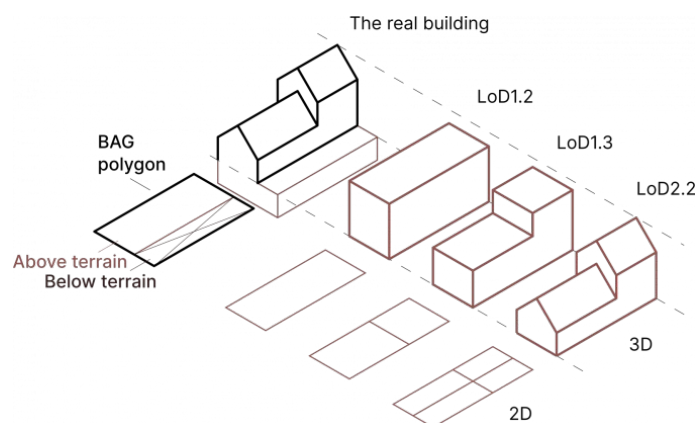


Figure 64: 3DBAG building geometries (adapted from 3D geoinformation research group, 2023).

For each BAG polygon, the 3DBAG extracts corresponding AHN point clouds to determine the roof shape, height and overall 3D building structure, resulting in 3D building geometry at three different levels of detail, LoD1.2, LoD1.3, and LoD2.2.

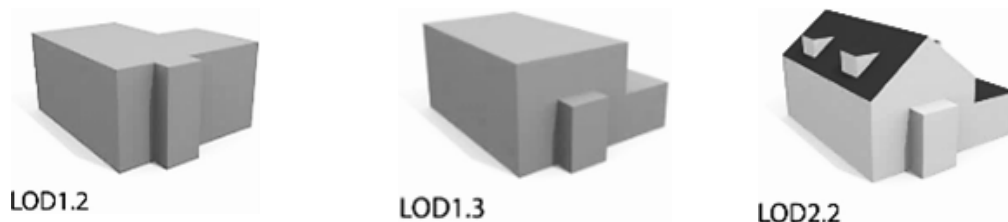


Figure 65: LoDs available from the 3DBAG. Adapted from (Biljecki et al., 2016).

In LoD1.2 the buildings are represented as blocks extruded from the 2D polygon. Smaller building parts or alcoves are represented but all walls are extruded to a single building height. LoD1.3 improves the roof structure, by representing differentiated wall heights, although still extrudes the individual roof surfaces to a single uniform level.

LoD2.2 offers the most detailed building geometry amongst the three available LoDs from 3DBAG, providing a defined roof structure, capturing sloped features as well as dormers.

Each building in the 3DBAG is identified by a Pand ID – the geo-identifier that links the geometry to the BAG registry.



Figure 66: Identifying buildings in the 3DBAG viewer. Adapted from (3DBAG Viewer, 2024).

The 3D geometry can be accessed by downloading the corresponding tile – a smaller grid square of the 3DBAG dataset. The tiles can be accessed in three formats:

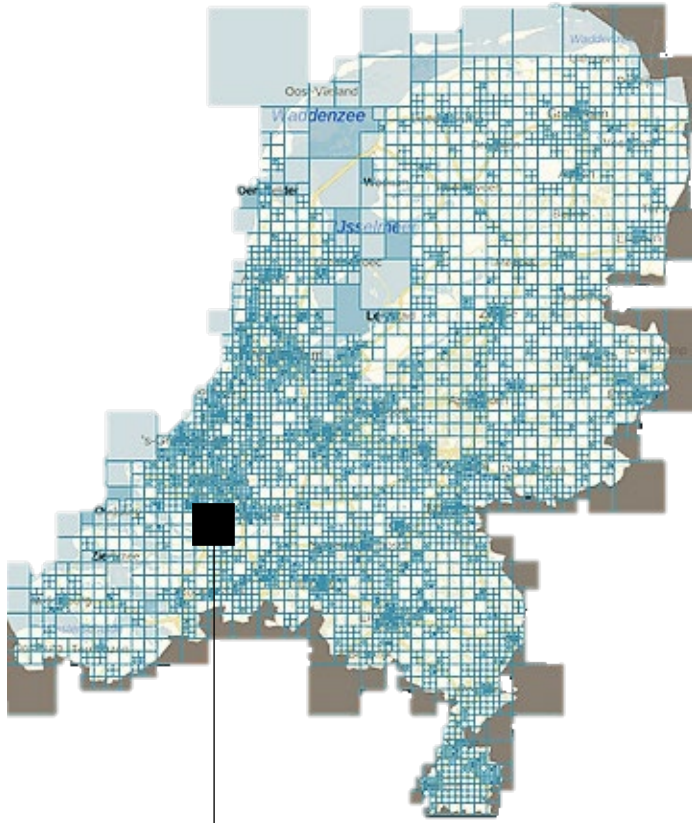


Figure 67: Geometry tile from 3DBAG (3DBAG Viewer, 2024) and tile visualized in Ninja viewer. Adapted from (CityJSON Ninja, n.d.).

1. CityJSON:

Compact JSON-based format designed specifically for storing large 3D city models, including object semantics such as buildings, and roads.

2. OBJ

Contains only 3D geometry of building models without attributes / semantic data.

3. GeoPackage:

An SQLite (C-language library) format for storing geospatial data, suitable for direct use in GIS software.

Both CityJSON and OBJ methods of geometry collection were explored in the study.

Geometry from CityJSON

The CityJSON tile can be viewed in ninja – a web interface for visualizing CityJSON data. Using Ninja, users can easily search for individual Pand IDs and extract the corresponding attribute data. The data includes geometry for all LoDs and building attributes such as the number of floors (bouwlagen), roof type (dak_type), building heights (h_dak_50p, h_dak_70p, h_dak_max, h_dak_min), and ground elevation (maaiveld).

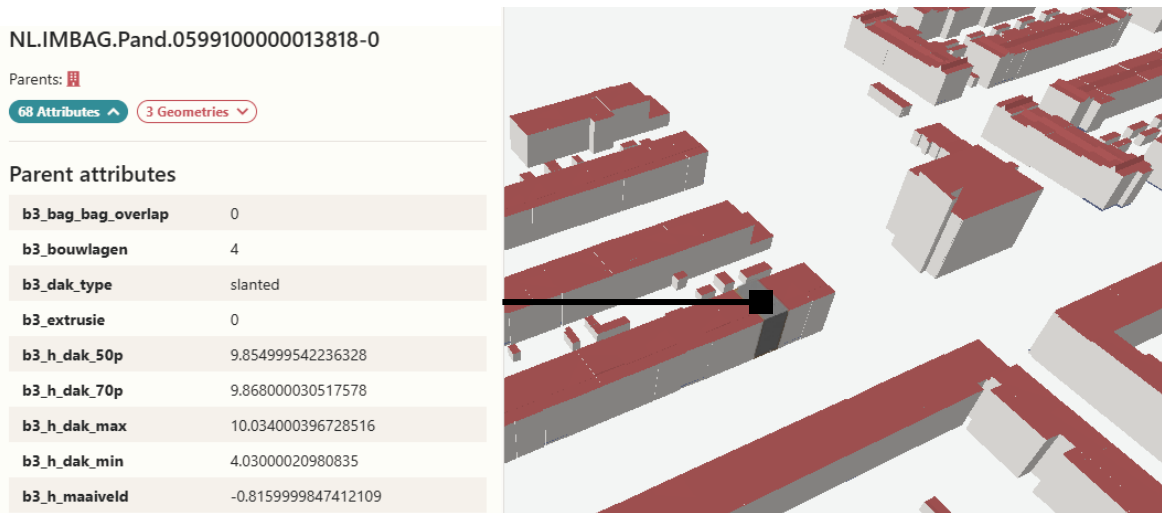


Figure 68: Viewing Pand ID attribute data in 3DBAG. Adapted from (3DBAG Viewer, 2024).

Geometry from OBJ

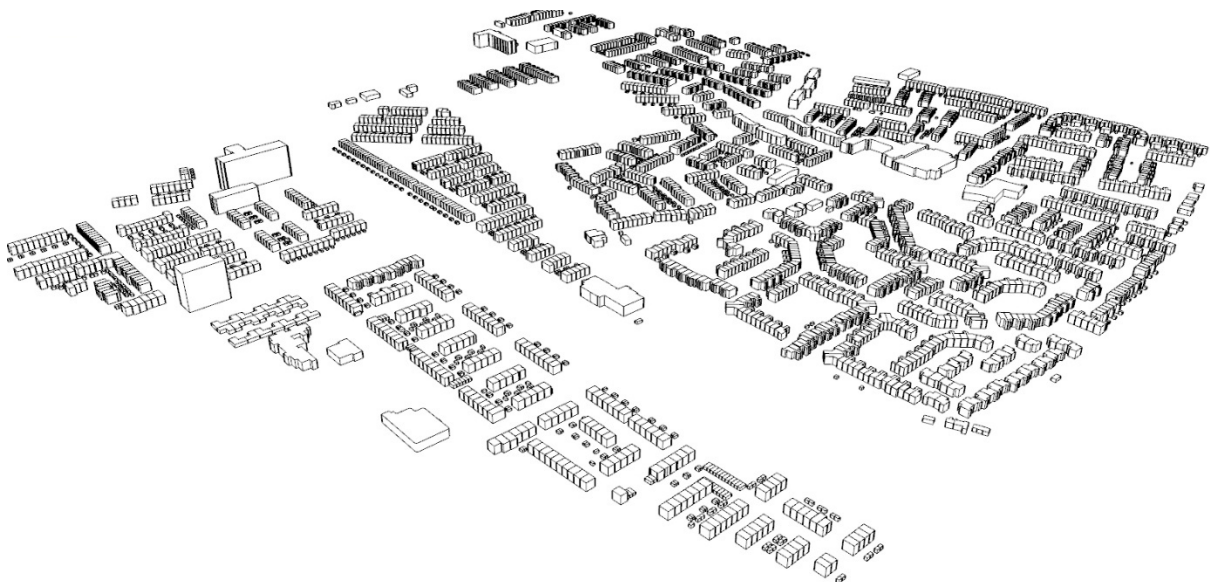


Figure 69: 3DBAG tile visualized in Rhino3D. Adapted from (3DBAG Viewer, 2024).

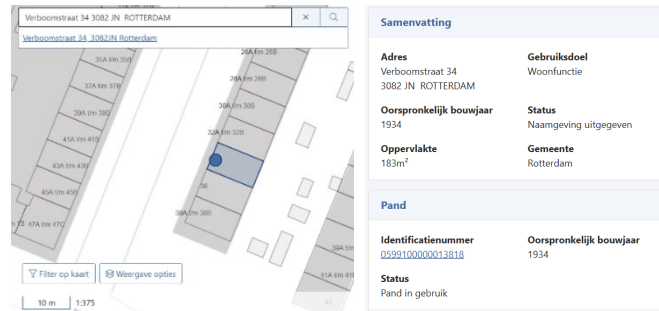
Viewing the OBJ format in Rhino3D provides a clear visual of the buildings. However, the OBJ files only provide geometric data and lacks the semantic detail necessary for extracting building properties at scale. As well since there are no building identifiers (Pand IDs) attached to the OBJ file it is impossible to locate individual buildings from the tile.

Thus, CityJSON was chosen as the primary data format because it offers a representation of both geometry and semantic information for each building. And CityJSON's structured format was suitable for the next stages of data handling to build IDF files for energy simulations and extract features for ML.

Scaling the collection

For an individual building study or a study with few buildings the following process for obtaining the building geometric and attribute data is effective:

1. Identify building address / Pand ID (Kadaster)



The screenshot shows a map interface with a search bar containing 'Verboomstraat 34 3082 JN ROTTERDAM'. The map displays several buildings, with one highlighted in blue. To the right, a 'Samenvatting' (Summary) panel provides the following information:

Samenvatting	
Adres Verboomstraat 34 3082 JN ROTTERDAM	Gebruiksdoel Woonfunctie
Oorspronkelijk bouwjaar 1934	Status Naamgeving uitgegeven
Oppervlakte 183m ²	Gemeente Rotterdam
Pand	
Identificatienummer 059910000013818	Oorspronkelijk bouwjaar 1934
Status Pand in gebruik	

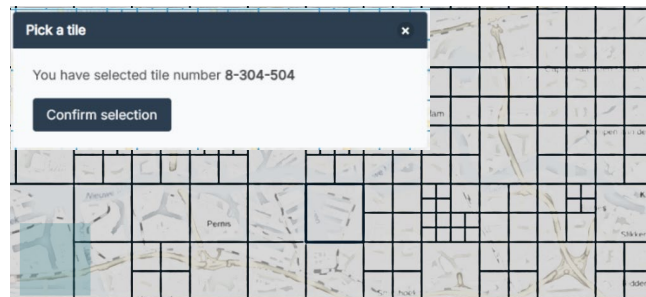
2. Find building (3DBAG)



The screenshot shows a 3D model of a building with a yellow marker. To the right, a table lists the following attributes and values:

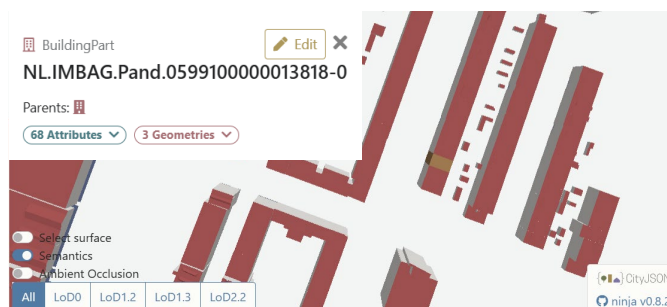
Attribute	Value
Tile number	8-304-504
identificatie	NL.IMBAG.Pand.059910000013818
status	Pand in gebruik
oorspronkelijkbouwjaar	1934
b3_bouwlagen	4
b3_kwaliteitsindicator	false
b3_h_maaiveld	-9.815999984741211
b3_volume_lod12	649.968933185469

3. Extract Tile (CityJSON)



The screenshot shows a grid of tiles. A dialog box titled 'Pick a tile' is open, displaying the message 'You have selected tile number 8-304-504' and a 'Confirm selection' button.

4. Extract JSON attributes (Ninja)



The screenshot shows a 3D model of a building with a red marker. The interface displays the following information:

- BuildingPart: NL.IMBAG.Pand.059910000013818-0
- Parents: []
- 68 Attributes (dropdown)
- 3 Geometries (dropdown)
- Buttons: Select surface, Semantics, Ambient Occlusion
- Buttons: All, LoD0, LoD1.2, LoD1.3, LoD2.2
- CityJSON logo and version: ninja v0.8.2

Figure 70: Collecting building data. Adapted from (BAG Viewer, n.d.), (3DBAG Viewer, 2024), (CityJSON Ninja, n.d.)

However, when scaling this process to city-level, several challenges occur. Large study areas often span numerous geographic tiles, meaning there is a need to manually identify, download, and manage tens (or possibly hundreds) of separate tiles, making the initial data acquisition difficult. Once the tile is downloaded, extracting specific building attributes is also a challenge, since the CityJSON files store attributes for all buildings within the tile in a dense, nested, structure. As well, not all buildings within the downloaded tile are needed, thus, extensive parsing and filtering is required to extract the attributes of interest for the select buildings within the study.

To overcome these challenges, a computational workflow was developed to automate the extraction of select buildings and corresponding building attributes. The workflow leverages the 3DBAG API – a web service to retrieve 3D building data from 3DBAG.

The API supports spatial queries, such as searching for all buildings within a certain bounding box – as well as Pand ID-based queries, allowing the retrieval of thousands of buildings and corresponding attribute data without downloading entire tiles, which was critical for this study.

From the defined list of buildings, each Pand ID was individually queried using a Python script. The script requests the necessary building features from the API, retrieves the data, and formats the retrieved data into a JSON file.

```
{
  "metadata": {
    "CityObjects": {},
    "metadata": {
      "referenceSystem": "https://www.opengis.net/def/crs/EPSG/0/7415",
      "transform": {
        "scale": [0.001, 0.001, 0.001],
        "translate": [92504.767875, 436464.981, -0.9814992370605466],
        "type": "CityJSON",
        "version": "2.0",
        "vertices": []
      }
    }
  },
  "CityObjects": {
    "NL.IMBAG.Pand.0599100000759798": {
      "attributes": {
        "b3_bag_bag_overlap": 0.0,
        "b3_bouwlagen": 5,
        "b3_dak_type": "slanted",
        "b3_extrusie": 0,
        "b3_h_dak_50p": 15.67700045776367,
        "b3_h_dak_70p": 16.160999298095703,
        "b3_h_dak_max": 17.423999786376953,
        "b3_h_dak_min": 13.769000053405762,
        "b3_h_maaiVELd": -0.9829999804496765,
        "b3_is_glas_dak": false,
        "b3_kas_warenhuis": false,
        "b3_mutatie_AHN3_AHN4": false,
        "b3_mutatie_AHN4_AHN5": false,
        "b3_n_vlakken": 7,
        "b3_nodata_fractie_AHN3": 0.0022123893722891808,
        "b3_nodata_fractie_AHN4": 0.0,
        "b3_nodata_fractie_AHN5": 0.0,
        "b3_nodata_radius_AHN3": 0.3778613209724426,
        "b3_nodata_radius_AHN4": 0.3239935338497162,
        "b3_nodata_radius_AHN5": 0.3978613209724426,
        "b3_opp_buitemuur": 289.94,
        "b3_opp_dak_plat": 0.0,
        "b3_opp_dak_schuin": 150.9,
        "b3_opp_grond": 112.88,
        "b3_opp_scheidingsmuur": 426.24,
        "b3_puntichtheid_AHN3": 19.636363983154297,
        "b3_puntichtheid_AHN4": 27.849557876586914,
        "b3_puntichtheid_AHN5": 18.026548385620117,
        "b3_pw_bron": "AHNS",
        "b3_pw_datum": 2023,
        "b3_pw_onvoldoende": false,
        "b3_pw_selectie_reden": "PREFERRED_AND_LATEST",
        "b3_rmse_lod12": 1.034056305885315,
        "b3_rmse_lod13": 1.034056305885315,
        "b3_rmse_lod22": 0.2296818494796753,
        "b3_succes": true,
        "b3_t_run": 113,
        "b3_val3dity_lod12": "[]",
        "b3_val3dity_lod13": "[]",
        "b3_val3dity_lod22": "[]",
        "b3_volume_lod12": 1924.8975830078125,
        "b3_volume_lod13": 1924.8975830078125,
        "b3_volume_lod22": 1868.6490478515625,
        "begingeldigheid": "2022-06-01",
        "documentdatum": "2022-06-01",
        "documentnummer": "Corsanr.22/12196",
        "eindgeldigheid": null,
        "eindregistratie": null,
        "fid": 12240266,
        "geconstateerd": false,
        "identificatie": "NL.IMBAG.Pand.0599100000759798",
        "oorspronkelijkbouwjaar": 1870,
        "rf_force_lod11": false,
        "status": "Pand in gebruik",
        "tijdstipinregistratie": null,
        "tijdstipinactief": null,
        "tijdstipinactiefvl": null,
        "tijdstipinactiefv": null,
        "tijdstipinactiefv": null,
        "tijdstipinactiefv": null,
        "2022-06-02T12:19:40Z",
        "tijdstipregistratie": "2022-06-02T12:19:48Z",
        "voorkomenidentificatie": 4,
        "children": ["NL.IMBAG.Pand.0599100000759798-0"],
        "geometry": {
          "boundaries": [[[0, 1, 2, 3]]],
          "lod": "0",
          "type": "MultiSurface",
          "type": "Building"
        },
        "NL.IMBAG.Pand.0599100000759798-0": {
          "geometry": {
            "boundaries": [[[[4, 5, 6, 7, 8, 9, 10]], [[11, 10, 9, 12]], [[13, 7, 6, 14]], [[14, 6, 5, 15]], [[12, 9, 8, 16]], [[16, 8, 7, 13]], [[17, 4, 10, 11]], [[15, 5, 4, 17]], [[15, 17, 11, 12, 16, 13, 14]]]],
            "lod": "1.2",
            "semantics": {
              "surfaces": [
                {
                  "type": "GroundSurface",
                  "on_footprint_edge": true,
                  "type": "WallSurface"
                },
                {
                  "type": "GroundSurface",
                  "on_footprint_edge": false,
                  "type": "WallSurface"
                },
                {
                  "type": "GroundSurface",
                  "on_footprint_edge": true,
                  "type": "WallSurface"
                }
              ]
            }
          },
          "b3_h_dak_50p": 15.618635177612305,
          "b3_h_dak_70p": 16.08927345275879,
          "b3_h_dak_max": 17.69110107421875,
          "b3_h_dak_min": 13.70636749265781,
          "type": "RoofSurface",
          "values": [[0, 1, 1, 1, 1, 1, 1, 3]],
          "type": "Solid",
          "boundaries": [[[[4, 5, 6, 7, 8, 9, 10]], [[11, 10, 9, 12]], [[13, 7, 6, 14]], [[14, 6, 5, 15]], [[12, 9, 8, 16]], [[16, 8, 7, 13]], [[17, 4, 10, 11]], [[15, 5, 4, 17]], [[15, 17, 11, 12, 16, 13, 14]]]],
          "lod": "1.3",
          "semantics": {
            "surfaces": [
              {
                "type": "GroundSurface",
                "on_footprint_edge": true,
                "type": "WallSurface"
              },
              {
                "type": "GroundSurface",
                "on_footprint_edge": false,
                "type": "WallSurface"
              },
              {
                "type": "GroundSurface",
                "on_footprint_edge": true,
                "type": "WallSurface"
              }
            ]
          }
        }
      }
    }
  }
}
```

Figure 71: Retrieved data from 3DBAG API (prior to formatting).

The data request was then adjusted to collect only LoD 1.2 geometry.

The filtered dataset contained approximately 75,000 Pand IDs, which were sampled to 20,000 for collection (maintaining the original distribution of archetypes). Using the API allowed for the simultaneous request of thousands of Pand IDs at once. The multi-processing aspect of this script – that enables the collection of multiple API requests at once, was critical to collect the building geometries in a timely manner.

Part of the geometry data collection process involved refining the request to target only the specific LoDs relevant to the study. Initially, the API returned all features across all LoDs. This resulted in unformatted JSON files with

Compared to higher LoDs, LoD 1.2 includes fewer vertices and surface indices which simplifies data structuring, as well as the dataset size to process. The workflow was designed to theoretically be compatible with all LoD levels, but working with LoD 1.2 provided a starting point to balance geometric accuracy and computational efficiency.

The request was adjusted to return a structured JSON file, where the meta data, features, and surface data can be easily identified, shown in Figure 72.

```
"metadata": {
  "CityObjects": {},
  "metadata": {
    "referenceSystem":
"opengis.net/def/crs/EPSG/0/7415"
  },
  "transform": {
    "scale": [
      0.001,
      0.001,
      0.001
    ],
    "translate": [
      91984.942125,
      438058.53075,
      -2.124498779296875
    ]
  },
  "type": "CityJSON",
  "version": "2.0",
}
```

META DATA

```
"buildings": [
  {
    "Pand ID": "0599100000012801",
    "Archetype ID": "TI.1946",
    "Status": "Pand in gebruik",
    "Construction Year": 1896,
    "Number of Floors": 3,
    "Roof Type": "slanted",
    "Wall Area": 139.48,
    "Roof Area (Flat)": 0.0,
    "Roof Area (Sloped)": 93.82,
    "Floor Area": 74.76,
    "Shared Wall Area": 238.03,
    "Ground Elevation (NAP)": -2.125,
    "LoD 1.2 Data": {
      "Building Height (Mean)": 8.95,
      "Building Height (70%)": 9.31,
      "Building Height (Max)": 10.15,
      "Building Height (Min)": 6.36
    }
  },
]
```

FEATURES

```
"vertices": [
  [
    4745,
    14003,
    2125
  ],
  [
    0,
    10729,
    2125
  ],
]

"Boundaries (LoD 1.2)": [
  [
    4,
    5,
    6,
    7,
  ]
],
```

SURFACE DATA

Figure 72: Formatted JSON file after collection of building metadata, building features, and building surface data.

PROCESSING FOR IDF

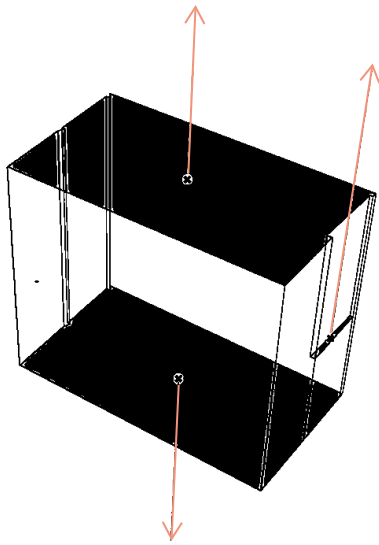


Figure 73: Surface normal for building geometry before flipping direction.

The data collection phases produced a JSON file containing building features and surface geometry, including all vertices. It was essential to verify the ordering of vertices for each surface, since EnergyPlus needs surfaces to be defined in a counterclockwise order with the surface normal pointing towards the thermal zone (inside the building).

This is especially important for horizontal surfaces, where an incorrect orientation can cause flipped boundaries leading to simulation errors – which was encountered when running the initial simulations.

To check and visualize the orientation of all surfaces, a Grasshopper script was developed, shown in Figure 74. Handling this step in Grasshopper (rather than Python) allowed to quickly inspect the vertex order and normal

direction, where it was found that all vertices from the original JSON were ordered clockwise, thus all surface normals pointed away from the thermal zone. Part of the data processing workflow thus involved flipping the order of the vertex data for input to EnergyPlus.

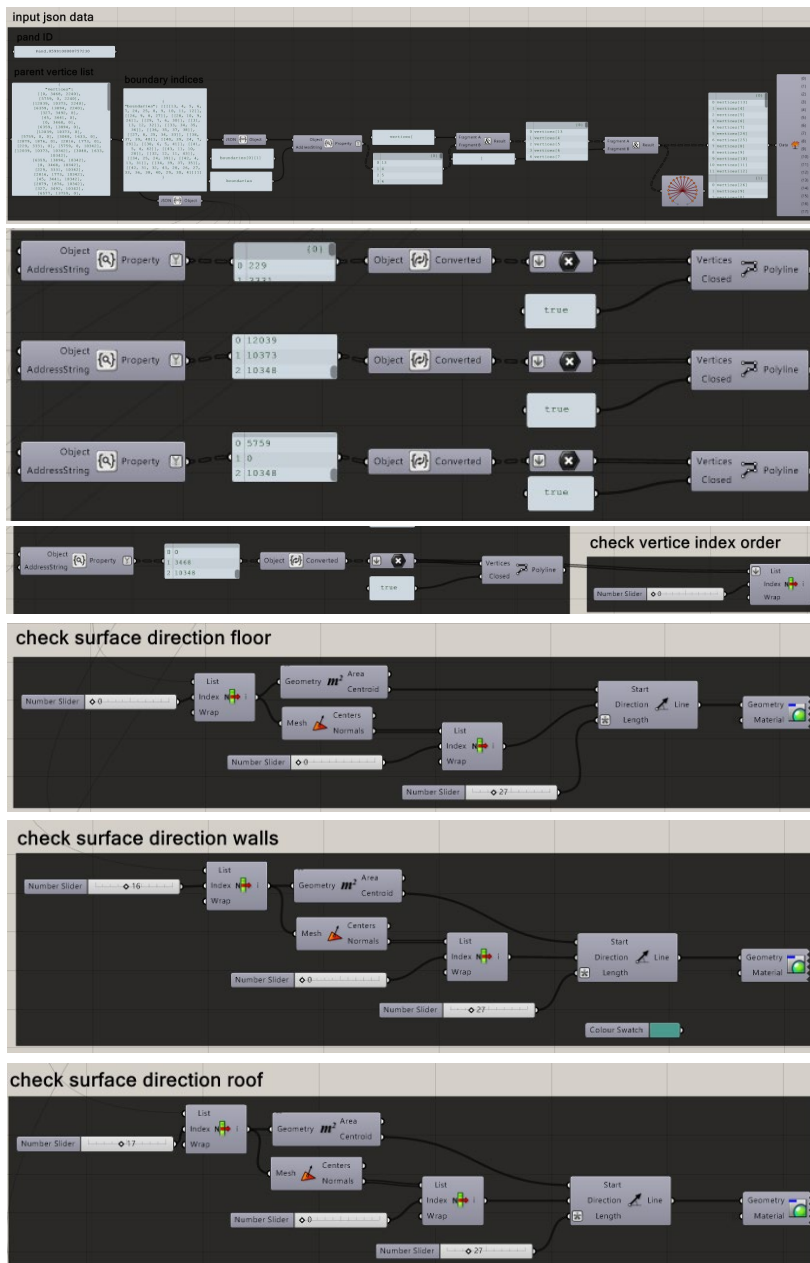
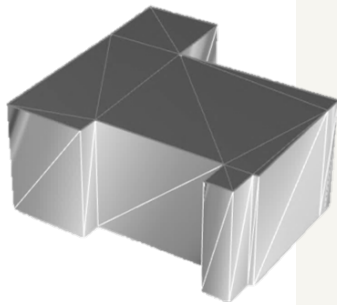


Figure 74: Grasshopper script to check vertex order and surface directions.

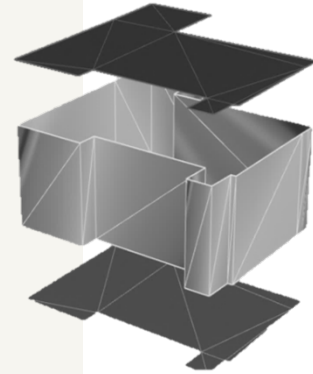
From the building JSON files, for each building, the boundary surfaces were defined as lists of vertex indices, but without explicit surface type (ground, façade, roof). A script was developed to iterate through each surface, extract the z-coordinates of its vertices, and assign as surface type based on the z-position. When all z-coordinates are minimum, the surface is classified as ground floor (G), when maximum, the surface is classified as roof (R) and all other surfaces are classified as façade (F). The resulting structured JSON included these new surface type labels for each surface, shown in Figure 75.



```

"0599100000012801": {
  "Archetype ID": "TI.1946",
  "Construction Year": 1896,
  "Number of Floors": 3,
  "Wall Area": 139.48,
  "Roof Area (Flat)": 0.0,
  "Roof Area (Sloped)": 93.82,
  "Floor Area": 74.76,
  "Shared Wall Area": 238.03,
  "Absolute Height (70%)": 11.44,
  "Surfaces": [
    "Coordinates": [
      0,
      10729,
      0
    ],
    "Type": "G"
  ]
}

```

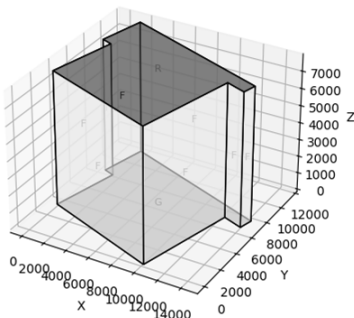


SURFACE JSON

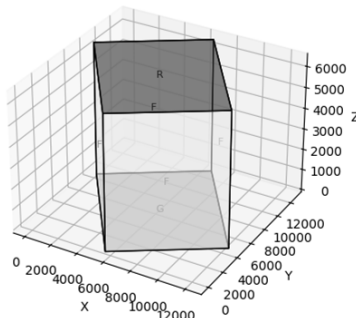
Figure 75: Surface type JSON.

To verify the correct mapping, the labelled surfaces were visualized using matplotlib, which plotted each building, and the surface labels, confirming the labelling corresponded to the expected surfaces for ground, façade, and roof. Example plots are shown below in Figure 76.

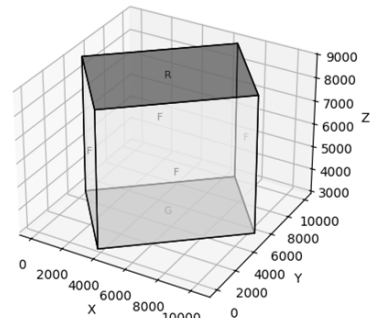
Building NL.IMBAG.Pand.0599100000012893



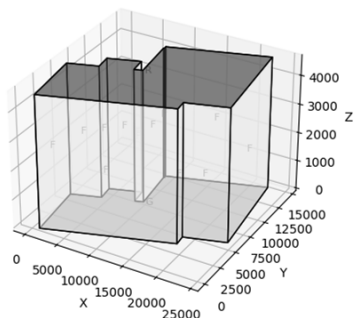
Building NL.IMBAG.Pand.0599100000011516



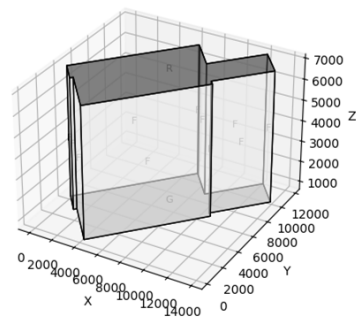
Building NL.IMBAG.Pand.0599100000012679



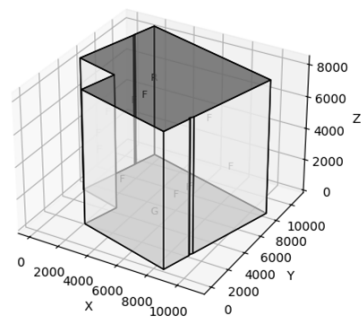
Building NL.IMBAG.Pand.0599100000012952



Building NL.IMBAG.Pand.0599100015002327



Building NL.IMBAG.Pand.0599100000416389



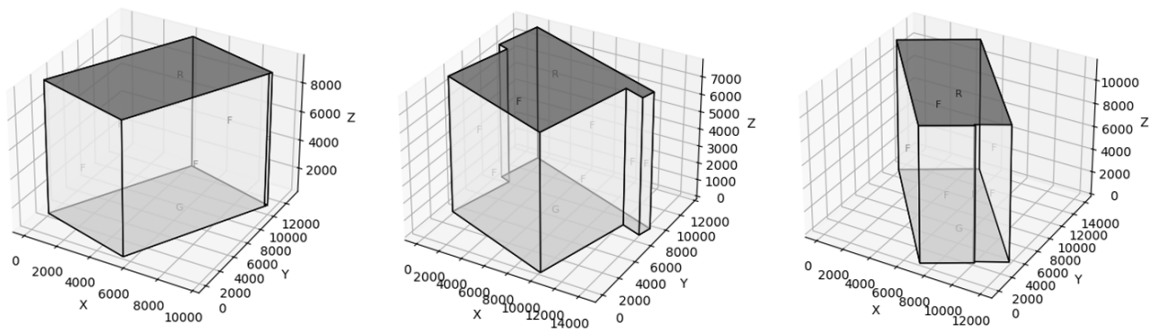


Figure 76: Building plots to verify surface labelling.

Finding building adjacencies.

To differentiate between the building types, Terraced Intermediate, Terraced Corner, and Detached it was necessary to define building adjacencies (shared walls) for the appropriate building surfaces. The Terraced Intermediate has a minimum of two shared walls, Terraced Corner with one, and Detached with zero. Defining building adjacencies allowed to classify the surfaces as adiabatic – boundaries that do not allow heat transfer with the external environment. This is a critical step to correctly represent the thermal energy demands for the different building types within the study.

To find building adjacencies for the dataset at scale (20,000 buildings), a computational workflow was developed using the following steps:

1. Extract the ground footprint:

Get the ground surface of each building from its JSON file by looking for the “G” surface type and converting its outline into a 2D polygon.

2. Apply a proximity buffer:

Expand this footprint by 20 cm in all directions to create a zone that where neighbours could be found.

3. Query API for bounding box

Find the smallest rectangle that fully contains the buffer footprint and query the 3DBAG API for all buildings inside the bounding box.

5. Retrieve candidate neighbours:

Get the list of buildings whose footprints fall within the bounding box. Any building found at this stage is considered a neighbour.

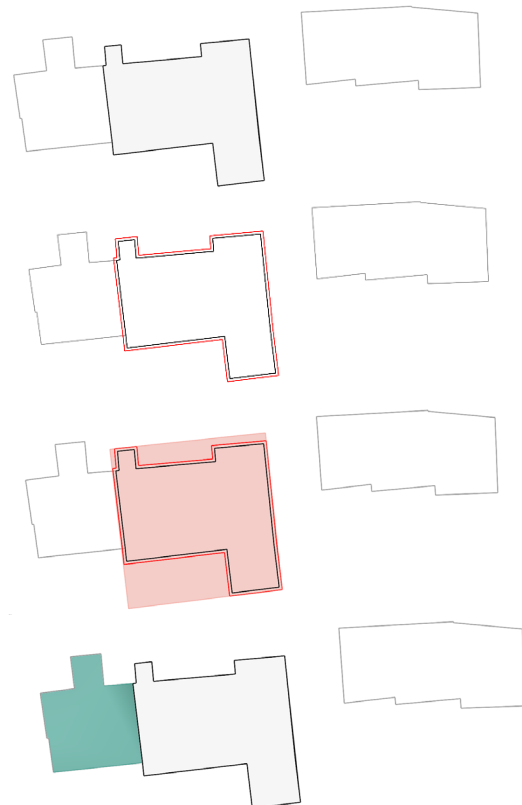


Figure 77: Methodology for finding building adjacencies.

Because the rectangular bounding box is a large area around the true base polygon, this method introduced “false-positive” neighbours just outside the 20 cm buffer. There were also cases of “false-negative”, where the bounding box did not capture all expected neighbours, for example in the case of Terraced Intermediate houses where only one adjacency was detected however, at least two adjacencies would be expected. Due to time constraints these false-positives and negative were not isolated from the dataset. Thus, some buildings were modelled with either more or less adjacencies than true for the geometry.

The surface labelling is shown in Figure 78 for Terraced Intermediate, where a minimum of two adiabatic surfaced are expected. Buildings with correctly identified adjacencies are shown in the top row and buildings with missing adjacencies are shown in the bottom row.

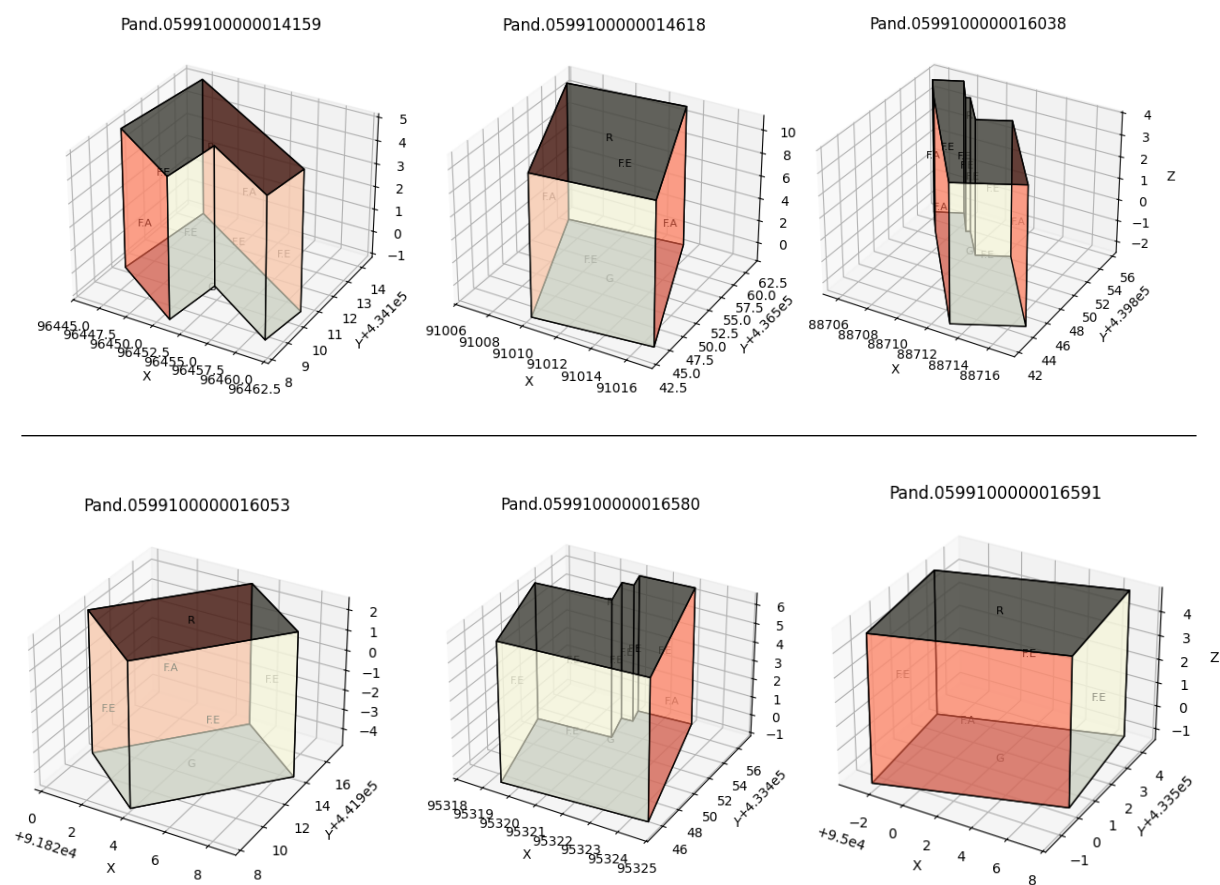


Figure 78: Building models with successful adjacency findings (top row) and buildings with false-negative adjacency findings or less adjacencies than expected (bottom row).

The surface labels Façade Exposed (F.E) and Façade Adiabatic (F.A) were then added into the building features JSON file for further processing.

ENERGY SIMULATIONS

GENERATING THE IDF FILE

```
Simulation Parameters
-----
[0001] Version
[0001] SimulationControl
[.....] PerformancePrecisionTradeoffs
[.....] Building
[.....] ShadowCalculation
[.....] SurfaceConvectionAlgorithm:Inside
[.....] SurfaceConvectionAlgorithm:Outside
[.....] HeatBalanceAlgorithm
[.....] HeatBalanceSettings:ConductionFiniteDifference
[.....] ZoneAirHeatBalanceAlgorithm
[.....] ZoneAirContaminantBalance
[.....] ZoneAirMassFlowConservation
[.....] ZoneCapacitanceMultiplier:ResearchSpecial
[0001] Timestep
[.....] ConvergenceLimits
[.....] HVACSystemRootFindingAlgorithm

Compliance Objects
-----
[.....] Compliance:Building

Location and Climate
-----
[0001] Site:Location
[.....] Site:VariableLocation
[.....] SizingPeriod:DesignDay
[.....] SizingPeriod:WeatherFileDays
[.....] SizingPeriod:WeatherFileConditionType
[0001] RunPeriod
[.....] RunPeriodControl:SpecialDays
[0001] RunPeriodControl:DaylightSavingTime
[.....] WeatherProperty:SkyTemperature
[.....] Site:WeatherStation
[.....] Site:HeightVariation
[.....] Site:GroundTemperature:BuildingSurface
[.....] Site:GroundTemperature:FCfactorMethod
[.....] Site:GroundTemperature:Shallow
[.....] Site:GroundTemperature:Deep
[.....] Site:GroundTemperature:Undisturbed:FiniteDifference
```

Figure 79: Input data file (IDF) interface in the IDF editor.

In energy simulation studies a large backlog can be the manual generation of the EnergyPlus input data files (IDFs) since it requires defining all building parameters, such as geometry, materials, schedules, internal gains, and the HVAC system (Zhang et al., 2024). When working with the dataset size required for this study, manually generating the IDF file for each of the 20,000 buildings would be impossible.

Different workflows for generating the IDF file were explored prior to the implementation of a Python workflow, as discussed below.

RHINO/ GRASSHOPPER/ HONEYBEE

Within Grasshopper, Honeybee was initially explored as a tool for generating IDF files based on its relatively simple visual programming environment. The Rhino interface makes it easier to check if geometry is accurately represented, and to visually confirm how input parameters – such as constructions and boundary conditions – are assigned to different building surfaces. This approach also supports some level of automation for generating batch IDF and EnergyPlus simulation files. A preliminary model output is shown in Figure 80, and the script to generate a basic IDF is shown in Figure 81.

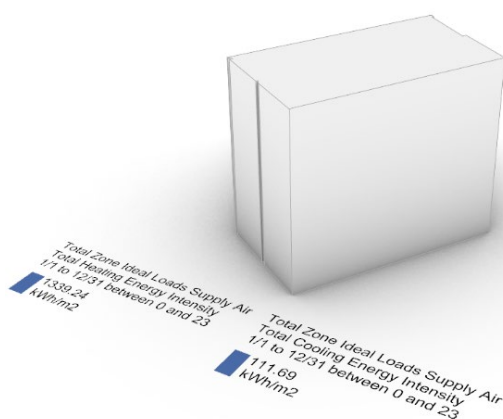


Figure 80: Output from exploration with Grasshopper and Honeybee to generate IDF and run EnergyPlus simulation.

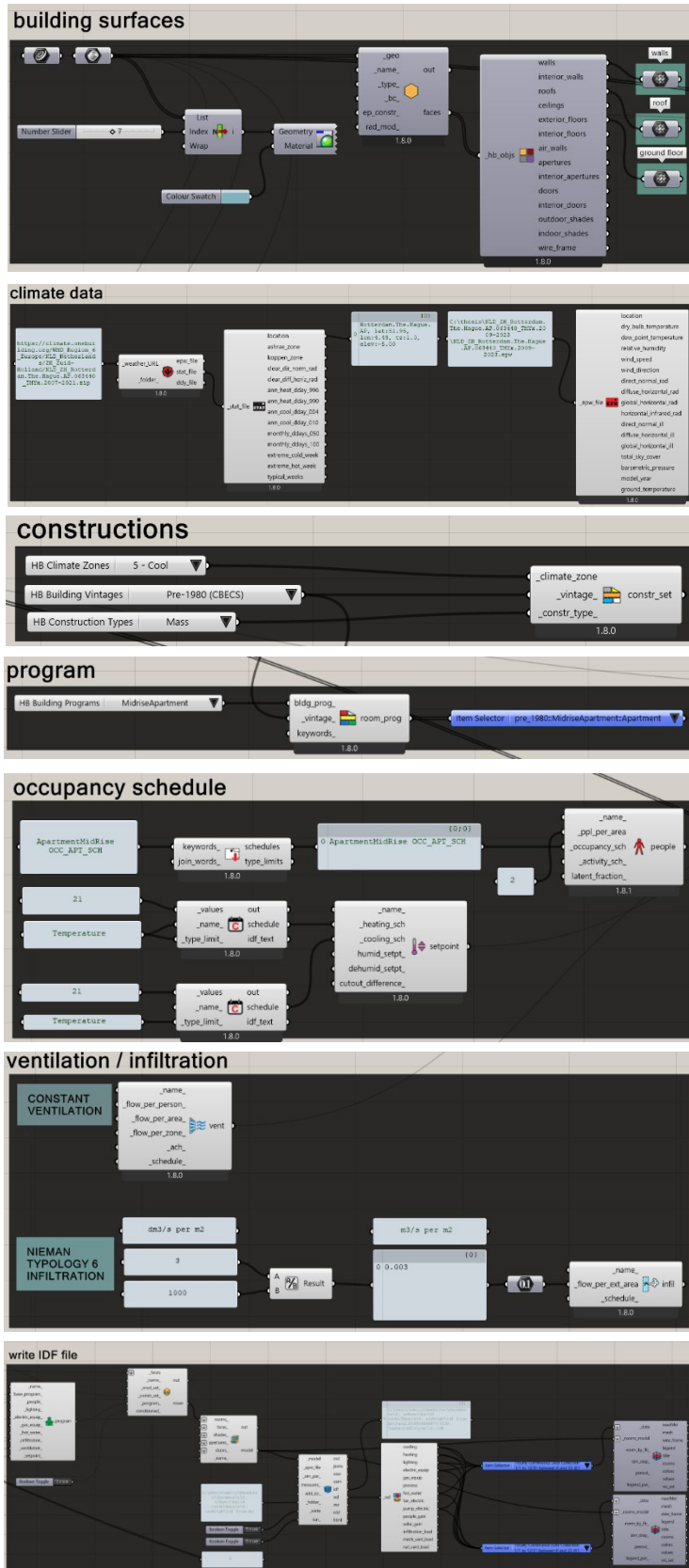


Figure 81: Preliminary Grasshopper script with simple inputs to generate an IDF file and run an EnergyPlus simulation.

Honeybee was ultimately not chosen as the primary workflow for this study because it proved challenging to set up efficient batch simulations for multiple archetypes and to set archetype-specific features (such as constructions) to the correct Grasshopper objects at scale.

PYTHON / EPPY

To overcome IDF generation at scale, a Python workflow was developed to automate the process. And generate IDF files for each building by parsing the JSON files containing the geometric and construction features for each building.

The input variables were defined with the Eppy Python library. Eppy is specifically designed for the creation, editing, and analysis of IDF files (Eppy, 2020), allowing to add building objects and parameters directly in Python, without manual editing in the IDFs editor. Key object definitions are shown below:

```
IDF.newIDFObject("BUILDING", Name=building_name, North_Axis=0.0, Terrain="City"),
    Loads_Convergence_Tolerance_Value=0.04,
    Temperature_Convergence_Tolerance_Value=0.4,
    Solar_Distribution="FullExterior",
    Maximum_Number_of_Warmup_Days=25)

IDF.newIDFObject("HVACTEMPLATE:ZONE:IDEALLOADSAIRSYSTEM", Zone_Name=zone_name)

IDF.newIDFObject("SCHEDULE:COMPACT", Name=f"HeatingSetpoint_{zone_name}",
    Schedule_Type_Limits_Name="Temperature", Field_1="Through: 12/31",
    Field_2="For: AllDays", Field_3="Until: 24:00", Field_4="21.0")

IDF.newIDFObject("MATERIAL", Name=mat_id, Roughness=mat["Roughness"],
    Thickness=mat["Thickness"], Conductivity=mat["Conductivity"],
    Density=mat["Density"], Specific_Heat=mat["Specific Heat
    Capacity"], Thermal_Absorptance=0.9, Solar_Absorptance=0.7)

IDF.nect("OUTPUT:VARIABLE", Key_Value="*",
    Variable_Name="Zone Ideal Loads Supply Air Total Heating Energy",
    Reporting_Frequency="Hourly")
```

Figure 82: Key object definitions for running an EnergyPlus simulation using Eppy Python library.

The main steps for generating the IDF include defining the following objects, showing in Table 17.

Table 15: IDF objects for EnergyPlus simulations.

IDF DEFINITIONS	
GEOMETRY	
BUILDING	Defines the overall building object that contains all zones and systems.
ZONE	Defines one thermal zone for each building to simulate the energy behaviour.
BUILDING SURFACE: DETAILED	Defines geometry and properties of each surface (floors, walls, roofs), including coordinates and constructions.
SITE	
SITE: GROUND TEMPERATURE	Sets monthly ground temperatures required for ground heat transfer calculations. Set to 18°C to avoid warnings in the simulation.
SYSTEMS	
HVAC: IDEAL LOADS AIR SYSTEM	Defines a basic HVAC system for the zone, using ideal air loads to simplify the heating/cooling definition and avoid inputting detailed HVAC inputs.
SCHEDULES	
SCHEDULE: COMPACT	Sets the schedule to 'always-on' to maintain infiltrations throughout the entire simulation.
THERMOSTATSETPOINT: DUALSETPOINT	Sets schedule type to 'dual setpoint' to define setpoints for both heating and cooling.
ZONE CONTROL: THERMOSTAT	Implements the setpoint schedules for the zone.
CONSTRUCTION	
MATERIAL	Defines the thermal properties (thickness, conductivity, density, etc.) for envelope components.
CONSTRUCTION	Assigns material layers to each envelope type to define an assembly.
WINDOW MATERIAL: SIMPLE GLAZING SYSTEM	Specifies window properties for U-factor, SHGC.
ZONE INFILTRATION: DESIGN FLOWRATE	Models air infiltration for each zone to simulate air leakage.
OUTPUT	
OUTPUT VARIABLE	Requests specific simulation outputs, in this case the heating and cooling demands.

The site, systems, and schedule inputs were held constant for each building, across all archetypes. Every building was modelled with a single-zone definition, ideal air loads, and the same thermostat set points and operation schedules, regardless of archetype or geometry.

```

"TI.1946": {
  "Infiltration": 0.003,
  "Materials": [
    {
      "Material ID": "G.TI.1946",
      "Roughness":
"MediumSmooth",
      "Insulation": 0.15,
      "Thickness": 0.15,
      "Conductivity": 1.0,
      "Density": 540.0,
      "Specific Heat Capacity": 1210
    },
    {
      "Material ID": "F.TI.1946",
      "Roughness": "Rough",
      "Insulation": 0.35,
      "Thickness": 0.3,
      "Conductivity": 0.85,
      "Density": 1920.0,
      "Specific Heat Capacity": 840
    },
    {
      "Material ID": "R.TI.1946",
      "Roughness": "MediumRough",
      "Insulation": 2.0,
      "Thickness": 0.2,
      "Conductivity": 0.1,
      "Density": 1500.0,
      "Specific Heat Capacity": 1000
    },
    {
      "Window ID": "W.TI.1946",
      "U_Factor": 2.9,

      "SHGC": 0.6
    }
  ]
}

```

CONSTRUCTIONS JSON

Using Python, the material ID table was first converted to a structured dictionary JSON file. Where each archetype represents an object and the 'Materials' dictionary defines the thermal parameters for each floor, wall, window, and roof element.

For each building, the code parsed the archetype ID from the Features JSON. The corresponding material properties for that archetype ID were then retrieved from the Constructions JSON.

```

"0599100000012801": {
  "Archetype ID": "TI.1946",
  "Construction Year": 1896,
  "Number of Floors": 3,
  "Wall Area": 139.48,
  "Roof Area (Flat)": 0.0,
  "Roof Area (Sloped)": 93.82,
  "Floor Area": 74.76,
  "Shared Wall Area": 238.03,
  "Absolute Height (70%)": 11.44,
  "Surfaces": [
    "Coordinates": [
      0,
      10729,
      0
    ],
    "Type": "G"
  ]
}

```

FEATURES JSON

Using Eppy, each building surface (ground, façade, window, and roof) was assigned its corresponding materials and thermal properties according to the surface type and building archetype.

Similarly, window objects were automatically generated in the IDF for all surfaces labeled as "exposed", shown in Figure 84. The total window area was determined by the predefined WWR for the archetype.

By using Eppy, it was possible to automate the generation of all required IDF objects and reproduce the input parameters for each archetype.

Figure 83: Example excerpts from the Constructions JSON file (left) and Features JSON (right).

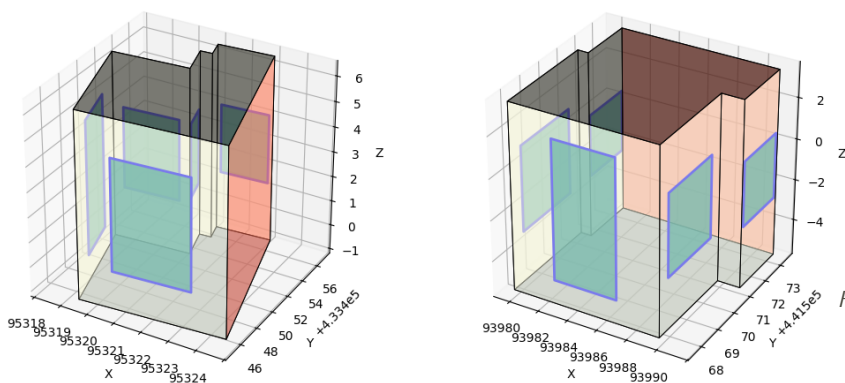


Figure 84: Window surfaces assigned to building models based on archetype WWR.

This workflow allowed for the creation of 20,000 IDF files (per scenario) for simulation – where one IDF file represents one building or Pand ID. An excerpt from an IDF file is shown in Figure 85.

```
SimulationControl,
  No,                !- Do Zone Sizing Calculation
  No,                !- Do System Sizing Calculation
  No,                !- Do Plant Sizing Calculation
  No,                !- Run Simulation for Sizing Periods
  Yes,               !- Run Simulation for Weather File Run Periods
  No,                !- Do HVAC Sizing Simulation for Sizing Periods
  1;                 !- Maximum Number of HVAC Sizing Simulation Passes

BUILDING,
  Pand.0599100000012801, !- Name
  0,                 !- North Axis
  City,              !- Terrain
  0.04,              !- Loads Convergence Tolerance Value
  0.4,               !- Temperature Convergence Tolerance Value
  FullExterior,     !- Solar Distribution
  25,                !- Maximum Number of Warmup Days
  1;                 !- Minimum Number of Warmup Days

Timestep,
  6;                 !- Number of Timesteps per Hour

Site:Location,|
  Rotterdam.The.Hague.AP_ZH_NLD Design_Conditions, !- Name
  51.96,             !- Latitude
  4.45,              !- Longitude
  1,                 !- Time Zone
  -4.5;              !- Elevation
```

Figure 85: Example section of IDF for EnergyPlus simulation.

BATCH RUN SIMULATIONS

For each generated IDF file, the EnergyPlus simulations were run using a multi-processing script to process multiple buildings in parallel. Again, when working at such scale, the multi-processing functionality of the script was instrumental to complete the simulations in a time-efficient way.

The IDF is configured for a continuous, annual simulation (January – December) using Rotterdam climate data. Or De Bilt climate data for the future weather simulations. Outputs are generated at 10-minute intervals for the entire year. The output variables set in the IDF record:

- Zone Ideal Loads Supply Air Total Heating Energy [J] (hourly)
- Zone Ideal Loads Supply Air Total Cooling Energy [J] (hourly)

For every simulation, two files are collected:

1. **eplusout.err** – logs all warnings, and errors during the simulation.
2. **eplusout.eso** – records all simulation outputs defined in the IDF file (i.e., zone heating/cooling loads).

The eso file contains outputs at each time step, recording the:

- **Run period location:** latitude and longitude.
- **Time step:** marks each reporting time step (day of simulation, month, hour, start minute, end minute, day of week)
- **Output:** Outputs for heating and cooling energy at each timestep (measured in joules).

```
RUN PERIOD:  
1, 51.96, 4.45, 1.00, -4.50  
  
TIME STEP:  
2,1, 1, 1, 0, 1, 0.00,60.00, Sunday  
  
HEATING: 141,1.0  
COOLING: 190,0.0
```

Figure 86: EnergyPlus eso file output, showing incremental heating and cooling demand at a single time step.

The eso file format is shown in Figure 86, where for each simulation there are thousands of incremental outputs (capturing each time step throughout the full run period). Thus, requiring post-processing to understand the total annual energy demands for each building.

PROCESS DEMANDS

A Python script was used to parse each EnergyPlus eso file for all 20,000 buildings within the dataset. For each building the incremental heating and cooling demands at each time step are summed over the complete simulation run period. The total demand is then converted from Joules to kilowatt-hours (kWh).

The script retrieves each building's geometric data and uses it to normalize the annual heating and cooling demands by the total floor area to produce results in kWh/m²/year. The final output is a single structured JSON file containing annual heating and cooling demands for each building.



6

DEMAND ANALYSIS

CURRENT CLIMATE

FUTURE CLIMATE

VALIDATION

6. DEMAND ANALYSIS

The building energy demand of all buildings simulated with EnergyPlus was analyzed to understand:

- Energy demand differences per archetype.
- Impact of building envelope improvements (increased insulation, reduced infiltration) on heating and cooling demands.
- Impact of future weather conditions (increased temperatures) on heating and cooling demands.

Note, a preliminary demand analysis of the EnergyPlus simulations was completed prior to the creation of the computational workflow for defining adiabatic surfaces and window objects and is referenced in APPENDIX C.

CURRENT CLIMATE

Analysis of total energy demand shows a clear trend where Detached (D) houses exhibit the highest energy consumption, followed by Terraced Corner (TC) houses, and Terraced Intermediate (TI).

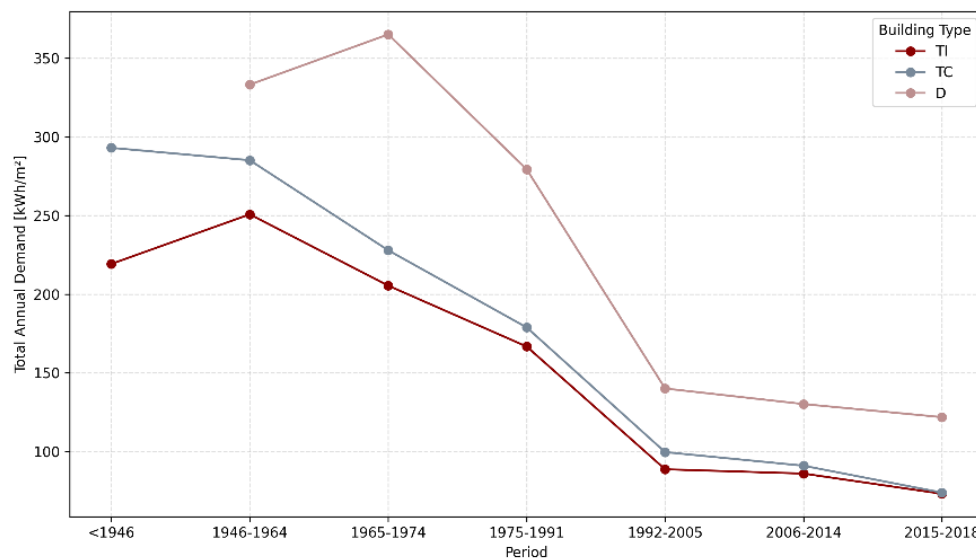


Figure 87: Total energy demand per archetype for simulation A1 (current constructions and current weather).

This trend can be explained by the proportion of exposed surfaces and WWR characteristics of each typology. Detached houses are fully exposed on all facades, resulting in the greatest external surface area. Thus, Detached houses experience more heat transfer with the external environment, which can increase both heating and cooling loads. Terraced Corner houses share at least one wall with a neighboring building, reducing heat losses or gains through that surface,

while Terraced Intermediate houses typically share two sides with neighbouring buildings, thus minimizing the exposed envelope area.

DETACHED HOUSE / VRIJSTAANDE WONING

For Detached houses, the average heating demand for archetypes pre-1965 and 1965-1974 is approximately 340–360 kWh/m² yr. The high heating demand can be attributed to archetype features including low insulation values, and a high infiltration of 0.004 m³/sm².

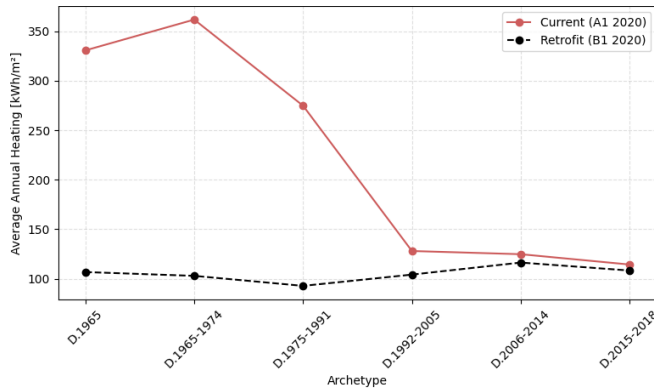


Figure 89: Detached average heating demand for simulations A1, B1.

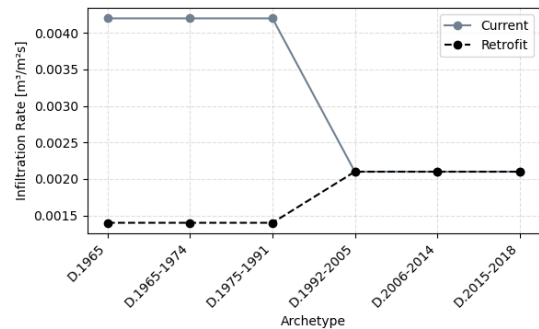


Figure 88: Detached infiltration rate [m³/m²s].

A large reduction in heating demand occurs for the 1992-2005 archetype, aligned with the implementation of airtightness standards, cavity wall insulation, and roof insulation in the Dutch building codes. During this period, heating demand drops sharply to approximately 130 kWh/m², even as the WWR ratio increases. Subsequent archetypes (2006-2014 and 2015-2018) show modest further reductions, reaching around 115 kWh/m². These incremental improvements can be primarily attributed to improvements in window performance ($U = 1.8 \text{ W/m}^2\text{K}$).

The retrofit heating demand remains consistently low across all archetypes, showing significantly reduced demands compared to the current scenario.

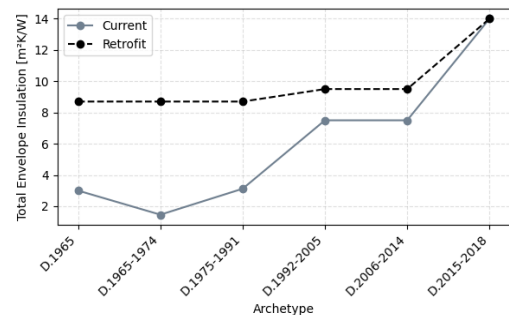


Figure 91: Detached total envelope insulation [m²K/W].

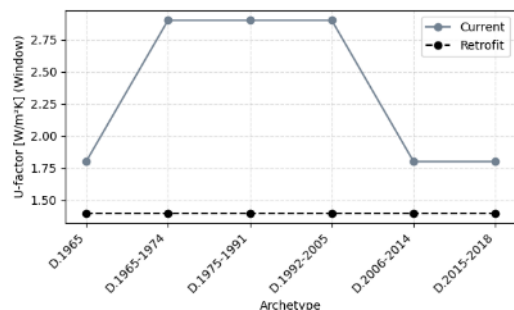


Figure 90: Detached window U-factor [W/m²K].

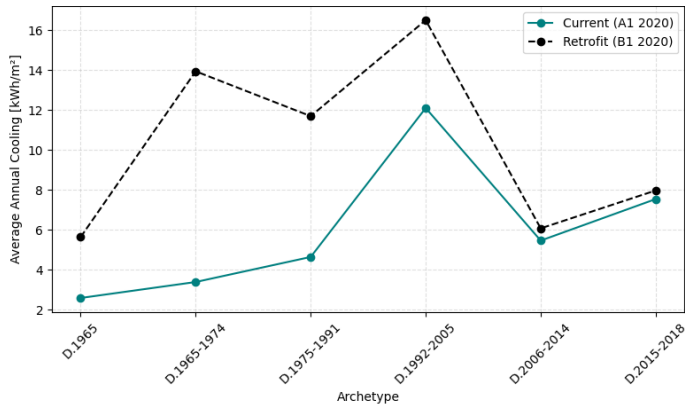


Figure 93: Detached average cooling demand A1, B1.

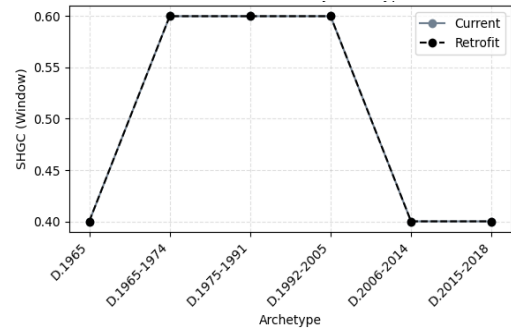


Figure 92: Detached SHGC.

The cooling demand for Detached houses shows that retrofit measures – such as improved infiltration, increased envelope insulation, and reduced window U-factor – can result in higher cooling demands compared to the current state. The SHGC and WWR values remain unchanged between scenarios, indicating that the increase in cooling demand is not due to changes in window solar gains but the combined effects of reduced infiltrations and reduced thermal transmittance. Specifically in the 1992-2005 archetype where there is a large spike in cooling demands, attributed to the steep decline in infiltration for that period.

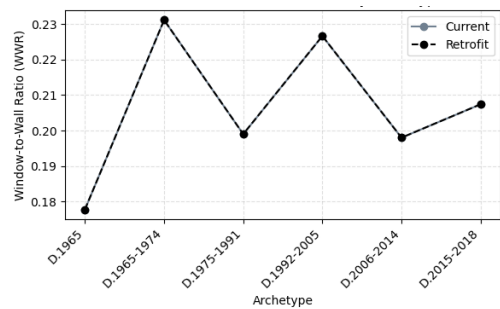


Figure 94: Detached WWR.

TERRACED CORNER / HOEKWONING

The heating demand for the Terraced Corner archetypes generally decreases over time, reflecting improvements in envelope insulation and reduced infiltration rates that significantly limit heat losses in winter. For the 1992-2005 archetype, the heating demands start to converge as the current construction parameters approach the same values as the retrofits.

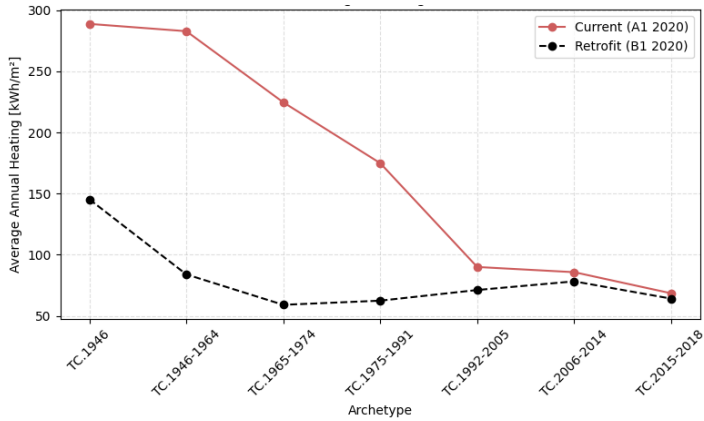


Figure 95: Terraced Corner average heating demand for simulations A1, B1.

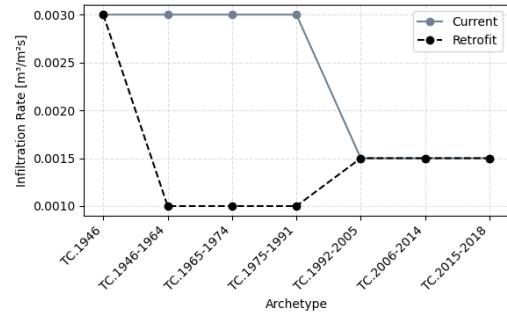


Figure 96: Terraced Corner infiltration rate [m^3/m^2s].

The cooling demand displays a more complex pattern, with a sharp increase for the 1965-1974 archetype. This spike can be attributed to the simultaneous spike in WWR and SHGC, which increase solar heat gains.

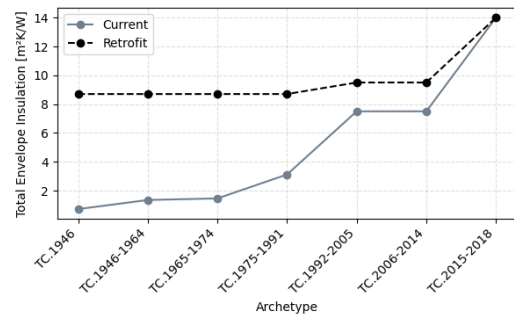


Figure 97: Terraced Corner total envelope insulation [m^2K/W].

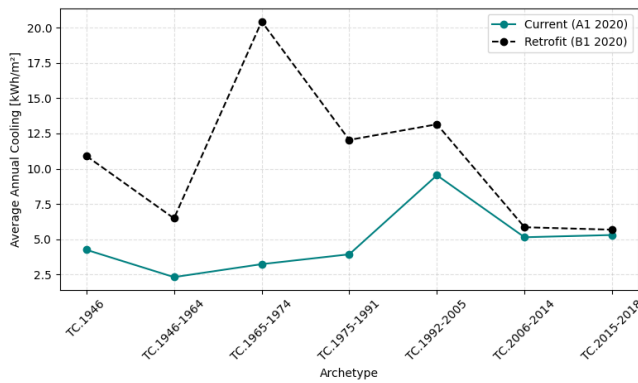


Figure 98: Terraced Corner average cooling demands (A1, B1).

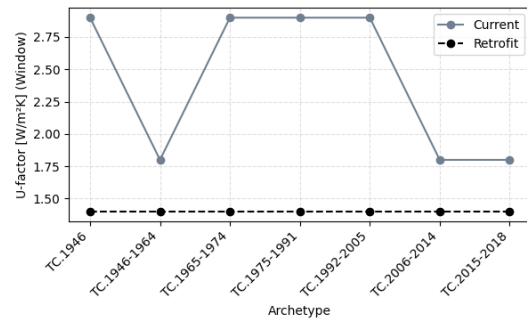


Figure 99: Terraced Corner window U-factor [W/m^2K].

As was observed for the Detached archetypes, the improved airtightness and highly insulated envelopes effectively trap heat in summer, increasing cooling loads. In the most recent archetypes, reductions in SHGC and window U-factor help reverse this trend, leading to lower cooling demands despite continued high levels of insulation and airtightness. This demonstrates the critical balance between envelope characteristics in achieving improved energy performance for both heating and cooling requirements.

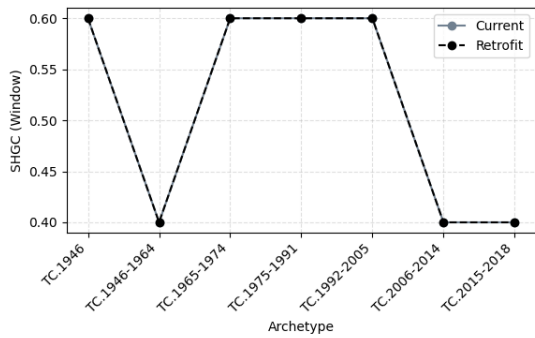


Figure 101: Terraced Corner SHGC.

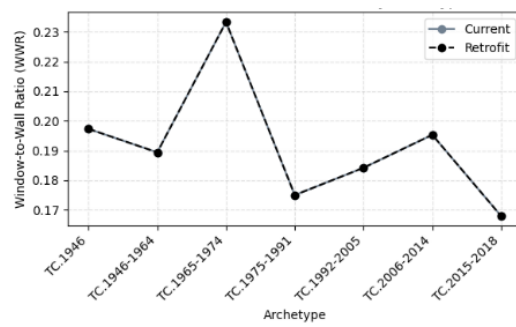


Figure 100: Terraced Corner WWR.

TERRACED INTERMEDIATE / TUSSENWONING

Similar to the Terraced Corner archetype, the heating demand for Terraced Intermediate archetypes shows a consistent decline, primarily driven by improvements in envelope insulation and airtightness.

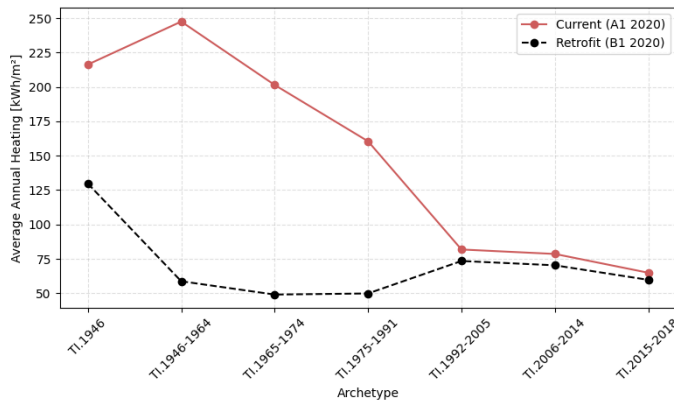


Figure 102: Terraced Intermediate average heating demand for simulations A1, B1.

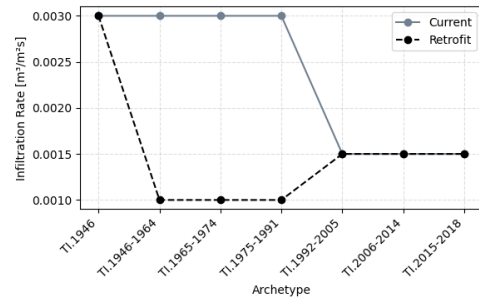


Figure 103: Terraced Intermediate infiltration rate [m³/m²s].

The WWR fluctuates, while the window performance (U-factor and SHGC) only improves in more recent archetypes, 1992-2005 and beyond.

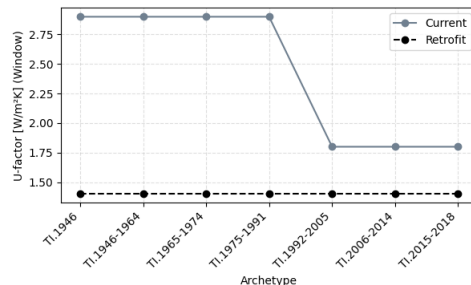


Figure 104: Terraced Intermediate window U-factor [W/m²K].

Again, the cooling demand rises from earlier to more recent archetypes, reflecting the combined impact of better insulation, reduced infiltration, and initially constant window properties until after 1992.

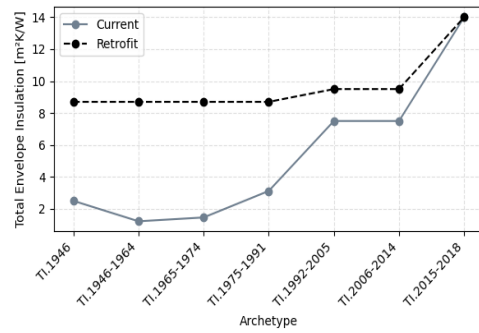


Figure 105: Terraced Intermediate total envelope insulation [m²K/W].

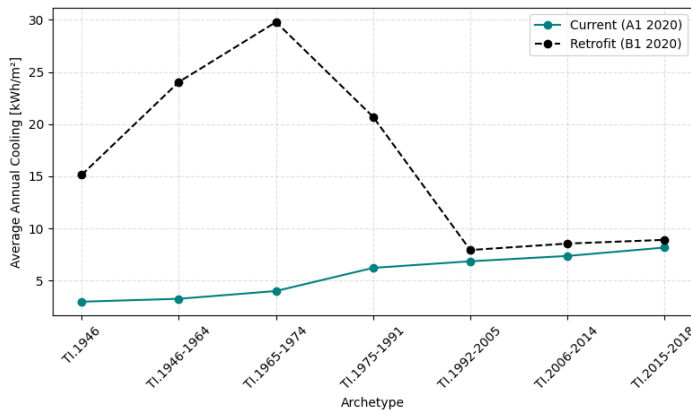


Figure 106: Terraced Intermediate average cooling demand for simulations A1, B1.

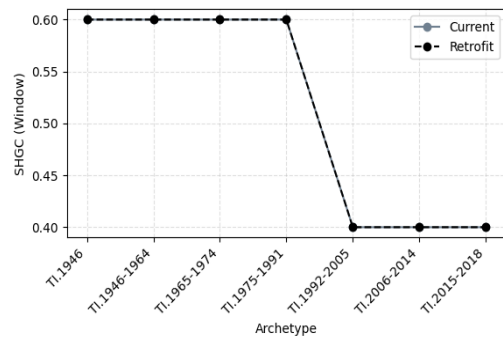


Figure 107: Terraced Intermediate SHGC.

When both SHGC and U-factor are reduced in 1992-2005, the increase in cooling demand is moderate.

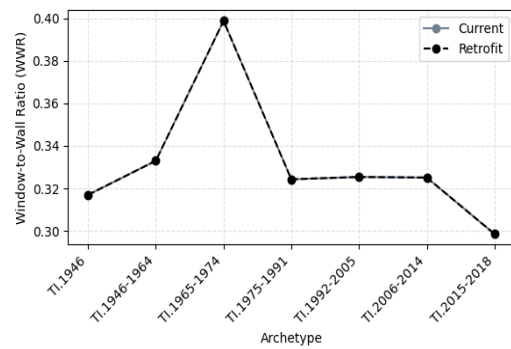


Figure 108: Terraced Intermediate WWR.

FUTURE CLIMATE

The results across Detached, Terraced Corner, and Terraced Intermediate houses show a consistent reduction in average heating demand when projecting to the 2050 and 2080 weather scenarios.

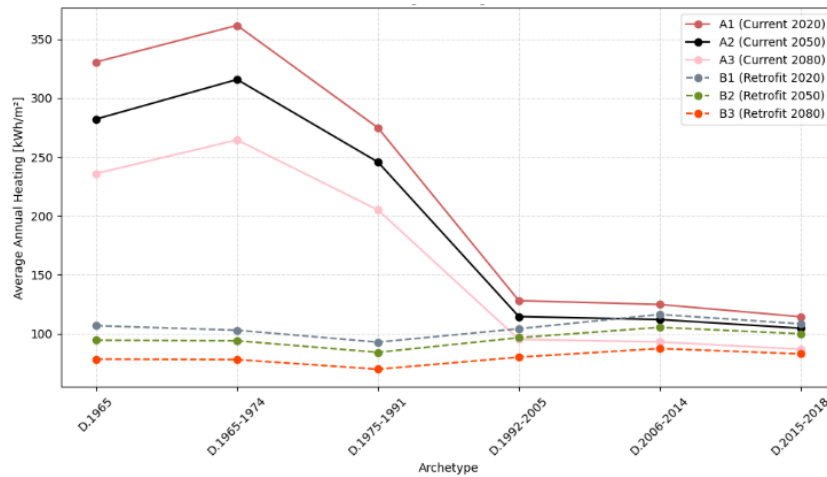


Figure 109: Detached average heating demand for all simulation scenarios.

This downward trend can be attributed largely to the anticipated milder winters under future climate conditions, which reduce the temperature difference between indoor and outdoor environments and therefore the need for space heating.

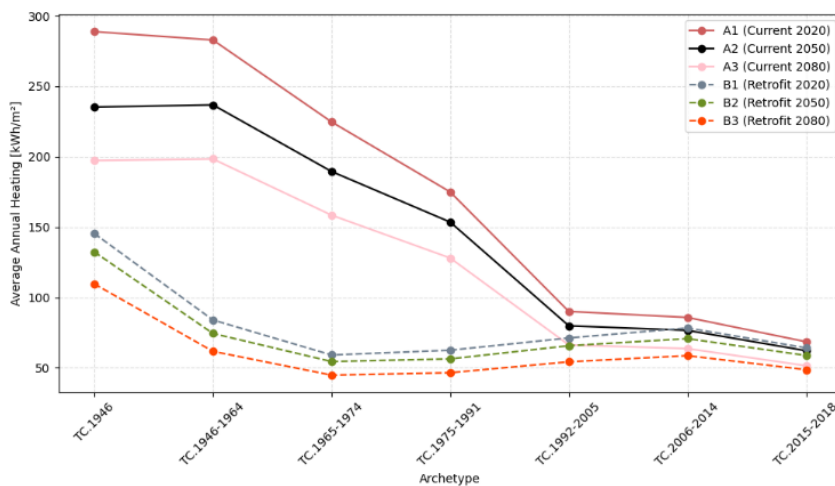


Figure 110: Terraced Corner average heating demand for all simulation scenarios.

The retrofit scenarios introduce further reductions in heating demand for each archetype and future weather scenario. The retrofits considered including improved airtightness (lower infiltration rates), increased envelope insulation and windows with reduced U-values, act to lower transmission heat losses.

Retrofit values for infiltration, insulation, and window U-values remain constant across future scenarios, isolating the effect of the future weather on heating demand. Notably, the heating demand is always lowest for simulation B3, considering a retrofit at the future climate 2080.

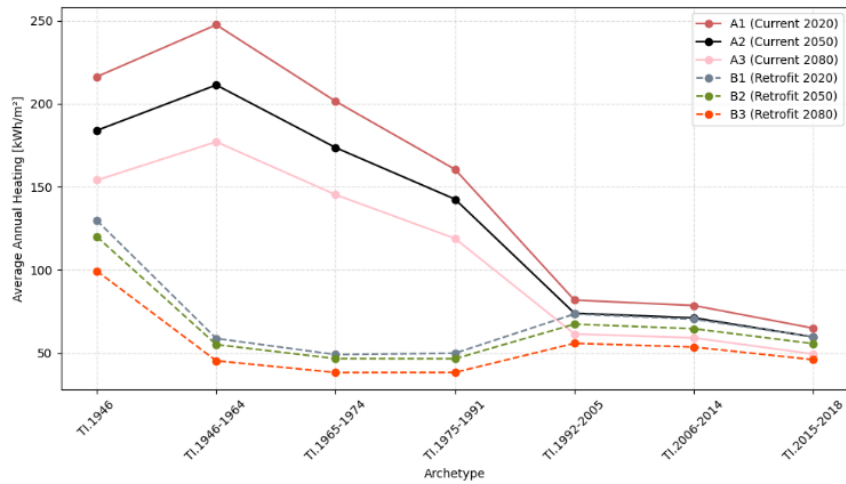


Figure 111: Terraced Intermediate average heating demand for all simulation scenarios.

Across all building typologies, the analysis shows an increase in average cooling demand under projected 2050 and 2080 weather scenarios. Unlike heating demand, where retrofits consistently reduce the demand, for cooling, the application of retrofit strategies results in an increased cooling demand.

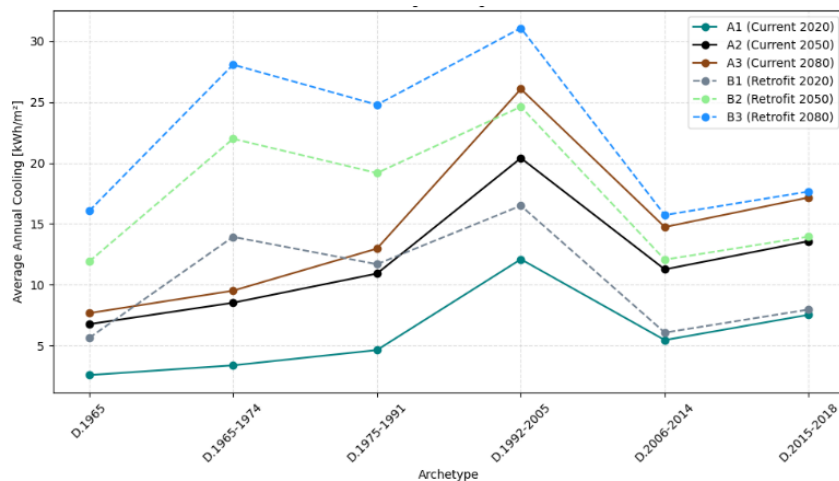


Figure 112: Detached average cooling demand for all simulation scenarios.

This trend again demonstrates that retrofits targeting the building envelope that are effective in reducing heat loss (and thus heating demand), may not adequately address solar gains that dominate summer cooling loads. Excessive airtightness and high insulation without adequate shading or ventilation measures, can increase overheating risk and significantly increase cooling demands.

The observed results thus highlight a fundamental challenge for future retrofit strategies: the need to balance reductions in heating demand with effective mitigation of cooling loads.

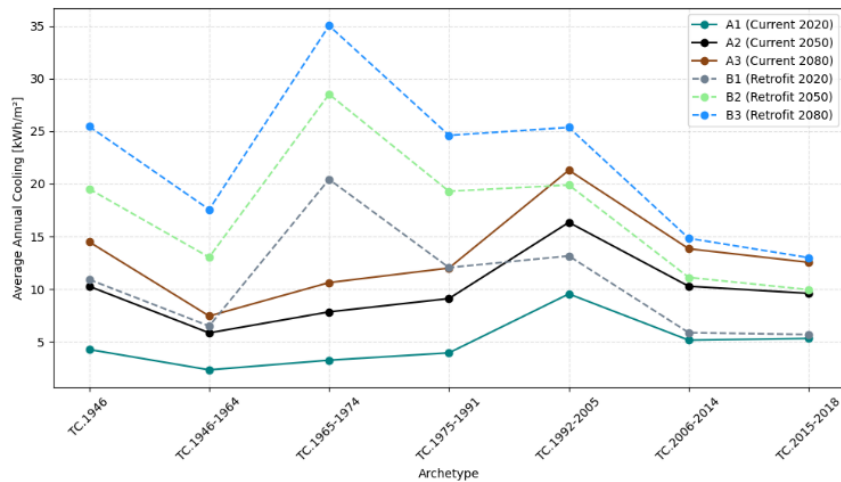


Figure 113: Terraced Corner average cooling demand for all simulation scenarios.

The analysis is based on a fixed retrofit scenario and does not account for parameters such as external shading, heat recovery ventilation, or internal loads and occupant behaviours. Future work should expand retrofit measures beyond envelope improvements, including external shading devices and improved glazing technologies (such as low SHGC coatings) to develop retrofit solutions that are resilient to both current and projected future climates.

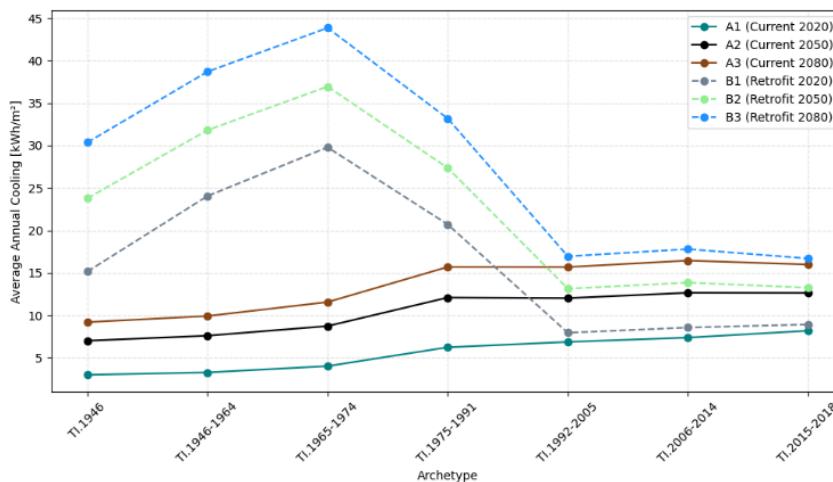


Figure 114: Terraced Intermediate average cooling demand for all simulation scenarios.

VALIDATION

Validating the EnergyPlus simulations was a challenge in this project. The NTA 8800 energy labels for primary energy consumption was used as a reference to interpret the simulated total energy demands (comprised of space heating and cooling). Following the NTA 8800 standard, which defines energy performance as the “measured or calculated energy required by building installations”, the total energy demands were mapped to the corresponding energy labels, to see how the archetypes translate to recognized performance classes (NTA 8800:2022 Nl, 2022). As well, this mapping was used check that the simulated demands were within the recognized energy label classes. Demands outside of these label classes, for example extreme outliers above 1000 kWh/m², were excluded from the dataset (in this case three Pand IDs were excluded).

Table 16: NTA 8800 energy labels.

ENERGY LABEL (NTA 8800)	PRIMARY FOSSIL ENERGY CONSUMPTION [kWh/m ²]
A++++	<= 0
A+++	<= 50
A++	> 50 <= 80
A+	> 80 <= 110
A	> 110 <= 165
B	> 165 <= 195
C	> 195 <= 255
D	> 255 <= 300
E	> 300 <= 345
F	> 345 <= 390
G	>390

The distribution of energy labels for the simulated dataset are shown in Figure 115, for simulations A1 and B1 (current and retrofit constructions at the current weather state).

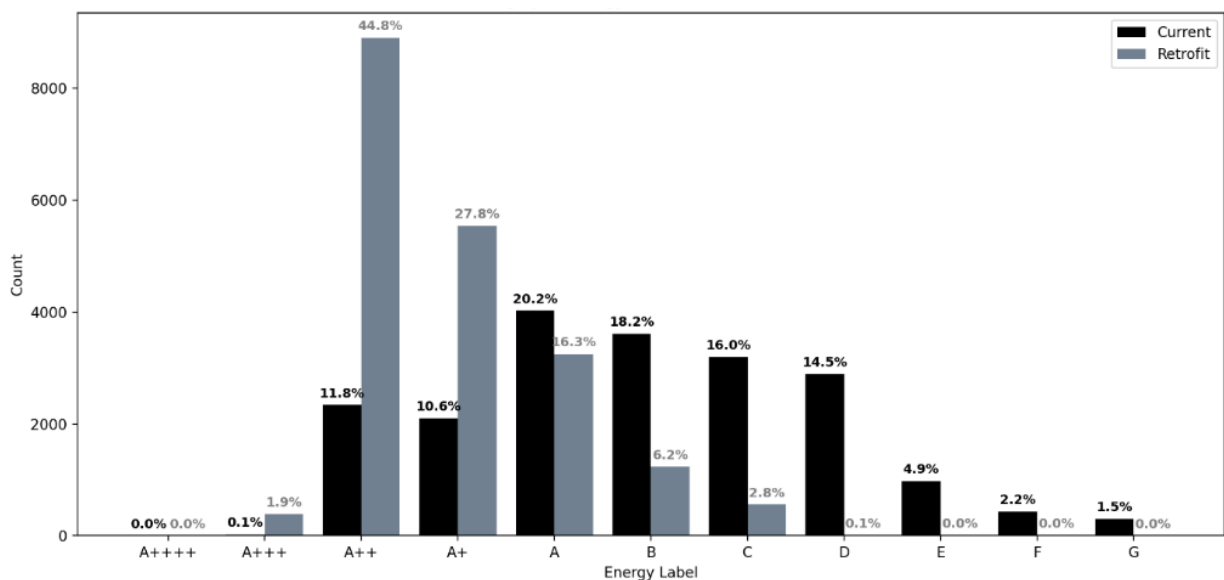
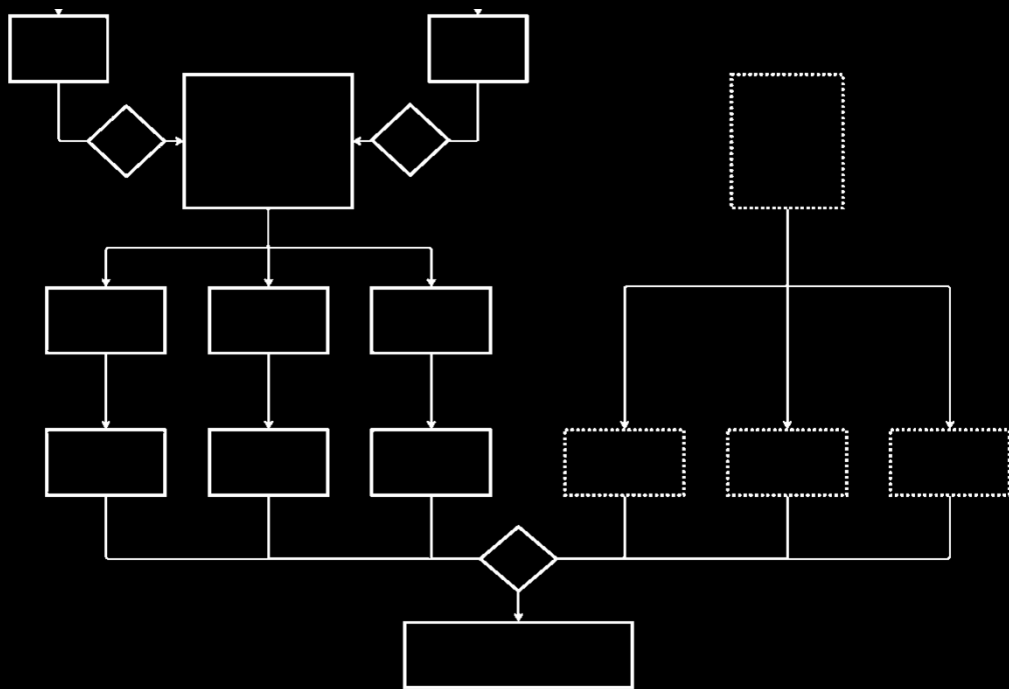


Figure 115: Distribution of simulated total energy demands within each energy label class for scenarios A1 and B1.

However, this method provides only a general indication if simulation results are reasonable, rather than building-specific validation.

A better strategy would involve direct comparison with measured values from EP-Online, the NL national database of building energy performance and energy performance indicators (*EP-Online*, n.d.). Using the EP-Online tool, users can search for individual Pand IDs and retrieve the corresponding heating demands. Note EP-Online does not provide cooling demands. This method is useful for spot-checking results; however, it is impractical to manually validate tens of thousands of buildings. As well differences in modelling assumptions present further limitations.

It is technically feasible to request large batches of energy label data via the EP-Online API, which would theoretically enable large-scale validation and comparison. However, this approach was not implemented within the scope of the study. Future work should prioritize the development of a scalable validation methodology to enhance the confidence in simulation outputs.



7

DATA STRUCTURE

WORKFLOW
VERTEX DATA
FEATURE SET

7. DATA STRUCTURE

The data structuring phase involved preparing the input datasets for ML. This process was highly iterative, involving understanding an appropriate way to handle the dataset size, complexity, scaling, and merging.

WORKFLOW

The input datasets were flattened from the JSONs to CSVs to create tabular structures that could be easily read to check for issues such as missing values. This involved structuring building features (geometric properties), constructions (envelope and window properties), weather data (average monthly temperatures), and vertex data (surface vertices).

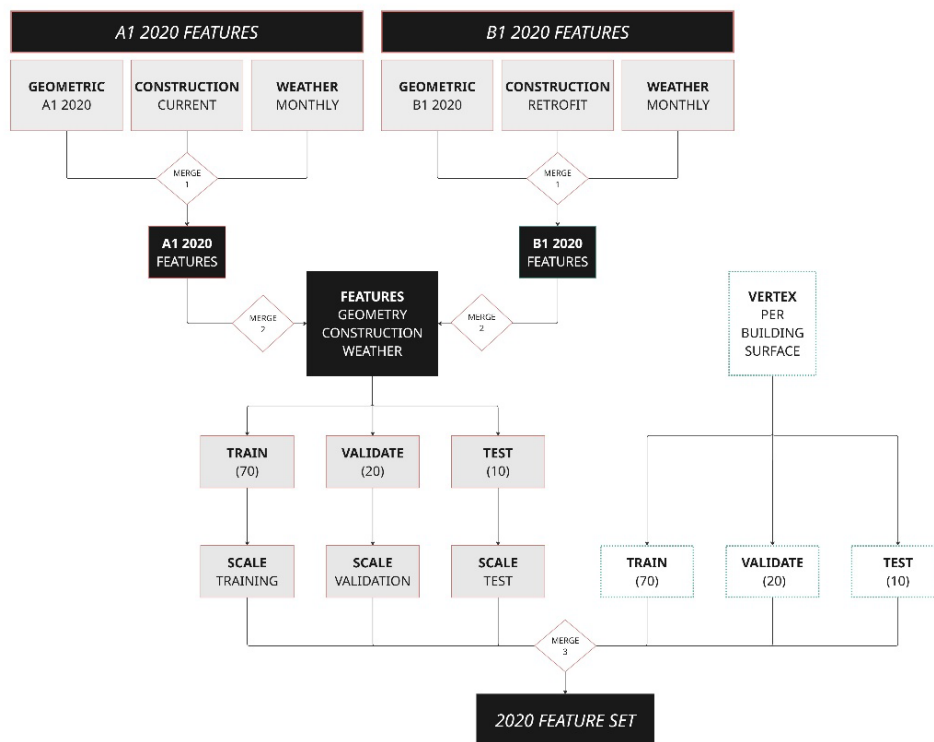


Figure 116: Data structuring workflow.

Merging steps combined the geometric, constructions, weather, and vertex datasets into a single dataset with all relevant input variables. Additional merging was required to combine the current A1 feature set with the B1 feature set to capture both current and retrofit construction features.

Once merged, the data was split into training, validation, and test sets using a 70/20/10 split. The input features were scaled using both standard scaling and min-max scaling to normalize the feature ranges. The data structure methodology is presented in Figure 116.

VERTEX DATA

The building surface data, represented by vertices, provides additional spatial information that can enhance the heating and cooling demand predictions. The vertices were structured as model inputs using the distances from each vertex to surface centroid, and corresponding orientation, as a unit vector.

The vertex angles (θ) were transformed into unit pairs (u_x, u_y) to avoid discontinuity at $0^\circ/360^\circ$, where 0° and 360° represent the same direction, but numerically they are at opposite ends of the scale.

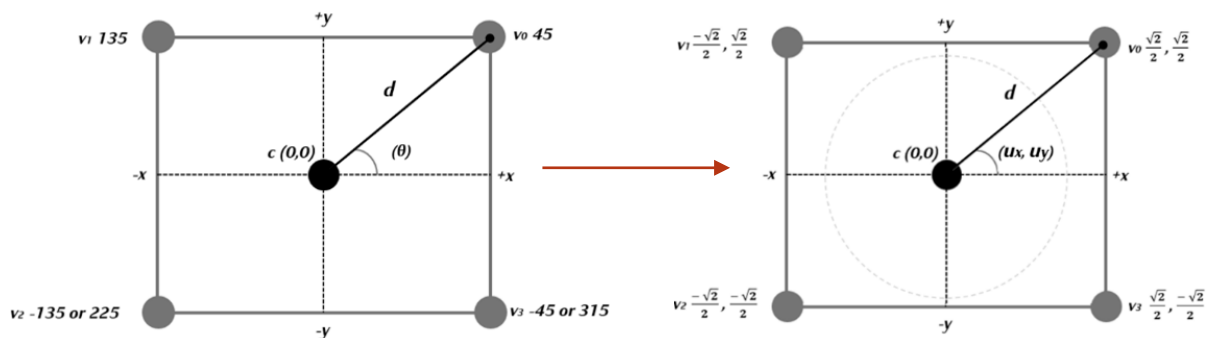


Figure 117: Structuring vertex data to polar coordinates.

An example of the data structure for a single building or Pand ID is shown in Table 17. Note, to represent the surface data, there are multiple rows of data for each Pand ID. The impact of this data structure on model predictions is discussed in section, FEATURE SET B.

Table 17: Structure of building surface data.

Pand ID	Surface Index	Surface Type	d_1	u_{x1}	u_{y1}
0599100000013430	0	G	d_{G1}	u_{xG1}	u_{yG1}
0599100000013430	1	F	d_{F1}	u_{xF1}	u_{yF1}
0599100000013430	2	F	d_{F1}	u_{xF1}	u_{yF1}
0599100000013430	3	F	d_{F1}	u_{xF1}	u_{yF1}
0599100000013430	4	F	d_{F1}	u_{xF1}	u_{yF1}
0599100000013430	5	R	d_{R1}	u_{xR1}	u_{yR1}

FEATURE SET

Feature engineering was conducted to introduce key features to the dataset, which capture important aspects of the building form and relate to energy performance:

Equation 15: Total floor area, expressed in m².

$$\text{Total floor area} = \text{Floor area} \times \text{Number of floors}$$

Equation 16: Building volume, expressed in m³

$$\text{Building volume} = \text{Floor area} \times \text{Building height}$$

Equation 17: Compactness ratio, expressed in m⁻¹.

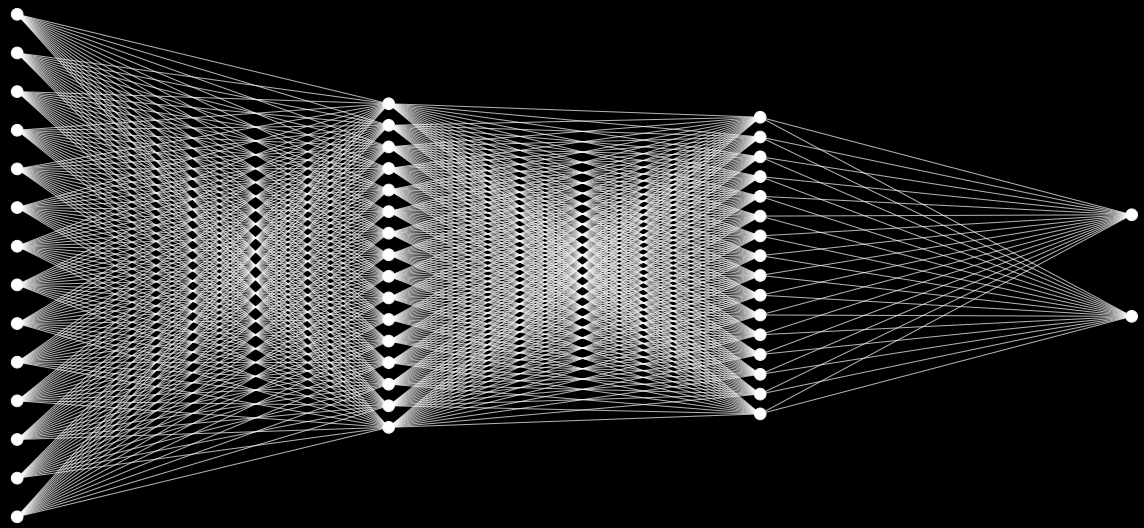
$$\text{Compactness ratio} = \text{Wall area} / \text{Building volume}$$

The complete feature set used for the ML development stage is shown in Table 18.

Table 18: Complete feature set for ML development.

Feature	Units	Variable Type	Normalization
IDENTIFIERS			
Pand ID	-	Categorical	-
Archetype	-	Categorical	-
Construction Year	-	Discrete	-
GEOMETRIC			
Number of Floors	-	Discrete	Standard-Scale
Wall Area	m ²	Continuous	Standard-Scale
Roof Area (Flat)	m ²	Continuous	Standard-Scale
Roof Area (Sloped)	m ²	Continuous	Standard-Scale
Floor Area	m ²	Continuous	Standard-Scale
Shared Wall Area	m ²	Continuous	Standard-Scale
Building Height (70%)	m	Continuous	Standard-Scale
Building Volume	m ³	Continuous	Standard-Scale
Total Floor Area	m ²	Continuous	Standard-Scale
Compactness Ratio	m ⁻¹	Continuous	Standard-Scale
CONSTRUCTION			
Ground Floor Insulation	m ² K/W	Continuous	Standard-Scale
Facade Insulation	m ² K/W	Continuous	Standard-Scale
Roof Insulation	m ² K/W	Continuous	Standard-Scale
Infiltration	m ³ /sm ²	Continuous	Standard-Scale
Window to Wall Ratio (WWR)	m ² /m ²	Continuous	Standard-Scale
U Factor	W/m ² K	Continuous	Standard-Scale
SHGC	-	Continuous	Standard-Scale

WEATHER			
Monthly average temperature	°C	Continuous	-
Monthly average solar radiation	kWh/m ² /day	Continuous	-
VERTICES			
Distance (d) from centroid	-	Continuous	Standard Scale
Angle (u _x)	-	Continuous	Polar Angle
Angle (u _y)	-	Continuous	Polar Angle
TARGETS			
Annual heating demand	kWh/m ²	Continuous	Min-Max Scale
Annual cooling demand	kWh/m ²	Continuous	Min-Max Scale



8

ML DEVELOPMENT

ARCHITECTURE

PHASE 1

PHASE 2

PHASE 3

8. ML DEVELOPMENT

A regression based artificial neural network (ANN) was developed to predict the energy demands, from the input building and climatic data. The objectives were to:

1. Understand the impact of retrofit strategies across different building archetypes as well as relationships between construction inputs and energy performance.
2. Test the model's prediction ability for future climate scenarios.

Training used the sampled dataset of 20,000 Pand IDs, using proportional sampling of the building archetypes from the full dataset of approximately 75,000 Pand IDs. This approach was chosen instead of an equal sampling of archetypes to avoid inflating the importance of less represented archetypes. For example, based on the significantly smaller distribution of Detached house types compared to Terraced Intermediate houses.

The development was a highly iterative process; several training iterations are referenced below as well as in APPENDIX C.

ARCHITECTURE

The ANN was initialized with an input layer, a single hidden layer, and an output layer, shown in Figure 118.

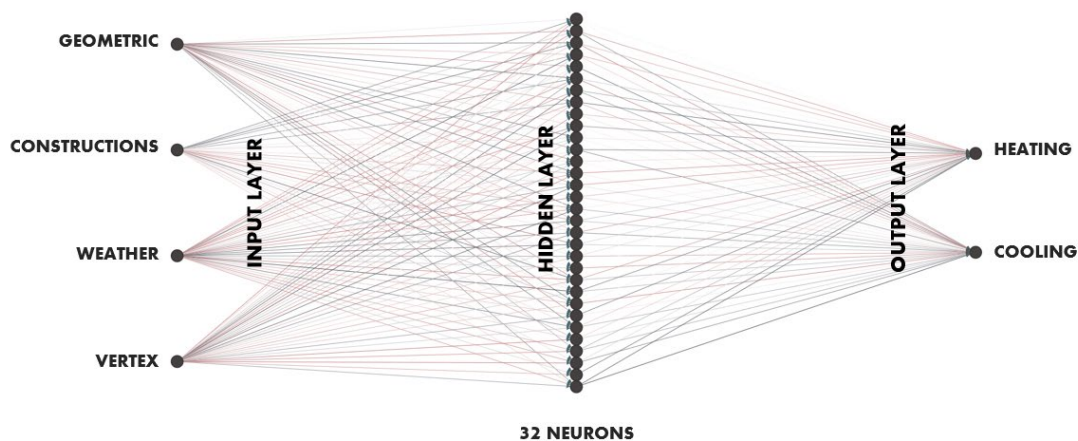


Figure 118: ANN model schematic.

A feed-forward architecture was used, meaning that the data moves forward from the input layer, through the hidden layer, and finally to the output layer, without looping back. The code excerpt to initialize the model is shown in Figure 119.

```
class ANN(nn.Module):
    def __init__(self, in_dim, hidden, out_dim=2):
        super().__init__()
        self.net = nn.Sequential(
            nn.Linear(in_dim, hidden), nn.ReLU(),
            nn.Linear(hidden, out_dim)
        )
    def forward(self, x):
        return self.net(x)
model = ANN(len(X_COLS), HIDDEN)
criterion = nn.MSELoss()
optimizer = optim.Adam(model.parameters(), lr=LR)
```

Figure 119: Code to initialize preliminary ANN.

INPUT LAYER

The input layer describes the features that the model uses to train from and make predictions. The number of features were varied between iterations to understand the model's prediction capabilities with different input sets, but in general were made up of geometric, weather, construction, and vertex features, as shown in Figure 118.

HIDDEN LAYER

The hidden layer is as an intermediate step in the ANN that transforms the inputs to predicted outputs through weighted connections to capture complex non-linear relationships that are not clearly defined from the input data. The model was initially defined using a single hidden layer with 32 neurons, meaning there are 32 independent computational units, enabling the model to learn complex patterns between building input features and corresponding energy outputs.

OUTPUT LAYER

The output layer was also varied throughout the model development phases. But in general, is comprised of the two prediction outputs:

- Annual Heating Demand [kwh/m²]
- Annual Cooling Demand [kwh/m²]

PHASE 1

The Phase 1 modelling approach involved explicitly training the ANN to predict four distinct outputs:

- Current Annual Heating Demand
- Current Annual Cooling Demand
- Retrofit Annual Heating Demand
- Retrofit Annual Cooling Demand

This preliminary setup was used to verify the ANN's capability to capture the differential impact of retrofit strategies on energy performance, using clearly labeled baseline and retrofit scenarios. The model architecture is shown in Figure 120.

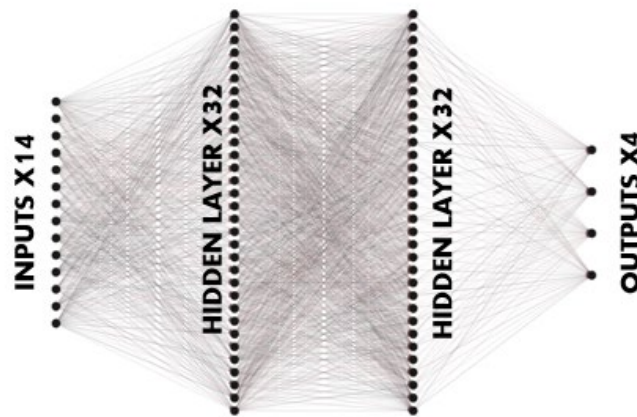


Figure 120: Phase 1 ANN model architecture.

The preliminary model uses a minimum number of features from the geometric feature set and was used to develop a stable and interpretable prediction model before increasing the complexity with added features. Note, Phase 1 training was conducted prior to the addition of adiabatic surface labels and the addition of windows. The Phase 1 training inputs are shown in Table 19.

Table 19: Phase 1 training features.

Feature	Units	Variable Type	Normalization
GEOMETRIC			
Number of Floors	-	Discrete	Standard-Scale
Wall Area	m ²	Continuous	Standard-Scale
Floor Area	m ²	Continuous	Standard-Scale
Building Height (70%)	m	Continuous	Standard-Scale
CURRENT CONSTRUCTION			
Ground Floor Insulation	m ² K/W	Continuous	Standard-Scale
Facade Insulation	m ² K/W	Continuous	Standard-Scale
Roof Insulation	m ² K/W	Continuous	Standard-Scale
Infiltration	m ³ /sm ²	Continuous	Standard-Scale
RETROFIT CONSTRUCTION			
Ground Floor Insulation	m ² K/W	Continuous	Standard-Scale
Facade Insulation	m ² K/W	Continuous	Standard-Scale
Roof Insulation	m ² K/W	Continuous	Standard-Scale
Infiltration	m ³ /sm ²	Continuous	Standard-Scale
WEATHER			
Annual average temperature	°C	Continuous	-
Annual average solar radiation	kWh/m ² /day	Continuous	-

During the training, the MSE was used to check for issues such as overfitting or underfitting. The model should depict a steady decrease in training loss, eventually stabilizing at a minimum value without excessive fluctuations between decreasing and increasing loss.

Multiple training iterations were conducted, each producing distinct training loss curves, shown in Figure 121, where the variations in model convergence between multiple runs can be observed. For each iteration, the MSE curves were analyzed to identify the model iteration with the lowest and most stable training loss.

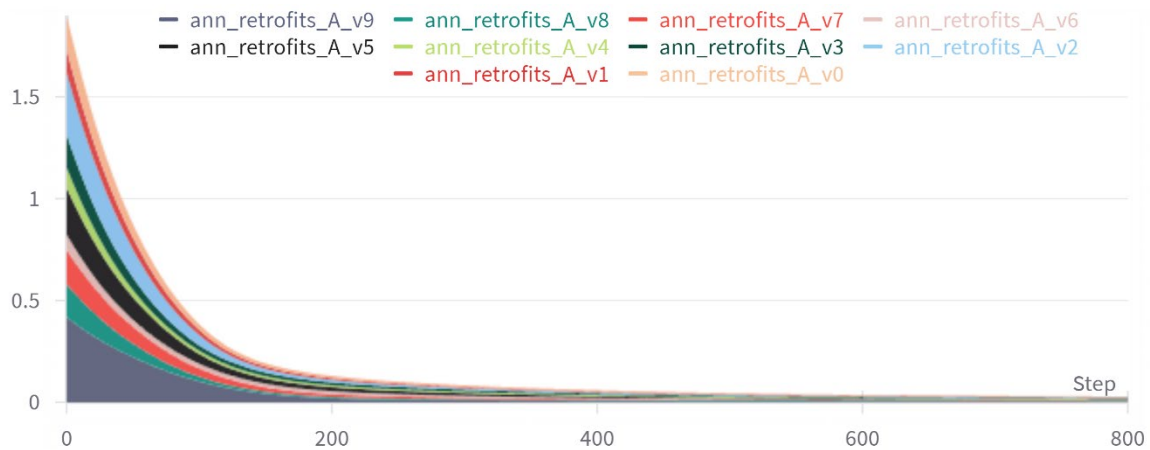


Figure 121: Phase 1 MSE loss curve, showing several iterations of training runs.

After selecting the best-performing iteration, the test-set predictions were used to assess the model's prediction ability. For heating, the model predictions at the current or baseline construction state (left) and retrofit construction state (right) are shown in Figure 122.

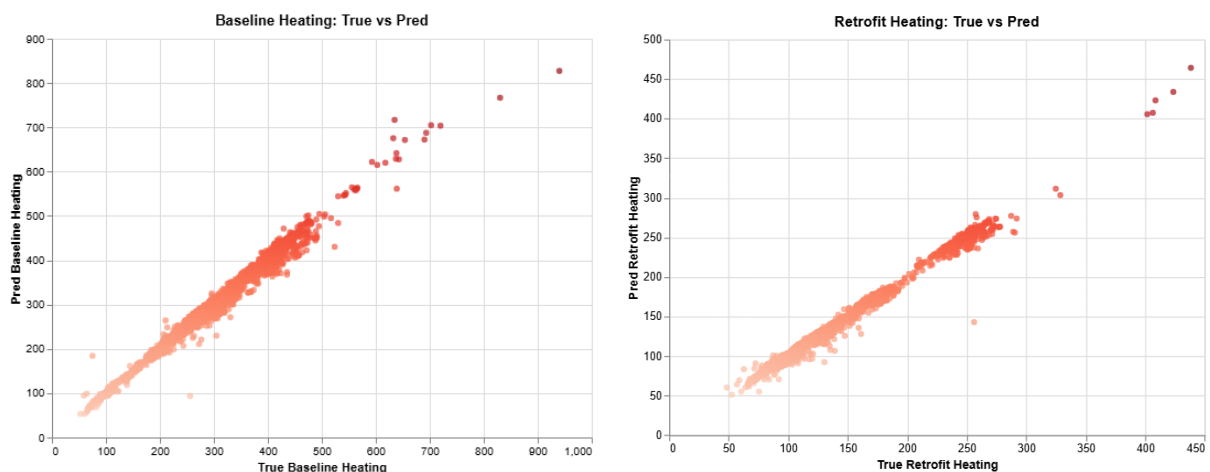


Figure 122: Annual heating demand predictions in $[kwh/m^2]$ at the current or baseline state (left) and retrofit construction state (right).

For cooling, the predictions for baseline and retrofit conditions are shown in Figure 123.

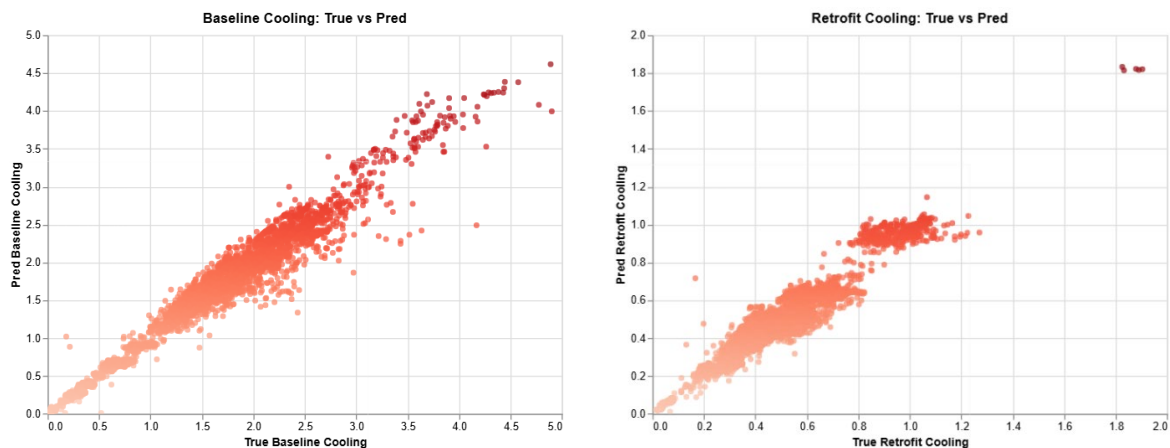


Figure 123: Annual cooling demand predictions in [kwh/m2] at the current or baseline state (left) and retrofit construction state (right).

Although valuable as an initial model development stage and validation of prediction ability with the input features, this approach has limited capacity for generalization. Since the construction inputs are explicitly labelled for current versus retrofit scenarios. Similarly, the heating and cooling demand outputs are explicitly labelled for current versus retrofit. This feature setup restricts the model's ability to generalize beyond these trained conditions.

PHASE 2

In Phase 2 the construction inputs were fed to the model without explicitly labelling as baseline or retrofit. Thus, the ANN is simplified by predicting only two outputs for

- Annual Heating Demand
- Annual Cooling Demand

With this structure, the objective was to improve the ANN's generalization to construction inputs, allowing flexibility to incorporate and evaluate a range of retrofit scenarios.

To understand the contribution of specific input features to the overall model performance, an ablation study was conducted. An ablation study involves training a model with all features then iteratively removing one feature or a group of features and observing the corresponding change in performance in terms of prediction accuracy and training loss (Ablation Studies, 2024).

This staged reduction approach was used to identify the minimum geometric data required for ANN predictions to simplify the input space and potentially improve model generalization. The study started with four datasets: geometric, construction, weather, and vertices. At each stage the weather and construction features were kept the same, and the number of geometric features used for training were reduced. As well later stages removed the vertex dataset from the training.

At Phase 2 model features still did not incorporate adiabatic surfaces or windows, however this phase provided a training framework to use at the next phase, once these input features were defined. The results are shown in APPENDIX C, PHASE 2.

PHASE 3

At Phase 3 the model features now included adiabatic surfaces labels and windows. The same staged reduction (ablation) approach was applied as in Phase 2, focusing on reducing geometric input features and assessing ANN predictions. However, in this phase, weather data was excluded from training. This decision was made since the weather variables were constant across the training dataset (i.e the monthly average temperatures and solar radiations were constant for all building archetypes). And therefore, did not provide additional information to the model. Although weather features were initially included to enable training with future weather scenarios, this was not implemented in Phase 3 due to time constraints. The primary goal of Phase 3 thus remained to simplify the input feature set while maintaining model performance.

FEATURE SET A

The initial model used all available geometric input features for heating and cooling predictions. The training feature set for stage A is shown below in Table 20.

Table 20: Feature Set A.

Feature	Units	Variable Type	Normalization
GEOMETRIC			
Number of Floors	-	Discrete	Standard-Scale
Wall Area	m ²	Continuous	Standard-Scale
Roof Area (Flat)	m ²	Continuous	Standard-Scale
Roof Area (Sloped)	m ²	Continuous	Standard-Scale
Floor Area	m ²	Continuous	Standard-Scale
Shared Wall Area	m ²	Continuous	Standard-Scale
Building Height (70%)	m	Continuous	Standard-Scale
Total Floor Area	m ²	Continuous	Standard-Scale
Building Volume	m ³	Continuous	Standard-Scale
Compactness Ratio	m ⁻¹	Continuous	Standard-Scale
CONSTRUCTION			
Ground Floor Insulation	m ² K/W	Continuous	Standard-Scale
Facade Insulation	m ² K/W	Continuous	Standard-Scale
Roof Insulation	m ² K/W	Continuous	Standard-Scale
Infiltration	m ³ /sm ²	Continuous	Standard-Scale
Window to Wall Ratio (WWR)	m ² /m ²	Continuous	Standard-Scale
U Factor	W/m ² K	Continuous	Standard-Scale
SHGC	-	Continuous	Standard-Scale

VERTICES			
Distance (d) from centroid	-	Continuous	Standard-Scale
Angle (u_x)	-	Continuous	Polar Angle
Angle (u_y)	-	Continuous	Polar Angle

FEATURE SET B

Next, the feature set removed specific area and height measurements and focused on using aggregated geometric descriptors: total floor area, building volume, compactness ratio, as well as surface vertices. The compactness ratio was used because it efficiently summarizes the relationship between a building's surface area and volume and is cited in several papers for its strong impact on thermal energy losses and gains, as well as influence as a feature for ML prediction (Wahi et al., 2024). This stage tested if the model could predict while relying on more generalized geometric features.

Table 21: Feature Set B.

Feature	Units	Variable Type	Normalization
GEOMETRIC			
Shared Wall Area	m^2	Continuous	Standard-Scale
Total Floor Area	m^2	Continuous	Standard-Scale
Building Volume	m^3	Continuous	Standard-Scale
Compactness Ratio	m^{-1}	Continuous	Standard-Scale
CONSTRUCTION			
Ground Floor Insulation	m^2K/W	Continuous	Standard-Scale
Facade Insulation	m^2K/W	Continuous	Standard-Scale
Roof Insulation	m^2K/W	Continuous	Standard-Scale
Infiltration	m^3/sm^2	Continuous	Standard-Scale
Window to Wall Ratio (WWR)	m^2/m^2	Continuous	Standard-Scale
U Factor	W/m^2K	Continuous	Standard-Scale
SHGC	-	Continuous	Standard-Scale
VERTICES			
Distance (d) from centroid	-	Continuous	Standard-Scale
Angle (u_x)	-	Continuous	Polar Angle
Angle (u_y)	-	Continuous	Polar Angle

It was found after training that the structure of the vertex data (shown in Table 17) created bias within the model. After merging the building features with the vertex data, the heating and cooling targets are copied once per surface, so for a building with 6 surfaces, the targets are represented 6 times.

The number of surfaces for a single building range from 6 to 38. Thus, the model is biased towards predictions for buildings with more complex geometries, with more surface data. The model's gradient is skewed to minimize the error for buildings with more surfaces, which may result in simpler building geometries being not being well predicted.

At the same time, since each surface of the building is mapped to the same heating and cooling targets, the surface features lose importance. The model is forced to output identical values for different surface vectors, which shrinks the weights to zero. Resolving this data structuring issue should be explored in future work.

FEATURE SET C

The reduction from feature set B to C involved removing the vertex data, and training with only the shared wall area, building volume, total floor area, and compactness ratio for geometric features. This stage helped to inform whether explicit geometry captured by vertex data was necessary for accurate model predictions, or if general geometric features were sufficient.

Table 22: Feature Set C.

Feature	Units	Variable Type	Normalization
GEOMETRIC			
Shared Wall Area	m ²	Continuous	Standard-Scale
Total Floor Area	m ²	Continuous	Standard-Scale
Building Volume	m ³	Continuous	Standard-Scale
Compactness Ratio	m ⁻¹	Continuous	Standard-Scale
CONSTRUCTION			
Ground Floor Insulation	m ² K/W	Continuous	Standard-Scale
Facade Insulation	m ² K/W	Continuous	Standard-Scale
Roof Insulation	m ² K/W	Continuous	Standard-Scale
Infiltration	m ³ /sm ²	Continuous	Standard-Scale
Window to Wall Ratio (WWR)	m ² /m ²	Continuous	Standard-Scale
U Factor	W/m ² K	Continuous	Standard-Scale
SHGC	-	Continuous	Standard-Scale

By eliminating vertices, and solely using aggregated geometric characteristics, the input data was largely simplified. This streamlined the data structuring process as well since there was no longer a need to merge the feature set with the surface vertex data. The simplified data structuring workflow is shown in Figure 124.

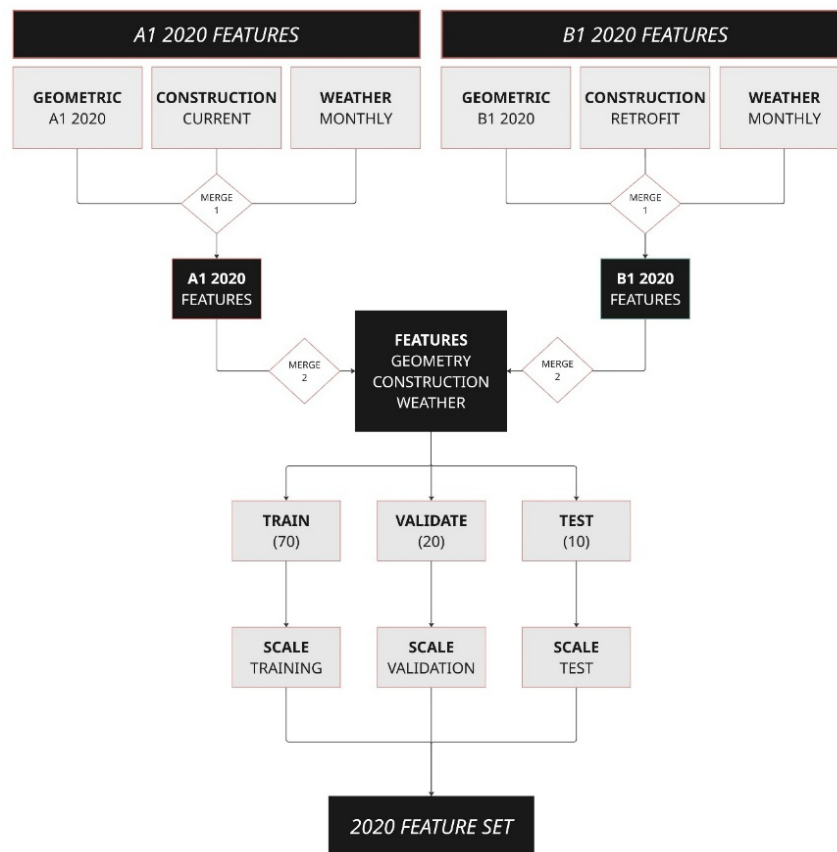


Figure 124: Data structuring workflow, without vertex data.

FEATURE SET D

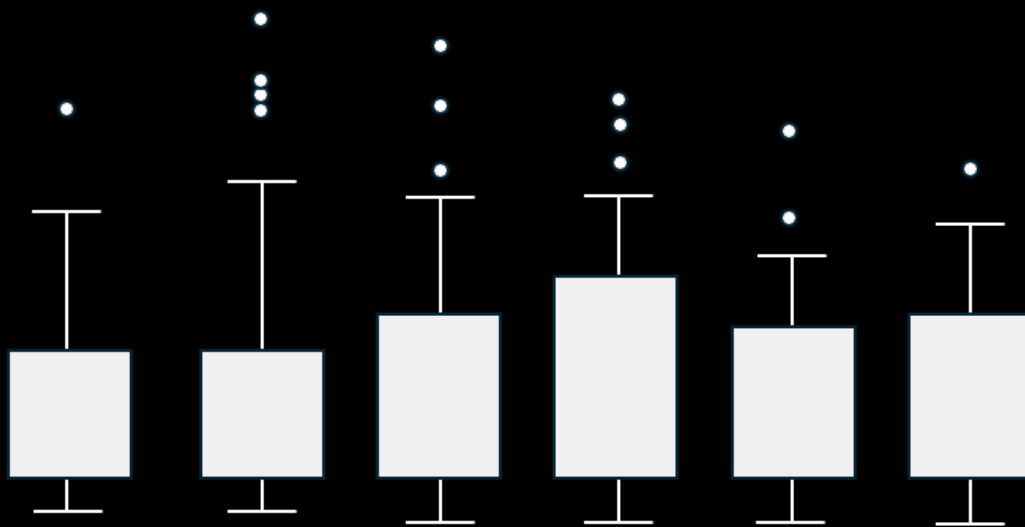
The last stage of training used the number of floors, wall area, floor area, shared wall area and building height, as geometric features. These features were selected to capture the most essential geometric properties to minimize redundancy and input complexity.

Number of floors and building height together provide an indication of compactness, which impacts the internal volume and heat transfer surfaces. The wall area is critical for modelling heat loss and gain, since it represents the primary envelope through which energy is exchanged. As well the shared wall area captures important boundary conditions (adiabatic surfaces). Floor area provides a measure of building size and conditioned space. The roof area was excluded to avoid redundancy in the input data since for LoD 1.2 geometry, the roof area can be directly inferred from the floor area. The final feature set is shown in Table 23.

Table 23: Feature Set D.

Feature	Units	Variable Type	Normalization
GEOMETRIC			
Number of Floors	-	Discrete	Standard-Scale
Wall Area	m ²	Continuous	Standard-Scale
Floor Area	m ²	Continuous	Standard-Scale
Shared Wall Area	m ²	Continuous	Standard-Scale
Building Height (70%)	m	Continuous	Standard-Scale
CONSTRUCTION			
Ground Floor Insulation	m ² K/W	Continuous	Standard-Scale
Facade Insulation	m ² K/W	Continuous	Standard-Scale
Roof Insulation	m ² K/W	Continuous	Standard-Scale
Infiltration	m ³ /sm ²	Continuous	Standard-Scale
Window to Wall Ratio (WWR)	m ² /m ²	Continuous	Standard-Scale
U Factor	W/m ² K	Continuous	Standard-Scale
SHGC	-	Continuous	Standard-Scale

The prediction results using Feature Set D are discussed in section 9. PERFORMANCE.



9

PERFORMANCE

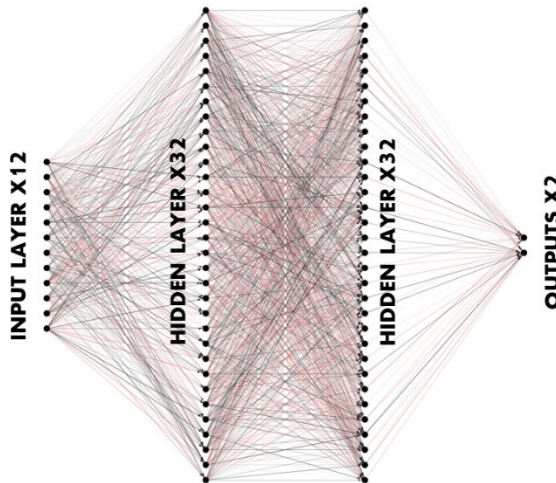
ARCHITECTURE

PREDICTION RESULTS

9. PERFORMANCE

ARCHITECTURE

The final ANN developed for the study is comprised of a fully connected feed-forward architecture with two hidden layers, each containing 32 neurons. The architecture is shown in Figure 125.



- **Input layer:** 12 features
- **First hidden layer:** 32 neurons, ReLU activation
- **Second hidden layer:** 32 neurons, ReLU activation
- **Output layer:** 2 targets for heating and cooling demands

Figure 125: Final ANN architecture using Feature set D.

Based on the ablation study results from the model development phase, Feature set D was used, consisting of 12 input features, normalized prior to training. All hidden layers utilize the rectified linear unit (ReLU) activation function to effectively handle non-linearity.

KEY HYPERPARAMETERS:

- **Learning rate:** 1e-4
- **Hidden neurons per layer:** 32
- **Epochs (max):** 20,000
- **Early stopping patience:** 400 epochs
- **Early stopping delta:** 0.0 (strict improvement)
- **Training set size:** 14,000 buildings

The model is trained using the Adam optimizer with a learning rate of 1e-4. The network is trained for up to 20,000 epochs, with early stopping based on validation loss improvement, using MSE for the loss function. Having the epochs set to 20,000 was found to be a safe metric to ensure training was not stopped too early (before reaching the lowest validation loss). The model incorporates an early stopping feature, by setting patience to 400, meaning the training stops if validation loss does not decrease for 400 consecutive epochs.

Model performance and loss curves are logged throughout training at regular intervals (every 10 epochs), enabling monitoring of convergence and overfitting.

Performance is evaluated on a test set using standard regression metrics, including MAE, RMSE, R², and MAPE. Metrics are computed on the original (unscaled) values to provide interpretable, error results.

PREDICTION RESULTS

The MSE curve from the training set is shown in Figure 126 for several model runs, to observe the model weights that contribute to the lowest validation loss.

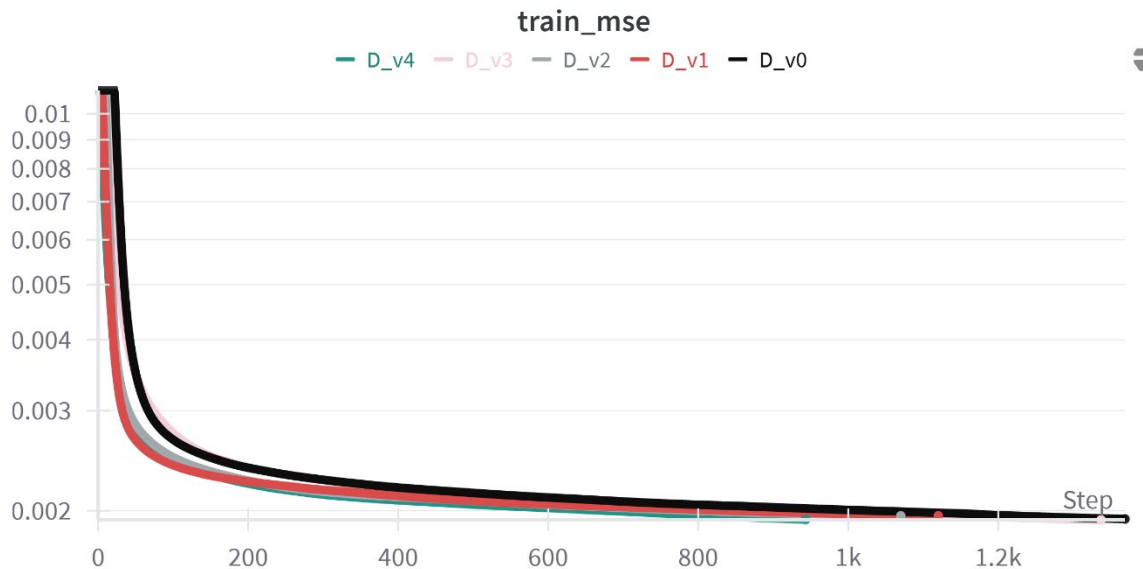


Figure 126: Phase 3 MSE loss curve, showing several iterations of training runs.

The MSE loss curves show a steep initial drop in loss, highlighting that the model quickly learns the relationships between input features and outputs. The loss curves show a smooth decay, decreasing gradually and flattening to a minimum loss between 9000 to 13,000 iterations (extending past the bounds shown in Figure 126). All runs show a similar loss curve, showing the stability of the training set.

HEATING PREDICTIONS

Tracking the error metrics for the test set for heating predictions, it was observed that run V4 produced the lowest MAPE at approximately 7% for heating, as well a strong R^2 of 0.98, indicating a good model fit. A summary of the error metrics is shown in Table 24.

Table 24: Heating prediction errors.

HEATING PREDICTION ERRORS					
RUN	EPOCH	RMSE	MAE	R2	MAPE
V4	9033	12.926	7.719	0.975	6.86%

Based on the low error metrics, the ANN predicts heating with high accuracy. The model predictions for heating are shown in Figure 127 where the predictions are closely aligned with the true values.

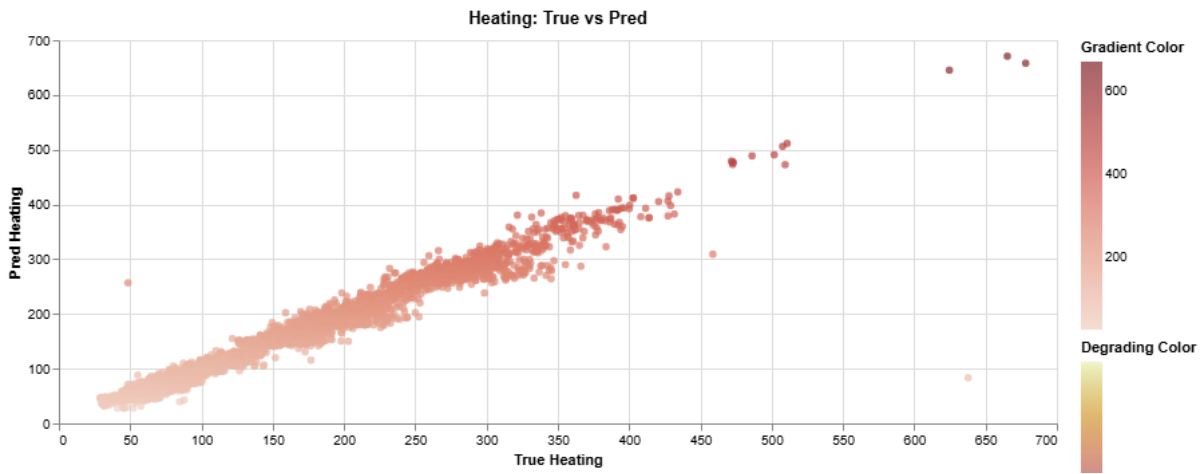


Figure 127: Annual heating predictions with feature set D.

The average heating MAPE is used to evaluate the model’s predictive accuracy across all archetypes, shown in Figure 128.

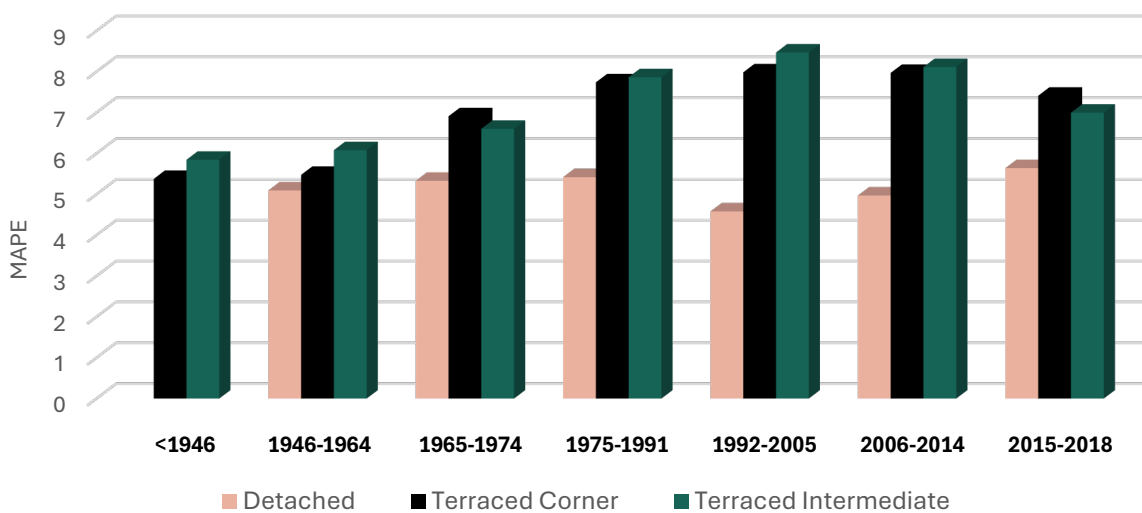


Figure 128: Average heating MAPE (%) per archetype.

The model’s prediction accuracy is highest for the Detached home type, where the average MAPE is around 5.1%, compared to 6.9% and 7.1% for Terraced Corner and Terraced Intermediate, respectively.

The heating MAPE box plots for each archetype show notable differences in model performance. Note that extremes were removed from the box plots for better interpretability but are discussed later in the section.

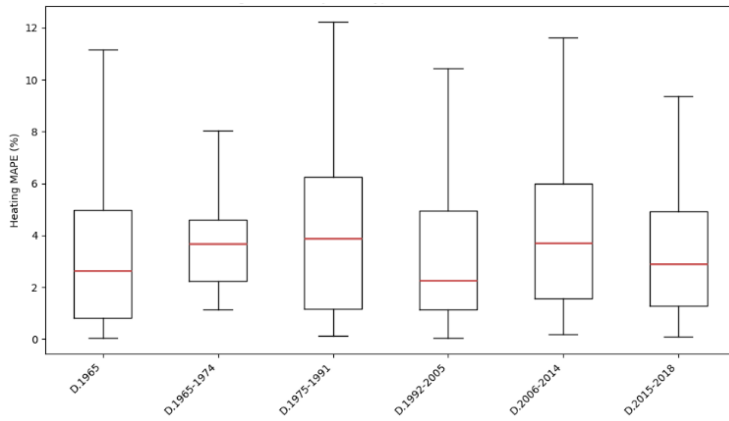


Figure 129: Heating MAPE (%) by archetype: Detached (outliers removed).

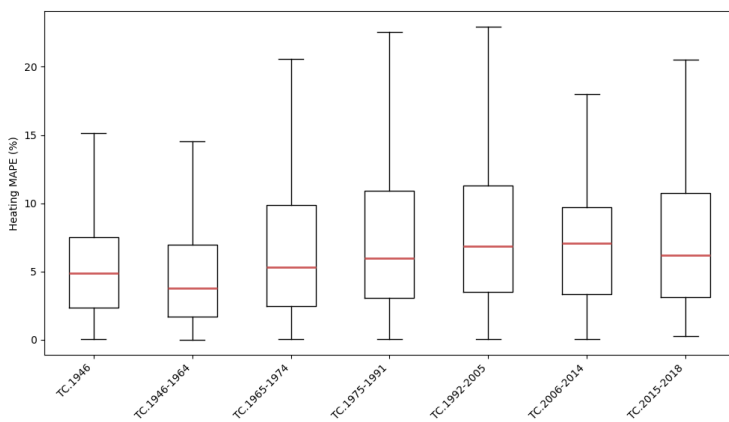


Figure 130: Heating MAPE (%) by archetype: Terraced Corner (outliers removed).

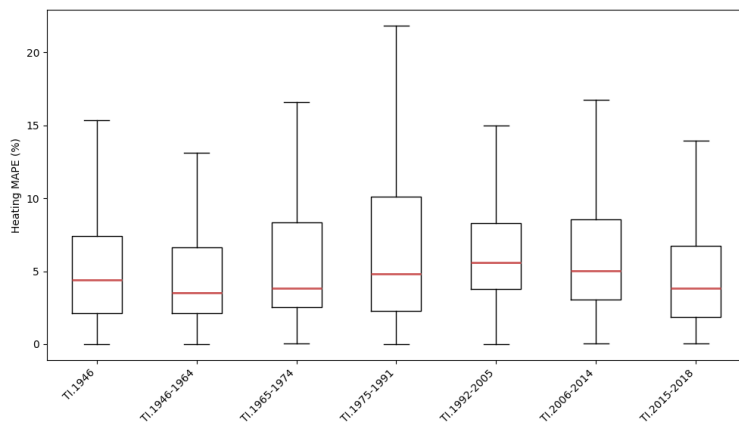


Figure 131: Heating MAPE (%) by archetype: Terraced Intermediate (outliers removed).

For the Detached home type, the median MAPE lies between 2-4% for all archetypes, reflecting strong predictive accuracy. The spread or interquartile range is moderate, with most archetype predictions falling below 10% MAPE. Higher MAPEs are observed, particularly for D.1975-1991 and D.2006-2014, but still below the 15% threshold considered reasonable.

Terraced Corner and Terraced Intermediate archetypes show higher medians compared to the Detached houses, across all archetypes. The increased spread and higher MAPE values suggest greater difficulty in capturing the heating dynamics of these typologies. The variability is particularly large for archetypes TC.1975-1991, TI.1975-1991.

It may seem counterintuitive that the model predicts Detached houses more accurately than terraced houses, since Detached houses typically have greater geometric complexity. However, without explicit vertex data, the model only sees high-level features like floor area and wall area and does not know the specific configuration or surface adjacencies. As well, for Detached houses, the lack of adiabatic

surfaces means heat loss is directly related to the wall area, making the thermal performance more straightforward to predict.

The model's higher prediction errors for terraced houses likely results from the lack of an explicit input for the number or size of adiabatic surfaces. While Detached houses are fully exposed, the adiabatic boundaries in terraced houses are only indirectly represented through the shared wall

area. This indirect encoding makes it more challenging for the model to learn the distinct thermal behaviour of terraced archetypes, and is likely a factor for the lower prediction accuracy.

Extreme values

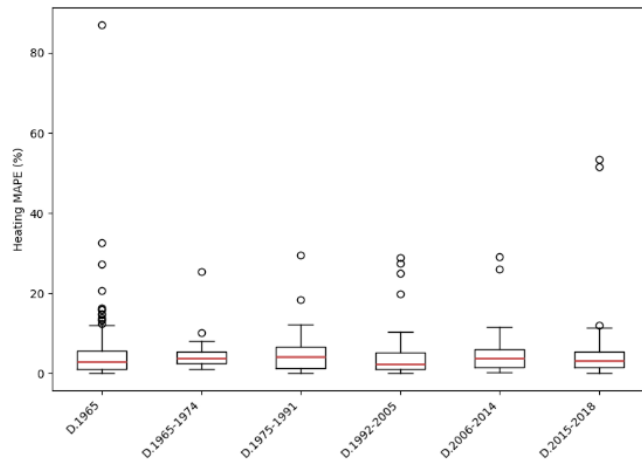


Figure 132: Heating MAPE (%) by archetype: Detached.

The box plots with outliers included highlight the presence of prediction extremes for each archetype. Both Detached and Terraced Corner typologies contain extreme outliers that exceed 80% and 40% MAPE respectively. And the Terraced Intermediate plot is largely skewed by an extreme outlier exceeding 400% MAPE.

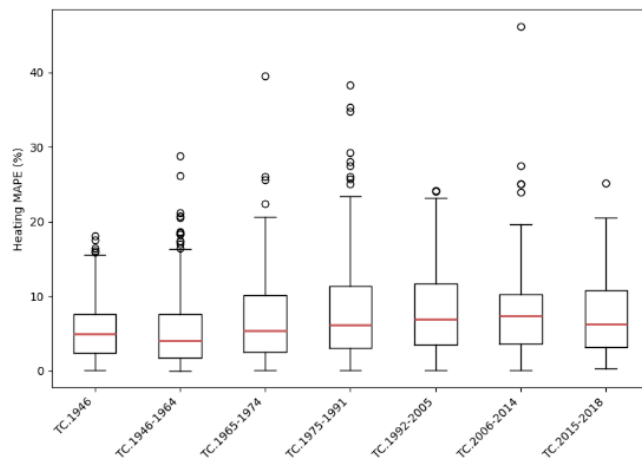


Figure 133: Heating MAPE (%) by archetype: Terraced Corner.

These prediction extremes are caused by cases where the model either dramatically underestimates or overestimates the true heating demand, as shown in Table 25. Such errors may result from the unique geometric features not well represented in the training data, or limitations in the feature set. For instance, a lack of explicit adjacency inputs (such as the number of adiabatic surfaces).

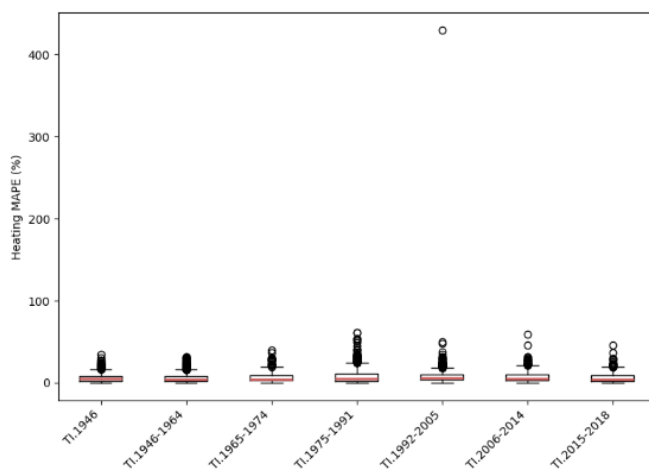


Figure 134: Heating MAPE (%) by archetype: Terraced Intermediate.

Table 25: Heating prediction extremes.

HEATING PREDICTION EXTREMES					
PAND ID	ARCHETYPE	TRUE	PREDICTED	MAE	MAPE
0599100000114990	D.1965	637.79	83.52	554.26	86 %
0599100000385588	T1.1992-2005	48.47	256.70	208.23	429 %
0599100000157120	D.1965	458.71	309.02	149.68	32 %

COOLING PREDICTIONS

Error metrics for cooling predictions on the test set also show that run V4 produces the lowest MAPE at approximately 51%, and R^2 of 0.58, indicating a moderate model fit. A summary of the error metrics is shown below:

Table 26: Cooling prediction errors.

COOLING PREDICTION ERRORS					
RUN	EPOCH	RMSE	MAE	R2	MAPE
V4	9033	6.785	4.007	0.579	51.09%

The model predictions for cooling are shown in Figure 135. While the model captures general trends there is significant dispersion, especially at higher true cooling values where predictions tend to underestimate the cooling demand. The relatively low R^2 (0.57) and high MAPE (51%) confirm moderate predictive accuracy with frequent large errors, particularly for cases with higher cooling loads. This highlights the model's limited reliability for accurately predicting cooling demands.

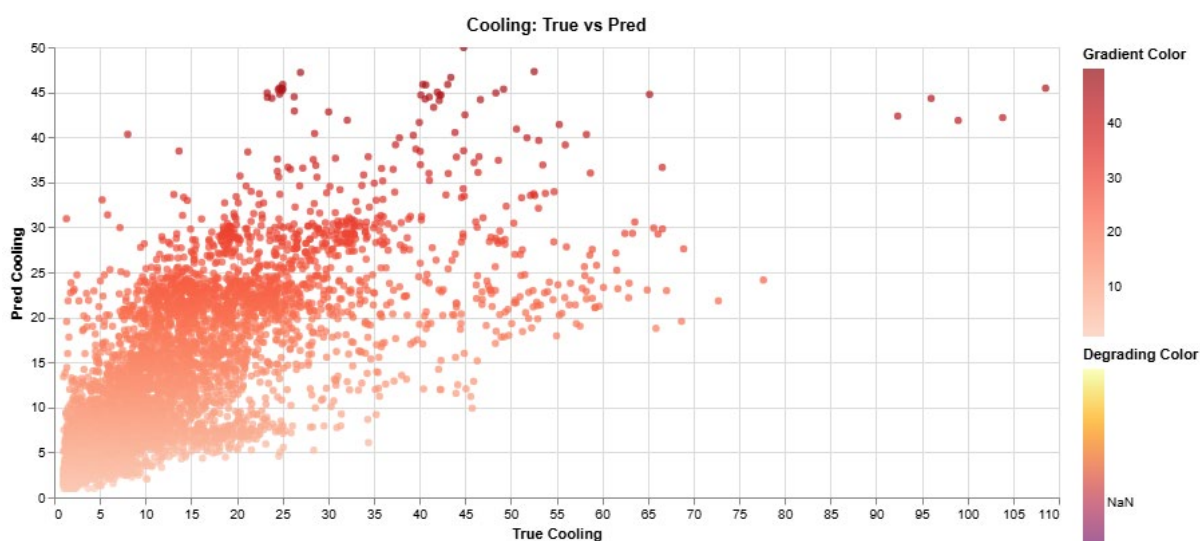


Figure 135: Annual cooling predictions with feature set D.

The bar chart shows that Terraced Intermediate houses consistently have the highest average MAPE for cooling demand predictions across all archetypes, reaching close to 80%.

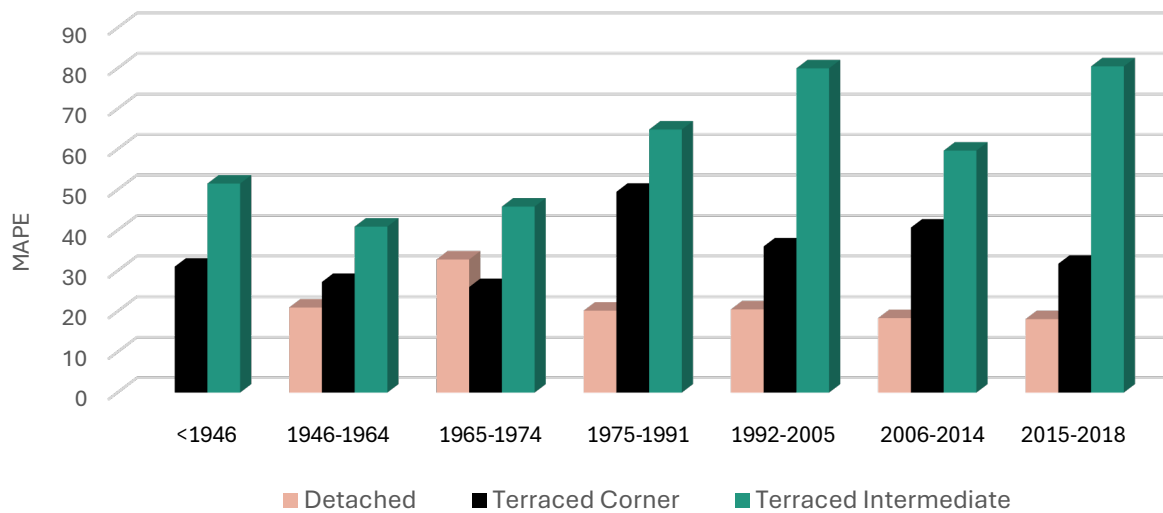


Figure 136: Average cooling MAPE per archetype.

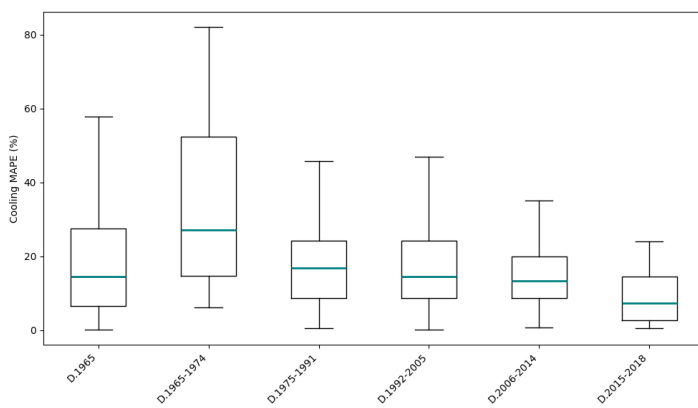


Figure 138: Cooling MAPE (%) by archetype: Detached (outliers removed).

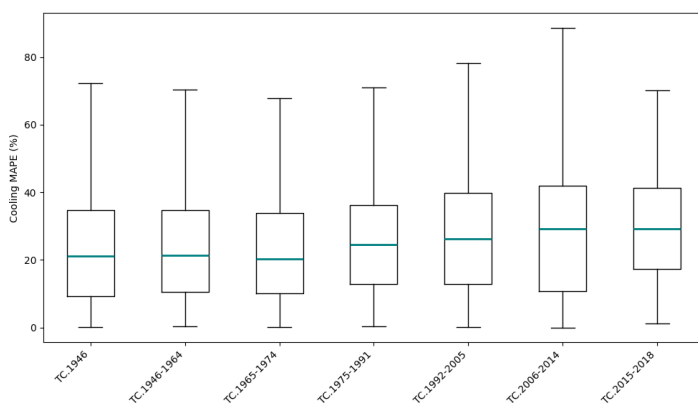


Figure 137: Cooling MAPE (%) by archetype: Terraced Corner (outliers removed).

The box plots of cooling MAPE (%) by archetype show that Detached archetypes generally show the lowest median and spread in cooling MAPE, indicating better model prediction for the Detached typology. In contrast, the Terraced Corner and especially the Terraced Intermediate archetypes display higher median MAPE and a wider spread, with the Terraced Intermediate showing some extremely high outliers. This pattern persists across all construction periods.

These results suggest the model struggles with cooling demand prediction for terraced buildings, particularly for the Terraced Intermediate.

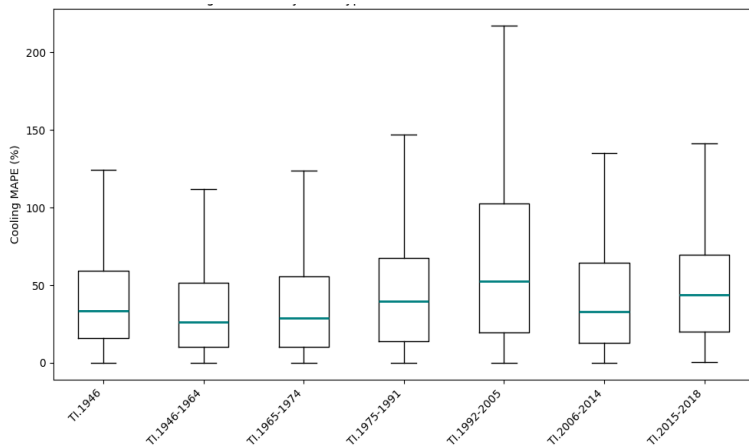


Figure 139: Cooling MAPE (%) by archetype: Terraced Intermediate (outliers removed).

The performance results can be attributed to two main factors:

1. The number and configuration of adiabatic surfaces are not directly included as an ML model input. Instead, the adiabatic surfaces are inferred through the shared wall area, potentially limiting the model's ability to capture the thermal interactions for terraced layouts.

2. From the model inputs, the Terraced Intermediate houses have a higher WWR, introducing greater variability and complexity in cooling performance, which may not be fully represented by the current input features. This limitation likely contributes to the higher and more variable MAPE values when compared to Detached houses.

Extreme values

The box plots showing the extremes highlight that Detached houses show fewer and less severe outliers, resulting in lower MAPE distributions.

Terraced Intermediate and Terraced Corner archetypes show higher extreme MAPE values, with numerous outliers exceeding several hundred percent. This outcome is largely due to the low true cooling demand in many terraced houses, which causes the MAPE to inflate rapidly even when absolute errors are moderate – a limitation of the MAPE metric.

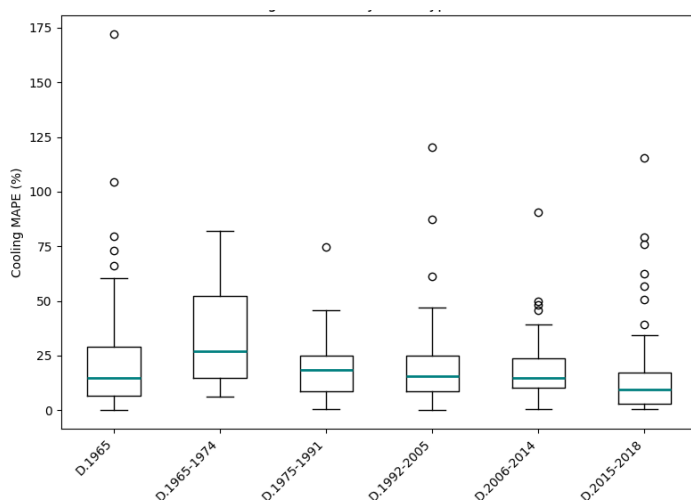


Figure 140: Cooling MAPE (%) by archetype: Detached.

This pattern suggests the model struggles most to accurately capture cooling performance in archetypes where adiabatic surfaces play a dominant role, and where the model input features may be insufficiently describing these parameters.

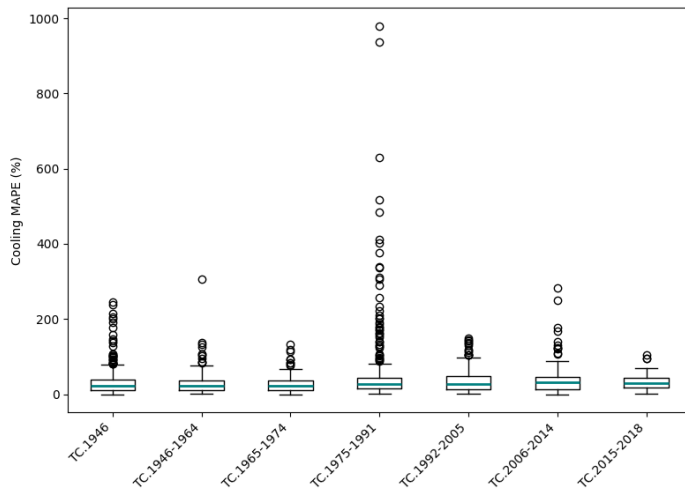


Figure 141: Cooling MAPE (%) by archetype: Terraced Corner.

Note for cooling, MAPE is not the most indicative metric for the model's performance. As a result of many of the true cooling demands being quite low absolute values, the resulting MAPE can reach extremes for a small or moderate difference in absolute value of predictions. The extreme cooling values are shown in Table 25, sorted based on the highest MAPE.

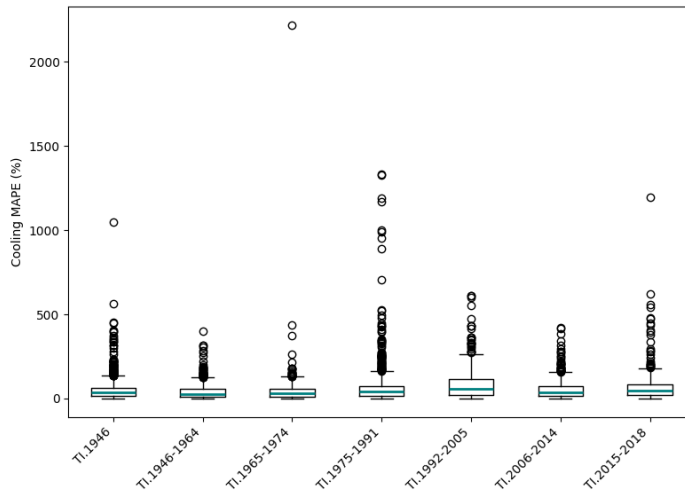


Figure 142: Cooling MAPE (%) by archetype: Terraced Intermediate.

The most extreme cooling predictions according to MAPE, are shown in Table 27, and comparatively, the most extreme cooling predictions according to MAE are shown in Table 28.

Table 27: Cooling prediction extremes ranked by MAPE.

COOLING PREDICTION EXTREMES					
PAND ID	ARCHETYPE	TRUE	PREDICTED	MAE	MAPE
0599100015004160	TI.1965-1974	1.3362	30.9458	29.61	2215.9 %
0599100000128483	TI.1975-1991	1.5254	21.8342	20.31	1331.3 %
0599100000335134	TI.1975-1991	1.3696	19.5267	18.15	1325.7 %

Table 28: Cooling prediction extremes ranked by MAE.

COOLING PREDICTION EXTREMES					
PAND ID	ARCHETYPE	TRUE	PREDICTED	MAE	MAPE
0599100000101293	TI.1946-1964	108.55	45.44	63.10	58.1 %
0599100015004542	TI.1992-2005	103.85	42.17	61.67	59.3 %
0599100015005154	TI.1965-1974	98.97	41.86	57.11	57.7 %

Methods to improve the cooling predictions should be explored further, including log-transforming the cooling values before training. This process can be applied to compress the range of cooling values and dominance of large cooling values. The reduced skew ideally allows the model to better predict both high and low true values.

Currently the model is predicting two largely different outputs – heating and cooling – for the same input features, which can make learning patterns more difficult. It may be advantageous to explore training a model specifically for cooling prediction to simplify the learning task and allow the model to focus only on the features and relationships most relevant to cooling.

10

CONCLUSIONS

RESEARCH QUESTIONS

NEXT STEPS

10. CONCLUSIONS

RESEARCH QUESTIONS

MAIN QUESTION

- **How can machine learning be used to predict energy performance for residential buildings at city-scale to reduce heating and cooling demands, considering future weather scenarios from climate change?**

Machine learning (ML) can be used to predict energy performance for residential buildings at city-scale by automating the collection of building geometry, generation of EnergyPlus input data files, and training an artificial neural network with minimal layers. This approach reduces the time and computational resources needed to run traditional EnergyPlus simulations from hours or days to minutes when calling predictions from the surrogate model. Using ML, heating predictions can achieve a minimal loss in accuracy, with an MAPE of 7%. For cooling the MAPE of 51% is largely dominated by low true cooling values. Additional work needs to be conducted to improve cooling predictions, such as adding input features to better represent building complexity, or applying data transformations such as log-transforming the cooling values before training.

Although the model is designed to incorporate future weather scenarios to allow for forecasting under climate change, this step was not implemented in the ML aspect of this project due to time constraints. To fully capture the impacts of climate change, the weather input features need to be handled thoughtfully. Originally, the logic involved using average monthly temperatures and solar radiations, but these values could likely be collapsed to the number of cooling degree days, heating degree days, and seasonal global horizontal irradiance. This reduces the dimensionality of the weather inputs and provides the model with metrics directly related to building energy demand.

SUB-QUESTIONS

RETROFIT INTERVENTIONS

- **How can ML be used to assess the impact of retrofit interventions across different building typologies?**

ML enables rapid assessment of retrofit strategies by learning the relationship between building properties, retrofit inputs, and resulting energy demands. The automated workflow, using simplified inputs allows for energy simulation across different archetypes, capturing how measures like improved insulation and reduced infiltration can reduce heating demands by over 50% especially for older, inefficient buildings. This workflow highlights the importance of targeted retrofits for specific archetypes – for example prior to 1992, where insulation improvements can move the energy label from F to A.

CITY-SCALE

- **How can computational methods be leveraged for energy modelling at city-scale?**

By developing a Python workflow for the entire process, involving API-based data collection, geometry processing, automated IDF generation, batch EnergyPlus simulation, feature structuring, and ML training, this study demonstrates that ML dramatically increases scalability, reproducibility, and time efficiency for large-scale energy modelling, compared to traditional approaches.

MACHINE LEARNING

- How can ML models improve the efficiency of building energy modelling?

The ML model improves the efficiency of building energy modelling by reducing both the number of required inputs and the time intensity of large-scale simulations. Through the staged model development and training process, the model showed strong predictive performance (specifically for heating) with using a small set of geometric and thermal envelope features.

For traditional energy modelling, generating an EnergyPlus IDF requires specifying many input parameters per building, including geometry, constructions layers, thermal properties, schedule data, internal loads, and system details. Even with a simplified and automated workflow, the IDF setup involves detailed inputs for each building surface. The ML model in this study simplified the feature set to 12 key features for training:

- floor area,
- number of floors,
- wall area,
- shared wall area,
- building height,
- ground floor insulation, façade insulation,
- roof insulation,
- infiltration rate,
- WWR,
- U Factor,
- SHGC.

And using this feature set, the ML model demonstrated strong prediction performance for heating demands.

- **What is an effective ML model, in terms of time efficiency and useability, for predicting building energy performance?**

The shallow ANN was an effective ML model based on the time efficiency, usability, and accuracy. Although, the ANN's architecture needs to be further developed for cooling predictions, the

model's structure can predict heating demands across a range of different archetypes, making it a practical tool for rapid energy assessment at scale.

- **What are the limitations of ML models compared to traditional energy modelling?**

One limitation is the need for extensive data structuring and pre-processing before ML training. All input features must be thoughtfully structured – flattened, merged, and standardized into a consistent tabular format. This process can be complex, time-consuming, and highly dependent on the chosen features.

In this project, a major portion of the workflow involved finding methods to flatten building data and merge various input sources into a clean dataset suitable for ML. EnergyPlus simulations are more straightforward in this respect: the defined inputs can be directly read by the simulation engine, with no need for data restructuring.

Although the ML predictions are rapid, the preparatory work to get the data ready for ML can be a significant and time-consuming part of the workflow.

NEXT STEPS

1. The current ML model is limited by using only two discrete values for R_c and infiltration per archetype – one for the baseline construction and one for the retrofit scenario. This restricts the model's flexibility to predict for a broader range of retrofit strategies. Future work should address this by incorporating a broader range of R_c and infiltration values, enabling the ANN to generalize better for different retrofit scenarios.
2. The impact of future weather scenarios on building energy demand was explored via EnergyPlus simulation, but results were not incorporated within the prediction model. The next objective would be to include the weather data representing the future climate scenarios within the feature set for training. In doing so it would be beneficial to consider more meaningful weather inputs such as the number of cooling degree days, heating degree days, and seasonal global horizontal irradiance.
3. Lastly, model improvements for cooling predictions should be explored to improve cooling prediction accuracy, including explicitly defining adiabatic surfaces, and vertex data – as well as structuring the vertex data to avoid prediction bias – and/or developing a separate ANN for cooling predictions.

11

REFLECTION

GRADUATION PROCESS

SOCIETAL IMPACT

11. REFLECTION

GRADUATION PROCESS

- *HOW IS YOUR GRADUATION TOPIC POSITIONED IN THE STUDIO?*

The sustainable design graduation studio investigates the design of sustainable structures, exploring topics such as innovation in structural materials, application of AI approaches, machine learning, and tools for structural optimization. The studio aims to design resource-efficient and resilient structures with reductions in non-renewable resources used throughout the building's life cycle. Looking at my graduation project, the goal was to simulate building energy use and model interventions that reduce a building's operational energy use. In making significant reductions in heating energy for example, this may allow for a transition to low-temperature heating systems like a heat pump, moving away from natural gas, and the dependence on non-renewable resources.

As well, my project investigates machine learning approaches to develop building energy models at scale, with the goal of achieving large-scale reductions in CO₂ emissions. This focus is in alignment with the studio's research interests in applying artificial intelligence methods to advance sustainability research and design.

- *HOW DID THE RESEARCH APPROACH WORK OUT (AND WHY OR WHY NOT)? AND DID IT LEAD TO THE RESULTS YOU AIMED FOR? (SWOT OF THE METHOD).*

Reflecting on my research, the approach was ultimately successful in meeting the core objectives of modelling residential heating and cooling demands at urban scale using computational workflows and machine learning. However, the process was not without challenges.

A major lesson was realizing the importance of aligning detailed data preparation with a clear machine learning strategy from the project start. I spent a lot of time at the early stages working with handling geometric surface data, and vertices, which slowed down research into enhancing the input representation of the EnergyPlus simulations and exploring different machine learning approaches. A more incremental approach, first identifying key predictive features, then increasing complexity could have been more efficient.

Similarly, at the start I was working with the full dataset (of over 74,000 buildings) in an effort to develop a method for modelling energy use at urban scale – inherent to my research question. However, this involved creating multiprocessing scripts and large file handling methods from the start. It could have been more effective to scale up my process after handling a smaller data set, to allow more time in earlier research stages for exploring a broader set of machine learning approaches. Although the focus on automation and computational efficiency resulted in a valuable workflow for handling energy modelling at large scale, stepping back periodically to reassess alignment with the overall research goals could have improved the process.

Finally, generating a synthetic dataset through repeated EnergyPlus simulations (for original building state, retrofit, current weather, and future weather) added substantial computational effort. While developing a purely Python-based workflow for the EnergyPlus simulation was an achievement that streamlined model input generation, relying on existing datasets could have freed time to focus more deeply on machine learning approaches.

Summarizing my research approach using the SWOT framework:

STRENGTHS	WEAKNESSES
<ul style="list-style-type: none"> ▪ Developed a scalable, automated workflow for 3D building model data at scale. ▪ Successfully implemented a pipeline for EnergyPlus simulations solely using Python. ▪ Developed a ML model that predicts building energy demand with reasonable accuracy for a wide range of building archetypes. 	<ul style="list-style-type: none"> ▪ Over-invested in data structuring before defining a clear ML approach. ▪ Shortened exploration of different ML models due to time spent on workflow development.
OPPORTUNITIES	THREATS
<ul style="list-style-type: none"> ▪ Enhance ML generalization ability using a range of input features to model more retrofit scenarios. ▪ Add more detail to the EnergyPlus simulations, to better represent the building archetypes. 	<ul style="list-style-type: none"> ▪ Some scripts of the computational workflow may be too tailored to this specific dataset.

- *IF APPLICABLE: WHAT IS THE RELATIONSHIP BETWEEN THE METHODOLOGICAL LINE OF APPROACH OF THE GRADUATION STUDIO (RELATED RESEARCH PROGRAM OF THE DEPARTMENT) AND YOUR CHOSEN METHOD?*

My research method is closely aligned with the approach of the sustainable design graduation studio and AiDAPT research group of using AI and data-driven methods to advance sustainability in the built environment. My research applied machine learning approaches to predict heating and cooling demands, directly contributing to an informed relationship of how insulation improvements impact building energy demand for a broad range of building archetypes. In developing a computational workflow and using AI methods for predictive modelling and large-scale data analysis, my approach is aligned with the studio's broader objectives of creating sustainable design interventions in the built environment.

- *HOW ARE RESEARCH AND DESIGN RELATED?*

Research involved understanding which building features and retrofit measures significantly affect energy performance and figuring out how to best represent these at a larger urban scale. The design involved making decisions on how to structure data, select machine learning methods, and develop a computational workflow. Insights from the research directly influenced my design decisions, such as selecting a level of detail for the building geometry, choosing the thermal properties for inputs, and investigating specific building archetypes. As well, the computational workflow itself informed my research by providing insights into retrofit effectiveness and building energy behaviour per archetype. Thus, there was a continuous interaction between research and design throughout my project that strengthened my approach to urban scale building energy modelling and prediction.

- *DID YOU ENCOUNTER MORAL/ETHICAL ISSUES OR DILEMMAS DURING THE PROCESS? HOW DID YOU DEAL WITH THESE?*

My research was driven from a technological viewpoint, leaving out essential social dimensions that were unfortunately beyond the scope of research. Retrofit strategies inherently involve the preferences, behaviours, and acceptance of building users, yet these critical factors were not integrated into my approach. Incorporating user perspectives to ensure interventions are both effective and representative of user behaviour would significantly strengthen the research.

SOCIETAL IMPACT

- *TO WHAT EXTENT ARE THE RESULTS APPLICABLE IN PRACTICE?*

The results from this research have substantial practical applicability, especially within the context of large-scale urban energy modelling and retrofit planning. The developed computational workflow – covering automated geometry collection, IDF file generation, and EnergyPlus simulations – provides a scalable solution for quickly analyzing heating and cooling demands for large-scale building datasets. The insights into energy demand differences between current and retrofit construction states for prevalent Dutch residential archetypes, especially those built before thermal performance regulations, directly support retrofit decision-making. Furthermore, the explored machine learning model demonstrates strong predictive performance for heating demands, indicating practical usability in scenarios where rapid demand estimation is needed. There remain opportunities to enhance the practical applicability of the prediction model by including additional inputs, particularly detailed retrofit parameters and improved weather data, and by extending the workflow to accommodate simulations for future climate scenarios.

- *TO WHAT EXTENT HAS THE PROJECTED INNOVATION BEEN ACHIEVED?*

The project explores the application of machine learning for energy performance at urban scale, addressing current gaps in the research domain in terms of scalability, and efficiency compared to traditional modelling approaches. Considering the expanding field of machine learning, this project offers insights into the applicability of machine learning approaches and computational methods to overcome data collection and availability challenges.

Key contributions to innovation include:

- Automated data collection pipeline and a fully automated EnergyPlus simulation workflow, enabling scalable energy modelling across a large-scale building dataset.
- Refined the archetype-based modelling approach by incorporating a broader range of construction periods.
- Application of machine learning to urban-scale energy prediction, addressing limitations of traditional modelling in terms of scalability and data availability.

- *DOES THE PROJECT CONTRIBUTE TO SUSTAINABLE DEVELOPMENT?*

Yes, this project contributes to sustainable development by exploring interventions for reducing energy consumption within the built environment. Rising global temperatures due to climate change can lead to higher cooling demands, exacerbating building energy consumption. Without intervention, this could lead to a greater reliance on non-renewable energy sources, contributing to increased air pollution and CO₂ emissions. Predicting building energy performance at scale allows us to identify key retrofits to reduce energy consumption and dependence on non-renewable energy sources for current and future weather scenarios.

Additionally, my project focus is on improving the energy performance of existing residential buildings. This focus is aligned with the sustainable development goal of preserving the existing building stock and reducing the environmental impact of new construction.

- *WHAT IS THE IMPACT OF YOUR PROJECT ON SUSTAINABILITY (PEOPLE, PLANET, PROFIT/PROSPERITY)?*

For people, this project focuses on retrofitting the existing Dutch housing stock and avoiding major demolitions, thus lends to preserving historical Dutch architecture. As well this project contributes to the long-term goals of creating more comfortable, affordable, and climate-resilient houses, particularly in older neighbourhoods.

For the planet, this project promotes reducing heating and cooling demands, thus lowering greenhouse gas emissions in the residential sector. By focusing on the existing Dutch housing stock, the intention is to avoid the environmental costs of demolition and new construction, aligning with circularity principles.

For prosperity, this project offers scalable methods for identifying energy-saving interventions, which can enable cost-savings and better allocation of resources when considering large-scale urban planning and retrofit investments.

- *WHAT IS THE SOCIO-CULTURAL AND ETHICAL IMPACT?*

From a positive perspective, my research work contributes to the objective of maintaining the character and identity of historic Dutch neighbourhoods by promoting retrofit of existing buildings over demolition.

From a critical lens, although my model offers data-driven insights for planning, it currently excludes the human dimension – such as occupant behaviour and user preferences – which are vital for socially acceptable retrofit interventions. Future development should integrate these factors to ensure interventions are aligned with societal needs.

Ethical considerations relate to the environmental impacts of using AI and machine learning for building energy modelling. The environmental impact of data-driven approaches, such as the significant energy and water demand to power large data centers, raises ethical questions about the use of AI and resource consumption. Using AI to address energy efficiency underscores the importance of reflecting on and balancing technological approaches with sustainability goals.

- *WHAT IS THE RELATION BETWEEN THE PROJECT AND THE WIDER SOCIAL CONTEXT?*

This project aims to better understand available retrofit interventions and enable stakeholders to prioritize interventions that offer maximum energy savings.

This project responds to broader societal challenges related to climate change, the energy transition, and housing quality. By developing a workflow that can enable large-scale retrofit planning, this project works to address the need for climate adaptation in the built environment. It also aligns with national and European level sustainability goals aimed at reducing energy consumption in existing buildings and reducing energy emissions. In doing so, it contributes to the wider social discourse on sustainable urban development, offering designers and planners data-driven tools for decision making.

- *HOW DOES THE PROJECT AFFECTS ARCHITECTURE / THE BUILT ENVIRONMENT?*

My project combines computational, architectural and climate design principals to understand retrofit interventions and the complexities of energy modelling at urban scale. This work provides a framework for data-driven decision making in architectural and urban planning processes.

There is a need in architecture, urban planning, and engineering professions for tools that integrate energy performance insights with building retrofit strategies. My project demonstrates how integrating simulation tools and machine learning can enhance our understanding of energy performance, particularly for the existing residential building stock – which is a critical area to achieve energy savings.

12

REFERENCES

REFERENCES

12. REFERENCES

Alabdullatief, Aasem & Omer, Siddig & Zein Elabdein, Rami & Alfraidi, Sultan. (2016). Green roof and louvers shading for sustainable mosque buildings in Riyadh, Saudi Arabia.

Aruta, G., Ascione, F., Bianco, N., Bindi, L., & Iovane, T. (2024). Energy classification of urban districts to map buildings and prioritize energy retrofit interventions: A novel fast tool. *Applied Energy*, 377, 124664. <https://doi.org/10.1016/j.apenergy.2024.124664>

BAG Viewer. (n.d.). <https://bagviewer.kadaster.nl/lvbag/bag-viewer/?searchQuery=Ring+613%2C+3195+XM+Pernis&objectId=0599200000427205&theme=BRT+Achtergrond&geometry.x=85859.295&geometry.y=434003.82999999996&zoomlevel=15>

Biljecki, F., Ledoux, H., Stoter, J., & Delft University of Technology. (2016). An improved LOD specification for 3D building models. *Computers, Environment and Urban Systems*. <https://doi.org/10.1016/j.compenvurbsys.2016.04.005>

Canada, N. R. (2025, January 14). *Keeping The Heat In - Section 4: Comprehensive air leakage control in your home*. Natural Resources Canada. <https://natural-resources.canada.ca/energy-efficiency/home-energy-efficiency/keeping-heat-section-4-comprehensive-air-leakage-control-your-home>

Carpino, C., Bruno, R., Carpino, V., & Arcuri, N. (2022). Improve decision-making process and reduce risks in the energy retrofit of existing buildings through uncertainty and sensitivity analysis. *Energy Sustainable Development/Energy for Sustainable Development*, 68, 289–307. <https://doi.org/10.1016/j.esd.2022.04.007>

CityJSON Ninja. (n.d.). <https://ninja.cityjson.org/>

Climate.onebuilding.org. (n.d.). <https://climate.onebuilding.org/>

De Vos, R. (2024, January 3). *Alweer die treurige NOS - Stichting Climate Intelligence Clintel*. Stichting Climate Intelligence Clintel. <https://clintel.nl/alweer-die-treurige-nos/>

ecoGlaze® Retrofit Double Glazing | green magazine. (2015, August 28). Green Magazine. <https://greenmagazine.com.au/product/ecomaster/ecoglaze-retrofit-double-glazing/>

EP-Online. (n.d.). <https://www.ep-online.nl/>

Eppy. (2020). https://eppy.readthedocs.io/en/latest/Main_Tutorial.html

epwshiftr. (2021). Github. <https://ideas-lab-nus.github.io/epwshiftr/articles/paper.html>

European Commission. (2021). Summary of the Commission assessment of the draft National Energy and Climate Plan 2021-2030. In *European Commission Assessment Report*. https://energy.ec.europa.eu/document/download/e1ed8d0a-54f9-4f95-bdd7-b97a54cf8c7e_en

Everything you should know about cavity wall insulation. . . (2022, September 1). Builders Insulation. https://buildersinsulation.co.uk/everything-you-should-know-about-cavity-wall-insulation-/?srsId=AfmBOor8GLm99P_OVcN0irJQyUd6sBissVmMI5MAh0dtYfVOAoQQKllo

Fathi, S., Srinivasan, R., Fenner, A., & Fathi, S. (2020a). Machine learning applications in urban building energy performance forecasting: A systematic review. *Renewable and Sustainable Energy Reviews*, 133, 110287. <https://doi.org/10.1016/j.rser.2020.110287>

Fathi, S., Srinivasan, R. S., Kibert, C. J., Steiner, R. L., & Demirezen, E. (2020b). AI-Based Campus Energy Use Prediction for Assessing the Effects of Climate Change. *Sustainability*, 12(8), 3223. <https://doi.org/10.3390/su12083223>

Franco, J. T. (2023, April 11). *How to calculate the thermal transmittance (U-Value) in the envelope of a building*. ArchDaily. <https://www.archdaily.com/898843/how-to-calculate-the-thermal-transmittance-u-value-in-the-envelope-of-a-building>

Geysen, D., De Somer, O., Johansson, C., Brage, J., & Vanhoudt, D. (2017). Operational thermal load forecasting in district heating networks using machine learning and expert advice. *Energy and Buildings*, 162, 144–153. <https://doi.org/10.1016/j.enbuild.2017.12.042>

Global Alliance for Buildings and Construction, Matteri, A., Summerfield, A., Maciel, A., Castillo Guzman, A., Gruner, A., Hermelink, A., Kleinschmidt, A., Manning, A., Zinnecker, A., Bierre, A. K., Lee, A., Cervera Mondragón, A., Chong, B., Erdnöß, B., Sifferlen, C., Gutierrez, C. B., Carrasco, C. A., Chan, C., . . . Liu, M. (2020). *2020 Global Status Report for Buildings and Construction: Towards a zero-emission, efficient and Resilient buildings and Construction sector*. United Nations Environment Programme. https://globalabc.org/sites/default/files/inline-files/2020%20Buildings%20GSR_FULL%20REPORT.pdf

González-Torres, M., Pérez-Lombard, L., Coronel, J. F., Maestre, I. R., & Yan, D. (2021). A review on buildings energy information: Trends, end-uses, fuels and drivers. *Energy Reports*, 8, 626–637. <https://doi.org/10.1016/j.egy.2021.11.280>

Heiranipour, M., Favoino, F., Miren, J. G., & Avesani, S. (2024). Typical and extreme (Heatwave) future weather files for building energy simulations: case studies for Turin and Bolzano, Italy, and De Bilt, Netherlands. *Zenodo*. <https://doi.org/10.5281/zenodo.14274362>

Hulsman, B. (2024, August 22). *The noble beauty of the terraced house*. The Low Countries. <https://www.the-low-countries.com/article/the-noble-beauty-of-the-terraced-house/>

Koh, C., Schollbach, K., Gauvin, F., & Brouwers, H. (2022). Aerogel composite for cavity wall rehabilitation in the Netherlands: Material characterization and thermal comfort assessment. *Building and Environment*, 224, 109535. <https://doi.org/10.1016/j.buildenv.2022.109535>

Konstantinou, T. (2014). Facade Refurbishment Toolbox: Supporting the design of residential energy upgrades. *journals.open.tudelft.nl*. <https://doi.org/10.7480/abe.2014.9.660>

KNMI. (2015). *Climate scenarios for the Netherlands* (Revised edition 2015). https://cdn.knmi.nl/system/data_center_publications/files/000/070/807/original/Brochure_KNM_I14_EN_2015.pdf?1653079346

KNMI *Klimaatscenario's*. (n.d.). <https://klimaatscenario's-data.knmi.nl/tijdreeks>

Li, Z., Ma, J., Tan, Y., Guo, C., & Li, X. (2023). Combining physical approaches with deep learning techniques for urban building energy modelling: A comprehensive review and future research prospects. *Building and Environment*, 246, 110960. <https://doi.org/10.1016/j.buildenv.2023.110960>

Menkveld, M., Sipma, J., & TNO PUBLIEK. (2022). Artikel 6 EED renovatieverplichting gebouwen van publieke instellingen. In TNO PUBLIEK & RVO, *TNO-rapport* (TNO 2022 P10681). TNO. <https://www.tno.nl>

Ministry of the Interior and Kingdom Relations. (2022). *Example homes 2022 existing construction*.

Nieman (2021). Report on standard and target values for existing housing Reference heat demand for existing buildings. In J. Hartlief, *Netherlands Enterprise Agency*

NTA 8800:2022 nl. (2022). <https://www.nen.nl/en/nta-8800-2022-nl-290717>

Olu-Ajayi, R., Alaka, H., Sulaimon, I., Sunmola, F., & Ajayi, S. (2021). Building energy consumption prediction for residential buildings using deep learning and other machine learning techniques. *Journal of Building Engineering*, 45, 103406. <https://doi.org/10.1016/j.jobbe.2021.103406>

Richards Partington Architects. (2012). Understanding overheating – where to start: An introduction for house builders and designers. In NHBC Foundation, *NHBC Foundation* (Guide NF 44). <https://www.nhbc.co.uk/binaries/content/assets/nhbc/foundation/understanding-overheating---where-to-start.pdf>

Rovers, R., Zikmund, A., Lupisek, A., Borodinecs, A., Novák, E., Matoušková, E., Haas, G. D., Kamphuis, J., Novák, J., Oorschot, J. V., Kuusk, K., Sojková, K., Almeida, M., Volf, M., Faltýnová, M., Kabrhel, M., Morck, O., Pihelo, P., Hejtmánek, P., . . . Ott, W. (2018). *A guide into renovation package concepts for mass retrofit of different types of buildings with prefabricated elements for (n)zeb performance*.

SIGA. (n.d.). *Thermal insulation – guide to a safe thermal envelope*. Vapour Control Layers, Tapes, Adhesives & Sealants. <https://www.siga.swiss/global/en/knowledge/building-solutions/thermal-insulation-the-ultimate-guide-to-a-safe-thermal-envelope>

Street View of Ring 613 · Google Maps. (n.d.). *Street View of Ring 613 · Google Maps*. <https://www.google.com/maps/place/Ring+613>

TABULA WebTool. (n.d.). <https://webtool.building-typology.eu/#bm>

The Royal Netherlands Meteorological Institute. (2023). *KNMI'23 climate scenarios*.

Thrampoulidis, E., Hug, G., & Orehounig, K. (2023). Approximating optimal building retrofit solutions for large-scale retrofit analysis. *Applied Energy*, 333, 120566. <https://doi.org/10.1016/j.apenergy.2022.120566>

Types and parts: Glazing. (2024, March 26). NFRC Consumer Guide to Windows. <https://efficientwindows.org/window-glazing/>

Van Bueren, E. M., Van Bohemen, H., Itard, L., & Visscher, H. (n.d.). Sustainable environment building [Book-chapter]. In *Energy in Buildings* (p. Chapter 5). <https://www.springer.com/gp/book/9789400712935>

Van Den Brom, P., Berben, J., Valk, H., Nieman, W/ E advisors, & RVO. (2022). *A description of the adjusted parameters and the validation procedure* (pp. 1–75).

Van Den Hurk, B., Ed, Siegmund, P., Ed, Klein Tank, A., Ed, KNMI, Jisk Attema, Alexander Bakker, Jules Beersma, Janette Bessembinder, Reinout Boers, Theo Brandsma, Henk van den Brink, Sybren Drijfhout, Henk Eskes, Rein Haarsma, Wilco Hazeleger, Rudmer Jilderda, Caroline Katsman, Geert Lenderink, Jessica Loriaux, . . . Gerd-Jan van Zadelhoff. (2014). KNMI'14: Climate Change scenarios for the 21st Century – A Netherlands perspective. In *KNMI'14 Climate Change Scenarios* (Scientific Report No. WR2014-01). KNMI. <https://www.climatescenarios.nl>

Vazquez-Canteli, J., Demir, A. D., Brown, J., & Nagy, Z. (2019). Deep neural networks as surrogate models for urban energy simulations. *Journal of Physics Conference Series*, 1343(1), 012002. <https://doi.org/10.1088/1742-6596/1343/1/012002>

Wahi, P. (2020). *Robustness of building envelope*. <https://resolver.tudelft.nl/uuid:f7743926-86dd-46be-9c08-6f00debb9a3c>

Wahi, P., Konstantinou, T., Visscher, H., & Tenpierik, M. J. (2024). Evaluating building-level parameters for lower-temperature heating readiness: A sampling-based approach to addressing the heterogeneity of Dutch housing stock. *Energy and Buildings*, 322, 114703. <https://doi.org/10.1016/j.enbuild.2024.114703>

Westermann, P., & Evins, R. (2021). Using Bayesian deep learning approaches for uncertainty-aware building energy surrogate models. *Energy and AI*, 3, 100039. <https://doi.org/10.1016/j.egyai.2020.100039>

Wittchen, K. B., & Aggerholm, S. (2000). Calculation of building heating demand in EPIQR. *Energy and Buildings*, 31(2), 137–141. [https://doi.org/10.1016/s0378-7788\(99\)00027-4](https://doi.org/10.1016/s0378-7788(99)00027-4)

Zero Carbon Hub. (2015). Overheating in Homes The Big Picture. In *Good Homes Alliance*. <https://www.shadeit.org.uk/wp-content/uploads/2016/09/ZCH-Overheating-In-Homes-The-Big-Picture.pdf>

Zhang, Y., Wang, D., Wang, G., Xu, P., & Zhu, Y. (2024). Data-driven building load prediction and large language models: Comprehensive overview. *Energy and Buildings*, 115001. <https://doi.org/10.1016/j.enbuild.2024.115001>

3D geoinformation research group. (2023). *Overview - 3DBAG*. <https://docs.3dbag.nl/en/>

3DBAG Viewer. (2024, December 16). <https://3dbag.nl/en/viewer>

6.2. Ablation Studies. (2024). <https://ml.recipes/notebooks/6-ablation-study.html>

A

APPENDIX A

GITHUB

APPENDIX A

GITHUB

The scripts created for the main computational workflow of this project are shared to the github repository, accessed at:

<https://github.com/elenarduzzi/buildingenergymetamodels>

B

APPENDIX B

MATERIAL ID TABLE

APPENDIX B

MATERIAL ID TABLE

The material inputs used to define the constructions for the EnergyPlus simulations are provided in the subsequent tables. Note the units for each parameter:

- Infiltration: m^3/sm^2
- Insulation (R_c): $\text{m}^2\text{K}/\text{W}$
- Thickness: m
- Thermal Conductivity: W/mK
- Density: kg/m^3
- Specific Heat Capacity: J/kgK
- Thermal Transmittance (U): $\text{W}/\text{m}^2\text{K}$
- SHGC: Unitless

Table 29: Material ID table for Terraced Intermediate (TI) archetypes.

Archetype ID	Infiltration	Material ID	Rc	Thickness	Conductivity	Density	Heat Capacity	U	SHGC
TI.1946	0.0030	G.TI.1946	3.5	0.15	0.04	540	1210		
		F.TI.1946	1.7	0.3	0.18	1920	840		
		R.TI.1946	3.5	0.2	0.06	1500	1000		
		W.TI.1946						1.4	0.6
TI.1946-1964	0.0010	G.TI.1946-1964	3.5	0.15	0.04	540	1210		
		F.TI.1946-1964	1.7	0.3	0.18	1920	840		
		R.TI.1946-1964	3.5	0.2	0.06	1500	1000		
		W.TI.1946-1964						1.4	0.6
TI.1965-1974	0.0010	G.TI.1965-1974	3.5	0.15	0.04	540	1210		
		F.TI.1965-1974	1.7	0.3	0.18	1920	840		
		R.TI.1965-1974	3.5	0.2	0.06	1500	1000		
		W.TI.1965-1974						1.4	0.6
TI.1975-1991	0.0010	G.TI.1975-1991	3.5	0.15	0.04	540	1210		
		F.TI.1975-1991	1.7	0.3	0.18	1920	840		
		R.TI.1975-1991	3.5	0.2	0.06	1500	1000		
		W.TI.1975-1991						1.4	0.6
TI.1992-2005	0.0015	G.TI.1992-2005	3.5	0.15	0.04	540	1210		
		F.TI.1992-2005	2.5	0.3	0.12	1920	840		
		R.TI.1992-2005	3.5	0.2	0.06	1500	1000		
		W.TI.1992-2005						1.4	0.4
TI.2006-2014	0.0015	G.TI.2006-2014	3.5	0.15	0.04	540	1210		
		F.TI.2006-2014	2.5	0.3	0.12	1920	840		
		R.TI.2006-2014	3.5	0.2	0.06	1500	1000		
		W.TI.2006-2014						1.4	0.4
TI.2015-2018	0.0015	G.TI.2015-2018	3.5	0.15	0.04	540	1210		
		F.TI.2015-2018	4.5	0.3	0.07	1920	840		
		R.TI.2015-2018	6	0.2	0.03	1500	1000		
		W.TI.2015-2018						1.4	0.4

Table 30: Material ID table for Terraced Corner (TC) archetypes.

Archetype ID	Infiltration	Material ID	Rc	Thickness	Conductivity	Density	Heat Capacity	U	SHGC
TC.1946	0.0030	G.TC.1946	3.5	0.15	0.04	540	1210		
		F.TC.1946	1.7	0.3	0.18	1920	840		
		R.TC.1946	3.5	0.2	0.06	1500	1000		
		W.TC.1946						1.4	0.6
TC.1946-1964	0.0010	G.TC.1946-1964	3.5	0.15	0.04	540	1210		
		F.TC.1946-1964	1.7	0.3	0.18	1920	840		
		R.TC.1946-1964	3.5	0.2	0.06	1500	1000		
		W.TC.1946-1964						1.4	0.4
TC.1965-1974	0.0010	G.TC.1965-1974	3.5	0.15	0.04	540	1210		
		F.TC.1965-1974	1.7	0.3	0.18	1920	840		
		R.TC.1965-1974	3.5	0.2	0.06	1500	1000		
		W.TC.1965-1974						1.4	0.6
TC.1975-1991	0.0010	G.TC.1975-1991	3.5	0.15	0.04	540	1210		
		F.TC.1975-1991	1.7	0.3	0.18	1920	840		
		R.TC.1975-1991	3.5	0.2	0.06	1500	1000		
		W.TC.1975-1991						1.4	0.6
TC.1992-2005	0.0015	G.TC.1992-2005	3.5	0.15	0.04	540	1210		
		F.TC.1992-2005	2.5	0.3	0.12	1920	840		
		R.TC.1992-2005	3.5	0.2	0.06	1500	1000		
		W.TC.1992-2005						1.4	0.6
TC.2006-2014	0.0015	G.TC.2006-2014	3.5	0.15	0.04	540	1210		
		F.TC.2006-2014	2.5	0.3	0.12	1920	840		
		R.TC.2006-2014	3.5	0.2	0.06	1500	1000		
		W.TC.2006-2014						1.4	0.4
TC.2015-2018	0.0015	G.TC.2015-2018	3.5	0.15	0.04	540	1210		
		F.TC.2015-2018	4.5	0.3	0.07	1920	840		
		R.TC.2015-2018	6	0.2	0.03	1500	1000		
		W.TC.2015-2018						1.4	0.4

Table 31: Material ID table for Detached (D) archetypes.

Archetype ID	Infiltration	Material ID	Rc	Thickness	Conductivity	Density	Heat Capacity	U	SHGC
D.1965	0.0014	G.D.1965	3.5	0.15	0.04	540	1210		
		F.D.1965	1.7	0.3	0.18	1920	840		
		R.D.1965	3.5	0.2	0.06	1500	1000		
		W.D.1965						1.4	0.4
D.1965-1974	0.0014	G.D.1965-1974	3.5	0.15	0.04	540	1210		
		F.D.1965-1974	1.7	0.3	0.18	1920	840		
		R.D.1965-1974	3.5	0.2	0.06	1500	1000		
		W.D.1965-1974						1.4	0.6
D.1975-1991	0.0014	G.D.1975-1991	3.5	0.15	0.04	540	1210		
		F.D.1975-1991	1.7	0.3	0.18	1920	840		
		R.D.1975-1991	3.5	0.2	0.06	1500	1000		
		W.D.1975-1991						1.4	0.6
D.1992-2005	0.0021	G.D.1992-2005	3.5	0.15	0.04	540	1210		
		F.D.1992-2005	2.5	0.3	0.12	1920	840		
		R.D.1992-2005	3.5	0.2	0.06	1500	1000		
		W.D.1992-2005						1.4	0.6
D.2006-2014	0.0021	G.D.2006-2014	3.5	0.15	0.04	540	1210		
		F.D.2006-2014	2.5	0.3	0.12	1920	840		
		R.D.2006-2014	3.5	0.2	0.06	1500	1000		
		W.D.2006-2014						1.4	0.4
D.2015-2018	0.0021	G.D.2015-2018	3.5	0.15	0.04	540	1210		
		F.D.2015-2018	4.5	0.3	0.07	1920	840		
		R.D.2015-2018	6	0.2	0.03	1500	1000		
		W.D.2015-2018						1.4	0.4
D.1965	0.0014	G.D.1965	3.5	0.15	0.04	540	1210		
		F.D.1965	1.7	0.3	0.18	1920	840		
		R.D.1965	3.5	0.2	0.06	1500	1000		
		W.D.1965						1.4	0.4

C

APPENDIX C

DEMAND ANALYSIS

ML DEVELOPMENT

PERFORMANCE

APPENDIX C

At the P4 project stage, the main workflow from data collection through model development and performance evaluation stages was complete. However, at this time there was not yet a solution for defining the shared wall surfaces or adiabatic surfaces of each building – a task that required additional computational effort. Without this information, it was also not possible to define window objects on the correct surfaces (i.e defining a window on surfaces that are not shared with neighbouring buildings).

Thus, the demand analysis, model development, and performance evaluation that follows was completed to satisfy the project requirements at the time, before the EnergyPlus simulations included windows and adiabatic surface definitions. It should be noted that the results deviate from the main demand analysis within the body of the report, for example as shown below the cooling loads decrease despite retrofit measures of improved insulation and infiltration. This response can be mainly attributed to the lack of windows within the simulation, which eliminate solar gains from driving cooling demands.

DEMAND ANALYSIS

The distribution of energy labels within the simulated dataset (including both current and retrofit construction states) at the current weather condition is shown in Figure 143.

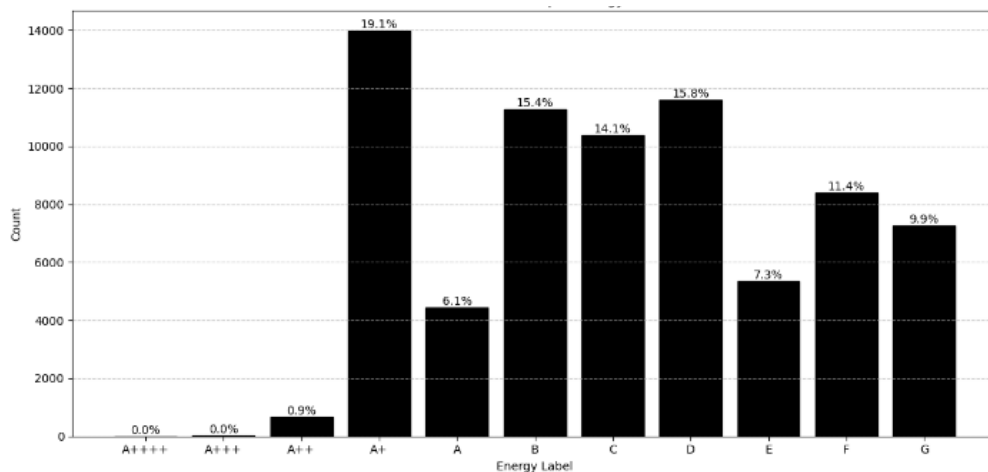


Figure 143: Number of Pand IDs per energy label, including both current and retrofit construction states.

DETACHED HOUSE / Vrijstaande woning

For Detached houses, the retrofit benefits are most noticeable in houses built before 1992. For houses built from 1992 onwards, the current envelopes perform very similar to the retrofit condition.

Detached houses show the highest heating demand compared to terraced houses due to the full exposure on all four façades, with the maximum current demand at 380 kWh/m² for houses built between 1965–1974.

Retrofit measures reduce pre-1992 heating demand by 60–70%, bringing it down to about 120 kWh/m². After 1992, the current demand drops to 130 kWh/m², reaching close to the retrofit scenario.

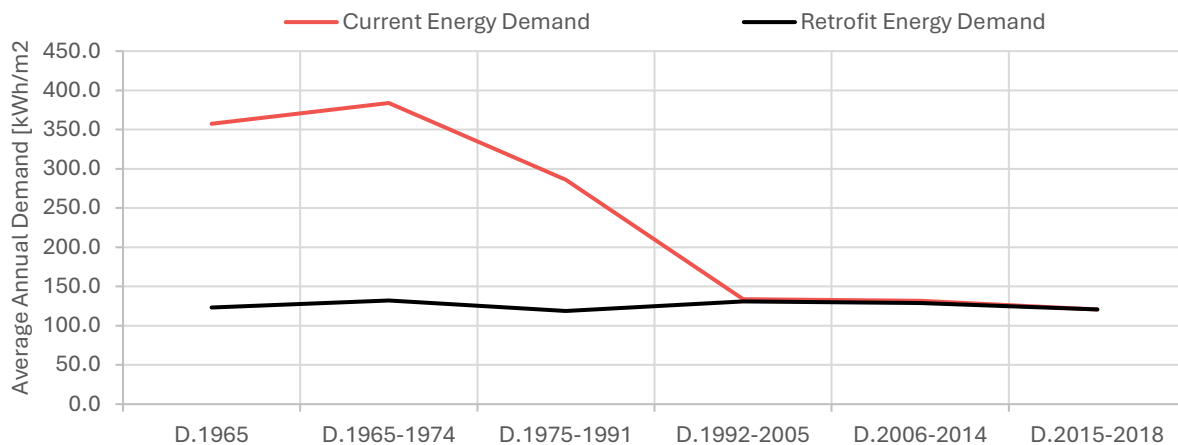


Figure 144: Detached house total energy demand for current condition and retrofit condition.

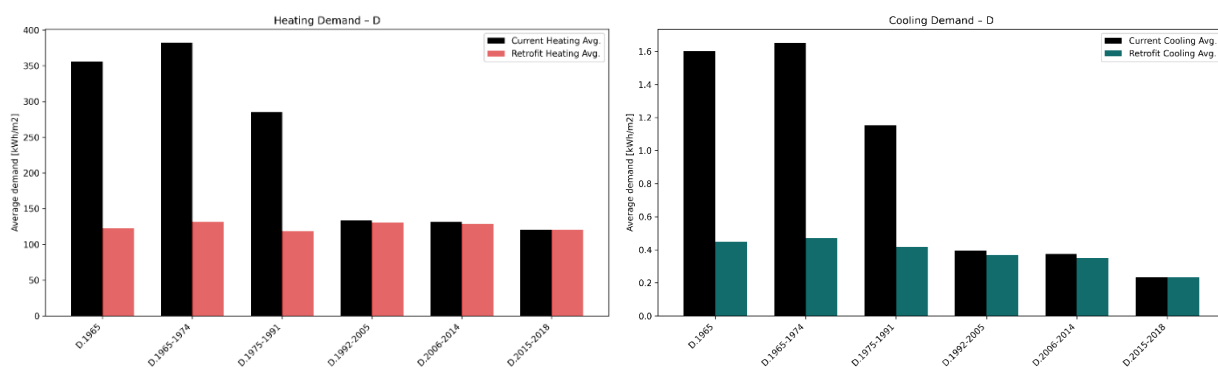


Figure 145: Current and retrofit heating and cooling demand for Detached archetypes.

For cooling, the demand stays very low at less than 1.7 kWh/m², with only minor improvements from retrofits in the older building periods. And no noticeable change after 1992. Compared to terraced houses, the pattern for Detached houses shows higher baseline demands and greater absolute retrofit potential for older archetypes.

Table 32: Detached total annual energy demand and energy label per archetype at current construction and retrofit construction states.

ARCHETYPE	CURRENT DEMAND [kwh/m ²]	CURRENT ENERGY LABEL	RETROFIT DEMAND [kwh/m ²]	RETROFIT ENERGY LABEL
D.1965	357.2	F	123.3	A
D.1965-1974	383.9	F	132.2	A
D.1975-1991	285.9	D	118.8	A
D.1992-2005	133.8	A	130.9	A
D.2006-2014	131.7	A	128.8	A
D.2015-2018	120.7	A	120.7	A

TERRACED CORNER / Hoekwoning

Similar findings for the Terraced Corner house show that the retrofit interventions have the greatest impact on buildings constructed before 1992, where poor insulation and high air leakage originally led to high energy demands and poor energy labels. For these older archetypes upgrading the roof, floor, and wall insulation, and reducing infiltration leads to significant reductions – up to 65% for heating and 70% for cooling demand.

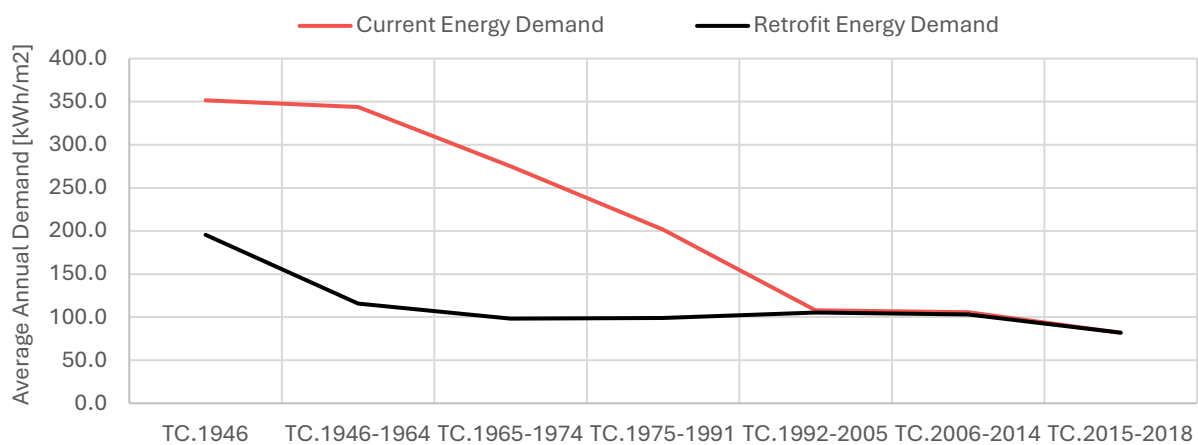


Figure 146: Terraced Corner total energy demand for current condition and retrofit condition.

For the most recent buildings (2015-2018), which already feature high-performance envelopes, the retrofits show virtually no effect. This pattern is visible from the Terraced Corner housing energy labels, shown in Table 33.

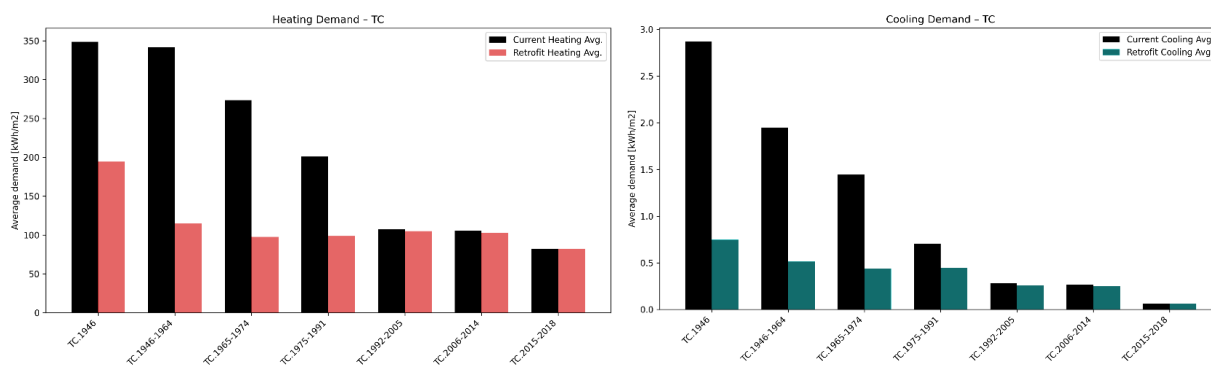


Figure 147: Current and retrofit heating and cooling demand for Terraced Corner archetypes.

Table 33: Terraced Corner total annual energy demand and energy label per archetype at current construction and retrofit construction states.

ARCHETYPE	CURRENT DEMAND [kwh/m ²]	CURRENT ENERGY LABEL	RETROFIT DEMAND [kwh/m ²]	RETROFIT ENERGY LABEL
TC.1946	351.6	F	195.5	C
TC.1946-1964	343.6	E	115.7	A
TC.1965-1974	275.2	D	98.1	A+
TC.1975-1991	201.7	C	99.1	A+
TC.1992-2005	108.0	A+	105.4	A+
TC.2006-2014	105.7	A+	103.2	A+
TC.2015-2018	81.9	A+	81.9	A+

TERRACED INTERMEDIATE / Tussenwoning

From the plot of total energy demand for Terraced Intermediate, Figure 148, shows that from 1946 to 1991, buildings had minimal insulation, and high air leakage, resulting in high average energy demands. When retrofits are applied that significantly improve insulation and reduce infiltration, the average energy demand drops quickly, as seen by the large gap between the red (current) and black (retrofit) lines at this period.

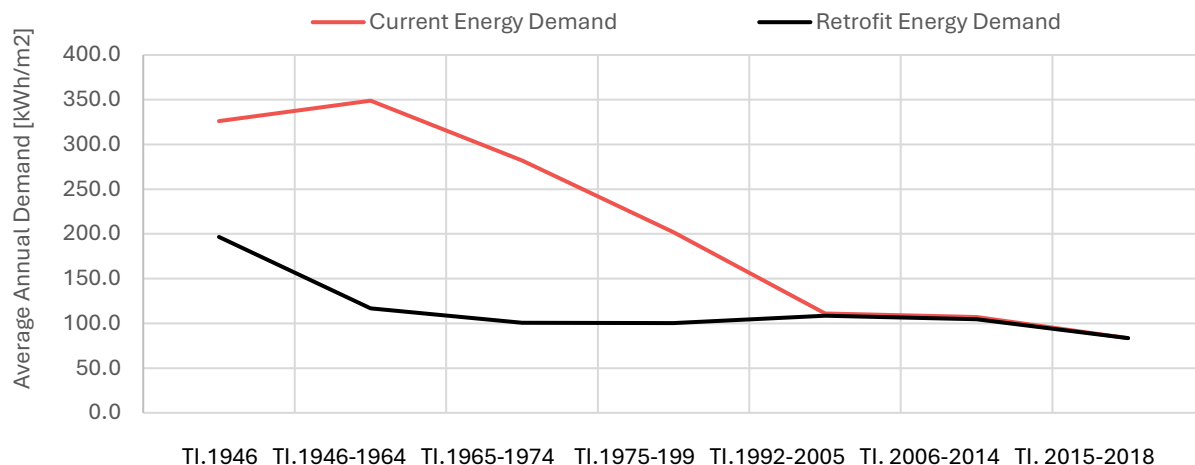


Figure 148: Terraced Intermediate total energy demand for current condition and retrofit condition.

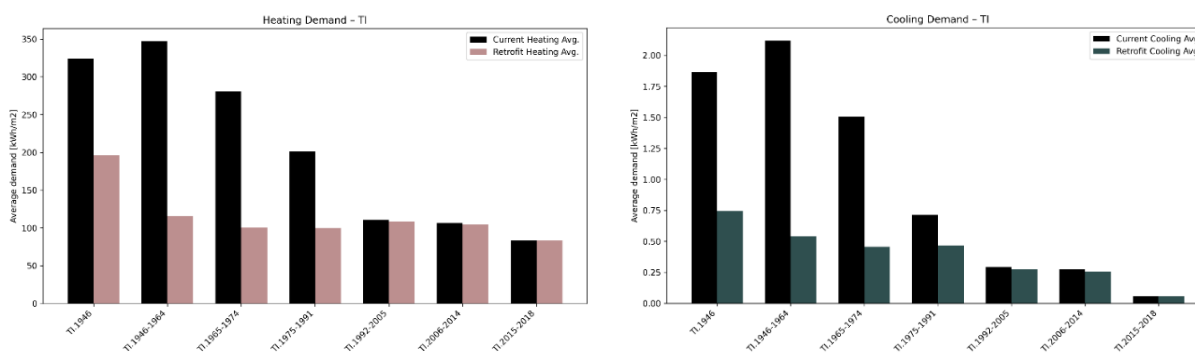


Figure 149: Current and retrofit heating and cooling demand for Terraced Intermediate archetypes.

However, from 1992 onward, the building envelopes is constructed to a higher standard (improved insulations and reduced infiltrations), so the retrofit upgrades show little additional improvement. As a result, the current and retrofit energy demand lines converge, highlighting that retrofit measures have the greatest impact on older, less efficient buildings.

Table 34: Terraced Intermediate total annual energy demand and energy label per archetype at current construction and retrofit construction states.

ARCHETYPE	CURRENT DEMAND [kwh/m ²]	CURRENT ENERGY LABEL	RETROFIT DEMAND [kwh/m ²]	RETROFIT ENERGY LABEL
TI.1946	326.1	E	196.6	C
TI.1946-1964	348.9	F	116.6	A
TI.1965-1974	282.2	D	100.7	A+
TI.1975-1991	202.1	C	100.3	A+
TI.1992-2005	111.2	A	108.5	A+
TI.2006-2014	107.1	A+	104.6	A+
TI.2015-2018	83.5	A+	83.5	A+

ML DEVELOPMENT

Note again that the model training described in this section was completed before the addition of windows and adiabatic surfaces for the EnergyPlus simulations. The model shows strong prediction performance based on the simplified input feature set, discussed below.

PHASE 2

The Phase 2 ANN predicts annual heating and cooling demands using a 20,000-building data set, with a train, test, validation split of 70%, 20%, 10%.

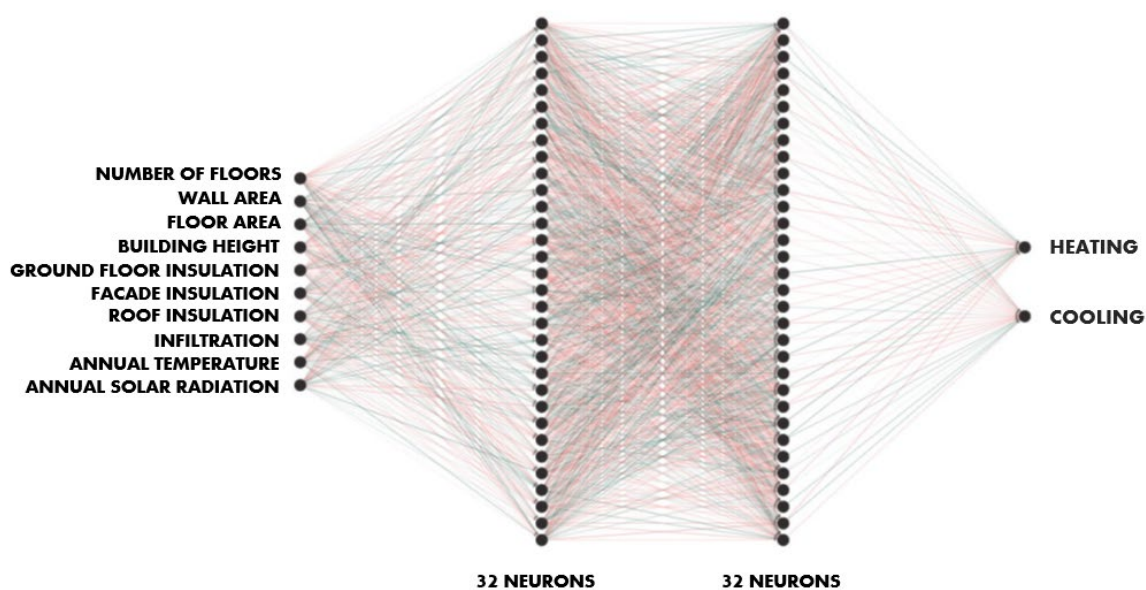


Figure 150: ANN architecture used for Phase 2 training (Feature Set D).

FEATURE SET A

The initial model aimed to leverage all available geometric features collected from the 3DBAG for heating and cooling demand predictions, shown in Table 35.

Table 35: Phase 2 Feature Set A.

Feature	Units	Variable Type	Normalization
GEOMETRIC			
Number of Floors	-	Discrete	Standard-Scale
Wall Area	m ²	Continuous	Standard-Scale
Roof Area (Flat)	m ²	Continuous	Standard-Scale
Roof Area (Sloped)	m ²	Continuous	Standard-Scale
Floor Area	m ²	Continuous	Standard-Scale
Shared Wall Area	m ²	Continuous	Standard-Scale
Building Height (70%)	m	Continuous	Standard-Scale

GEOMETRIC			
Total Floor Area	m ²	Continuous	Standard-Scale
Building Volume	m ³	Continuous	Standard-Scale
Compactness Ratio	m ⁻¹	Continuous	Standard-Scale
CONSTRUCTION			
Ground Floor Insulation	m ² K/W	Continuous	Standard-Scale
Facade Insulation	m ² K/W	Continuous	Standard-Scale
Roof Insulation	m ² K/W	Continuous	Standard-Scale
Infiltration	m ³ /sm ²	Continuous	Standard-Scale
WEATHER			
Annual average temperature	°C	Continuous	-
Annual average solar radiation	kWh/m ² /day	Continuous	-
VERTICES			
Distance (d) from centroid	-	Continuous	Standard-Scale
Angle (u _x)	-	Continuous	Polar Angle
Angle (u _y)	-	Continuous	Polar Angle

FEATURE SET B

Feature set B simplified the geometric inputs to the total floor area, building volume, and compactness ratio.

Table 36: Phase 2 Feature Set B.

Feature	Units	Variable Type	Normalization
GEOMETRIC			
Total Floor Area	m ²	Continuous	Standard-Scale
Building Volume	m ³	Continuous	Standard-Scale
Compactness Ratio	m ⁻¹	Continuous	Standard-Scale
CONSTRUCTION			
Ground Floor Insulation	m ² K/W	Continuous	Standard-Scale
Facade Insulation	m ² K/W	Continuous	Standard-Scale
Roof Insulation	m ² K/W	Continuous	Standard-Scale
Infiltration	m ³ /sm ²	Continuous	Standard-Scale
WEATHER			
Annual average temperature	°C	Continuous	-
Annual average solar radiation	kWh/m ² /day	Continuous	-
VERTICES			
Distance (d) from centroid	-	Continuous	Standard-Scale
Angle (u _x)	-	Continuous	Polar Angle
Angle (u _y)	-	Continuous	Polar Angle

FEATURE SET C

The reduction from Feature set B to C involved removing the vertex data. All other features remained the same.

Table 37: Phase 2 Feature Set C.

Feature	Units	Variable Type	Normalization
GEOMETRIC			
Total Floor Area	m ²	Continuous	Standard-Scale
Building Volume	m ³	Continuous	Standard-Scale
Compactness Ratio	m ⁻¹	Continuous	Standard-Scale
CONSTRUCTION			
Ground Floor Insulation	m ² K/W	Continuous	Standard-Scale
Facade Insulation	m ² K/W	Continuous	Standard-Scale
Roof Insulation	m ² K/W	Continuous	Standard-Scale
Infiltration	m ³ /sm ²	Continuous	Standard-Scale
WEATHER			
Annual average temperature	°C	Continuous	-
Annual average solar radiation	kWh/m ² /day	Continuous	-

FEATURE SET D

The last stage of training used the number of floors, wall area, floor area, and building height as geometric features. These features were selected to capture the most essential geometric properties to minimize redundancy and input complexity.

The number of floors and building height together provide an indication of compactness, which impacts the internal volume and heat transfer surfaces. Wall area is critical for modelling heat loss and gain, since it represents the primary envelope through which energy is exchanged. And the floor area provides a measure of building size and conditioned space.

Table 38: Phase 2 Feature Set D.

Feature	Units	Variable Type	Normalization
GEOMETRIC			
Number of Floors	-	Discrete	Standard-Scale
Wall Area	m ²	Continuous	Standard-Scale
Floor Area	m ²	Continuous	Standard-Scale
Building Height (70%)	m	Continuous	Standard-Scale
CONSTRUCTION			
Ground Floor Insulation	m ² K/W	Continuous	Standard-Scale
Facade Insulation	m ² K/W	Continuous	Standard-Scale
Roof Insulation	m ² K/W	Continuous	Standard-Scale
Infiltration	m ³ /sm ²	Continuous	Standard-Scale

WEATHER			
Annual average temperature	°C	Continuous	-
Annual average solar radiation	kWh/m ² /day	Continuous	-

The roof area was excluded as a feature to avoid redundancy in the input data since for LoD 1.2 geometry, the roof area can be directly inferred from the floor area.

The MSE loss curves across the Feature D training set show a steep initial drop in loss, highlighting that the model quickly learns the relationships between input features and outputs. The loss curves shown a smooth decay, decreasing gradually and flattening to a minimum loss between 10,000 to 15,000 iterations. All runs show a similar loss curve, showing the stability of the training set.

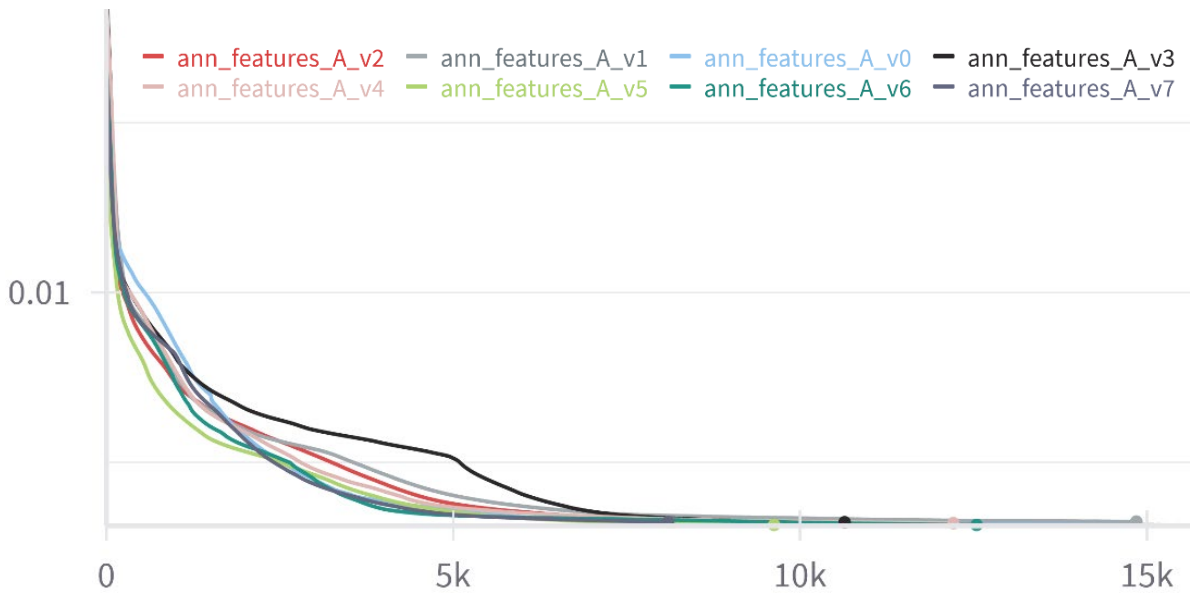


Figure 151: Phase 2 MSE loss curve, showing several iterations of training runs.

PERFORMANCE

Tracking the error metrics for the test set for heating and cooling demand predictions, it was observed that run V0 produced the lowest MAPE at approximately 3% for heating and 10% for cooling. As well as strong R^2 values of 0.98 and 0.97, indicating a good model fit for both heating and cooling models. A summary of the error metrics is shown in Table 39.

Table 39: Phase 2 heating and cooling demand prediction errors.

HEATING PREDICTION ERRORS					
RUN	EPOCH	RMSE	MAE	R2	MAPE
V0	13,319	0.01513	0.00709	0.98	2.9%
COOLING PREDICTION ERRORS					
RUN	EPOCH	RMSE	MAE	R2	MAPE
V0	13,319	0.02673	0.01727	0.97	10.2%

HEATING PREDICTIONS

Based on the low error metrics, the ANN predicts heating with high accuracy. The heating predictions are shown in Figure 152, where the predictions are closely aligned with the true values. At higher true heating values, there is slightly more spread in the predictions, with few outliers.

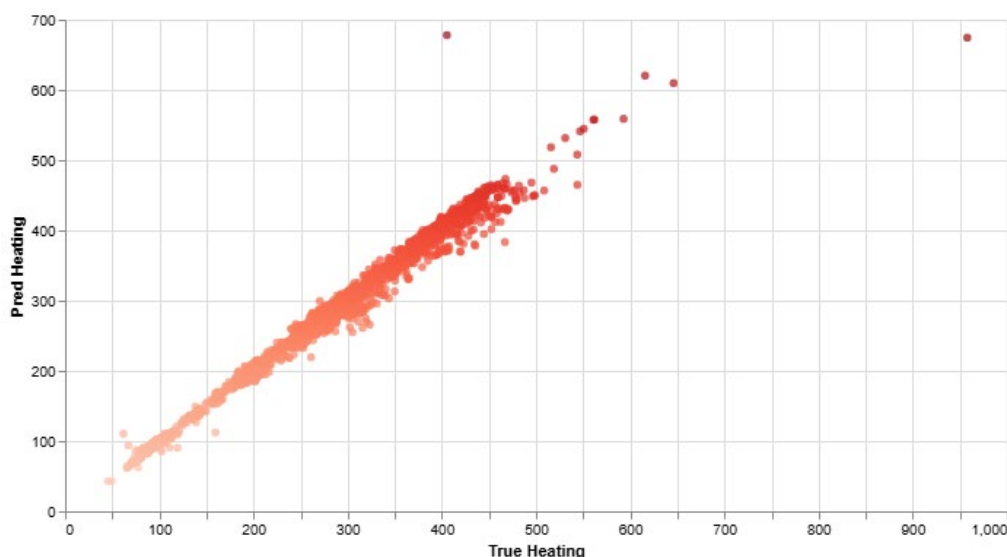
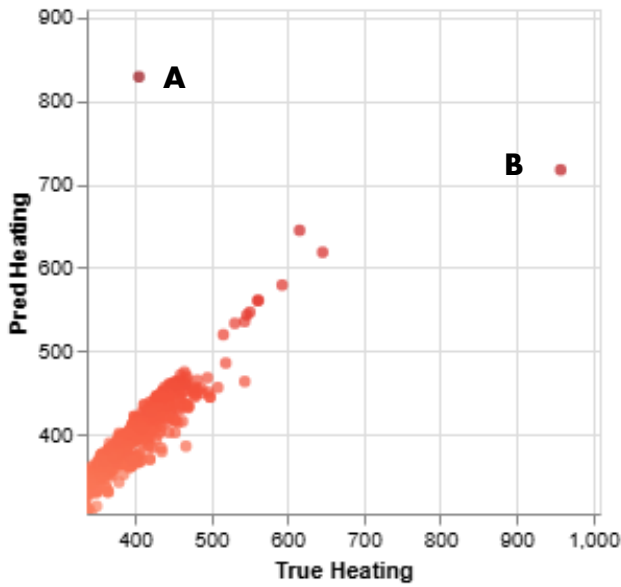


Figure 152: Phase 2 annual heating predictions with feature set D.

Table 40: Phase 2 heating prediction extremes.



HEATING PREDICTION EXTREMES			
	TRUE	PREDICTED	MAPE
A	405.4	828.6	104 %
B	957.9	717.2	25 %

Looking at a few of the prediction outliers in Figure 153, Extreme [A] represents a Terraced Intermediate house from the period 2006-2014. Extreme [B] is a Terraced Intermediate house from the pre-1946 construction period, notably with the highest true heating value from the test set.

Figure 153: Phase 2 heating prediction extremes.

The average MAPE across all archetypes is shown in Figure 154.

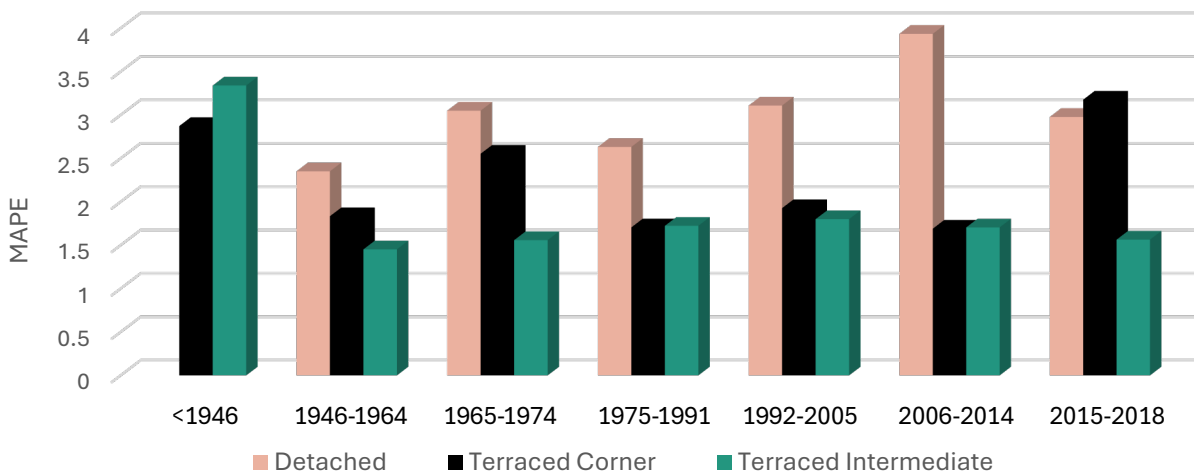


Figure 154: Phase 2 average heating MAPE per archetype.

For the Detached house type, the predictions show good accuracy. The median MAPE lies between 1-3%, for all building periods and from the box plots in Figure 155 there are few outliers overall, with the most extremes in the 1992-2005 building period. The maximum extreme MAPE is 26% for the 2006-2014 building period.

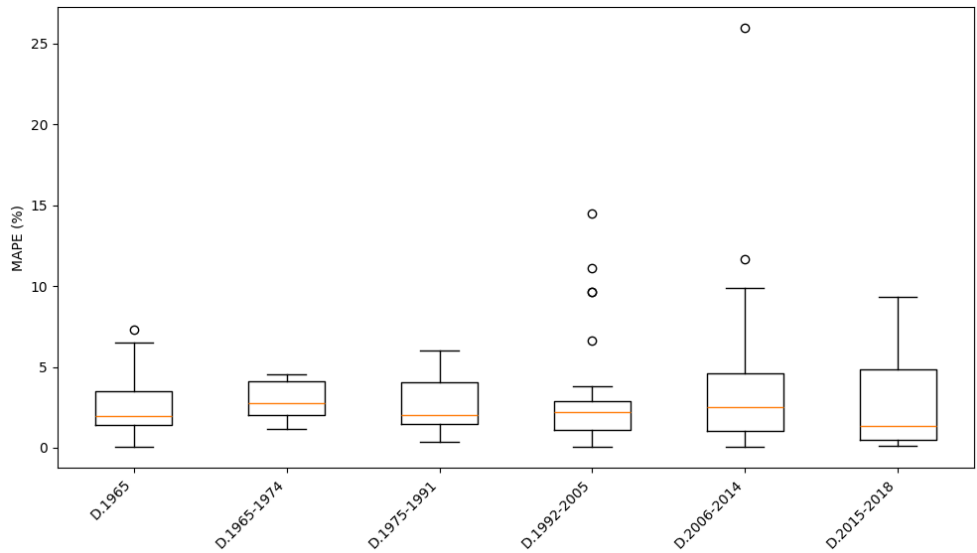


Figure 155: Phase 2 heating MAPE (%) by archetype: Detached.

For the Terraced Corner house, the median MAPE is consistent across all archetypes, below 2.5%. There is consistently less spread amongst the MAPE for each archetype. One extreme outlier is shown for the 2015–2016 period at 64%, with the predicted heating almost double that of the true heating value.

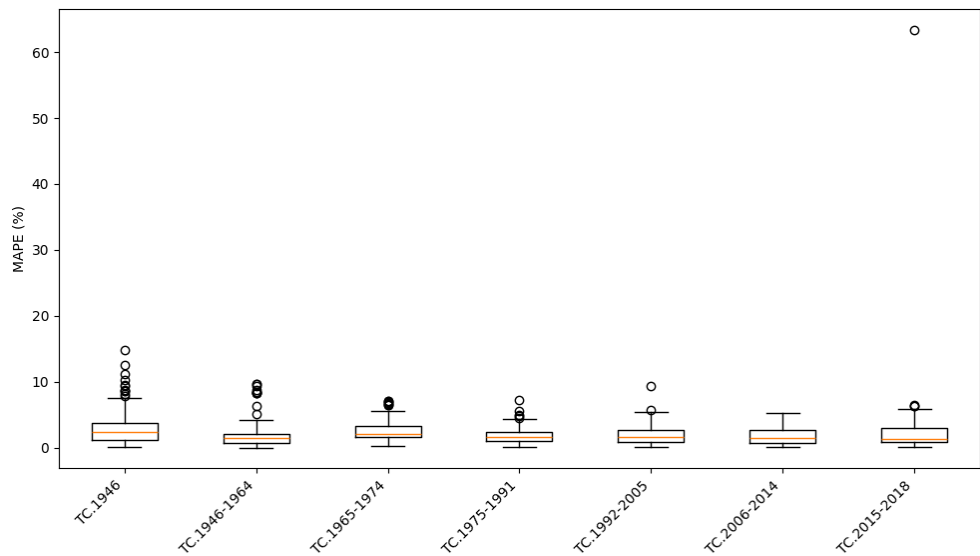


Figure 156: Phase 2 heating MAPE (%) by archetype: Terraced Corner.

Similar results are shown for the Terraced Intermediate house, with a median MAPE between 1–3% across all archetypes. One extreme outlier is shown for the 2006–2014 period at 104%, with the prediction over double that of the true value.

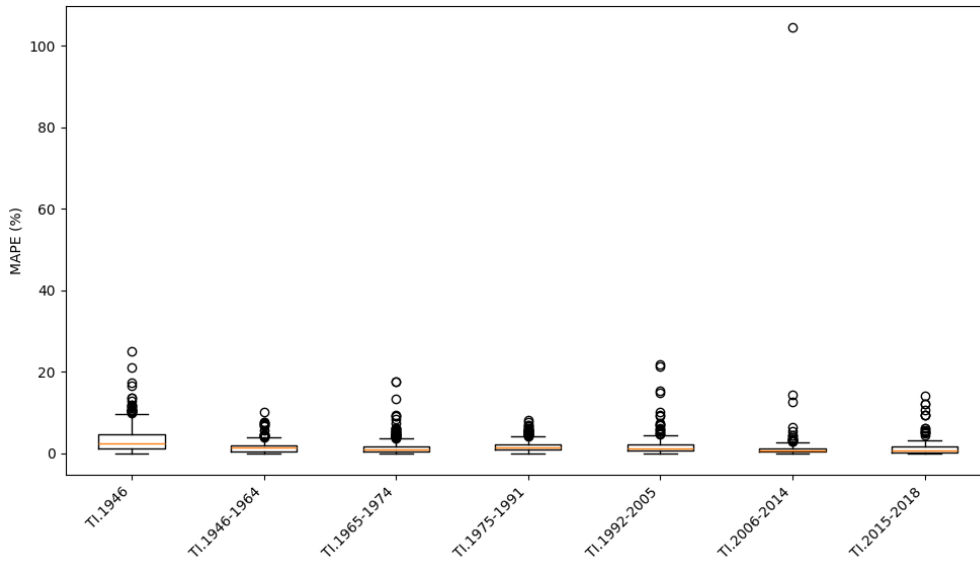


Figure 157: Phase 2 heating MAPE (%) by archetype: Terraced Intermediate.

COOLING PREDICTIONS

Cooling predictions are shown in Figure 158.

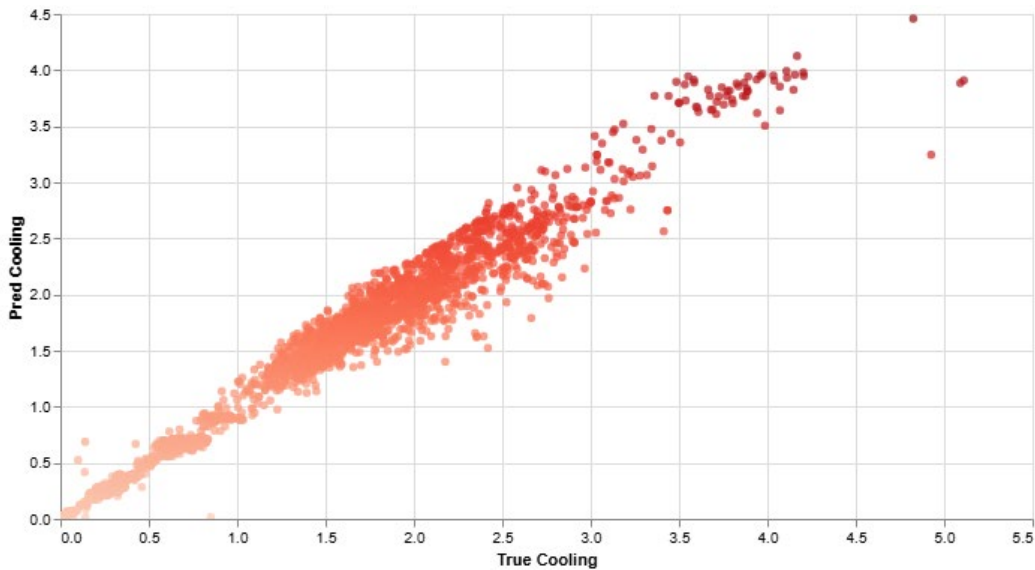


Figure 158: Phase 2 annual cooling predictions with feature set D.

Cooling predictions show a significantly higher MAPE compared to the heating predictions, with all archetypes above a 5% MAPE.

Because many of the true cooling demand values are very small, the resulting MAPE can reach extremes for a small difference in absolute prediction value – a limitation of the MAPE metric. For example, in Figure 159, Extreme A shows a MAE of 0.03 kWh/m², which translates to an MAPE of 243%.

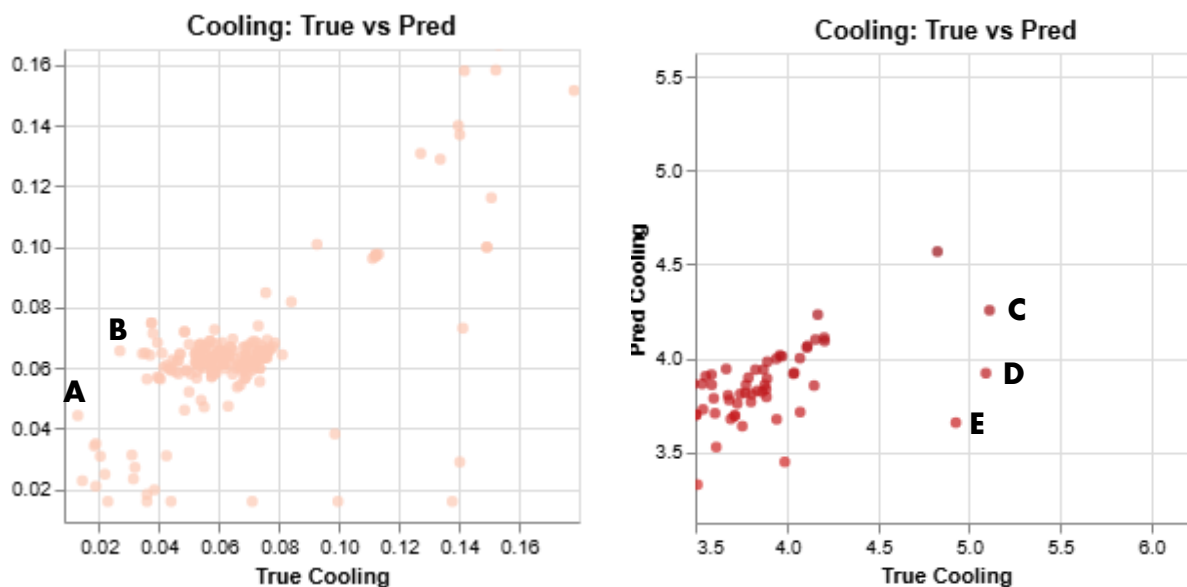


Figure 159: Phase 2 cooling prediction extremes for low true values (left) and high true cooling values (right).

Examples of some of the prediction extremes are shown in Table 41.

Table 41: Cooling prediction extremes.

COOLING PREDICTION EXTREMES					
	TRUE	PREDICTED	MAPE	ARCHETYPE	
A	0.012	0.044	243 %	Terraced Intermediate	2015-2018
B	0.026	0.065	143 %	Terraced Intermediate	2015-2018
C	5.11	4.25	16.7 %	Terraced Corner	< 1946
D	5.09	3.92	23.0 %	Terraced Corner	< 1946
E	4.92	3.65	25.8 %	Terraced Intermediate	< 1946

Looking at the average MAPE per archetype, in Figure 160, the predictions are particularly poor for terraced houses in the 2015-2018 building period, with a MAPE of 18% and 22% for the intermediate and corner houses respectively.

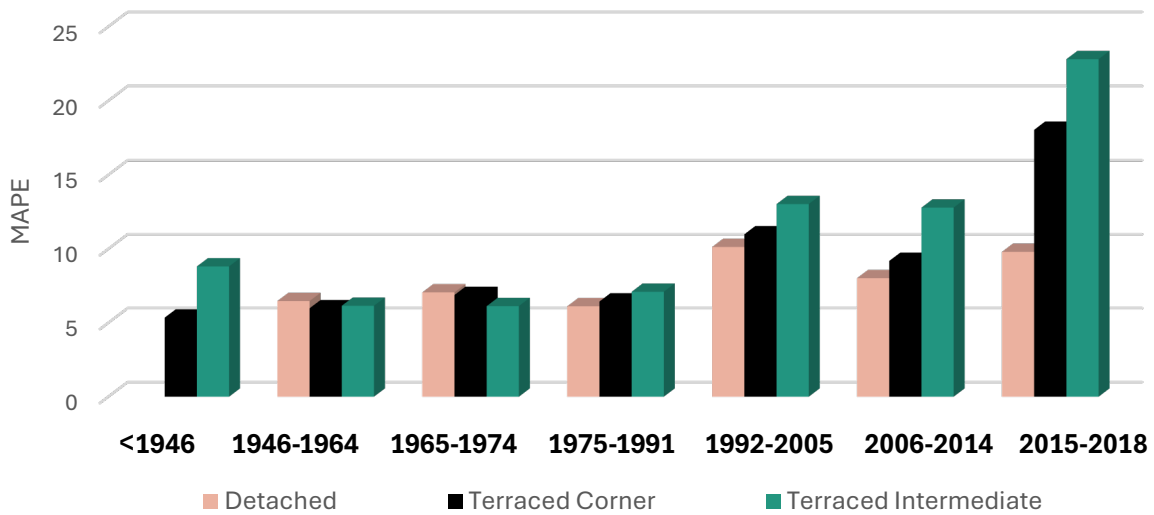


Figure 160: Phase 2 average cooling MAPE per archetype.

For the Detached house, the median error rises in newer construction periods and is highest for the 2015-2018 period at approximately 7%. Older building periods show a narrower distribution, with fewer extreme outliers.

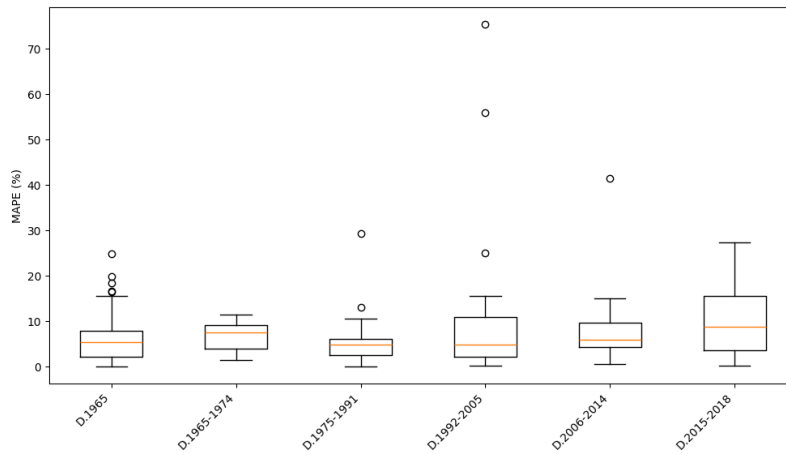


Figure 161: Phase 2 cooling MAPE (%) by archetype: Detached.

Similarly for the Terraced Corner, the MAPE is consistent across most archetypes, increasing in the most recent construction period, 2015-2018, to approximately 7.5%. Extreme outliers are also in the more recent construction periods: 2006-2014 and 2015-2018.

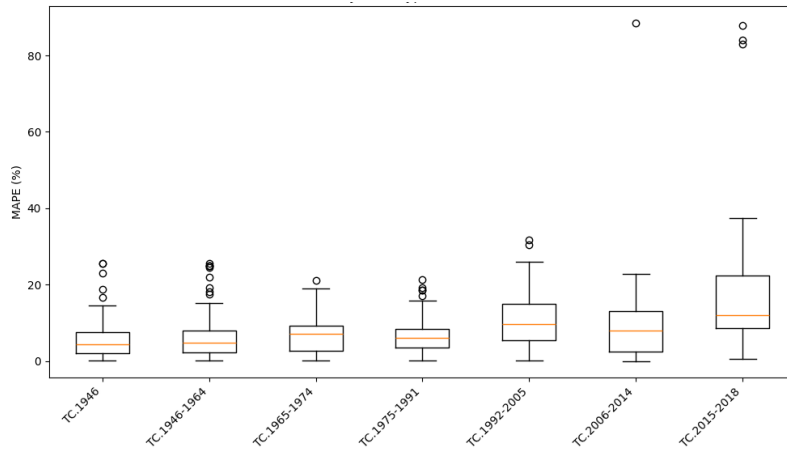


Figure 162: Phase 2 cooling MAPE (%) by archetype: Terraced Corner.

For the Terraced Intermediate housing type, the median MAPE is quite low across all building periods, also reaching 7.5% in the 2015-2018 period. Many outliers are found in the more recent periods, with extreme outliers shown from 1992-2018.

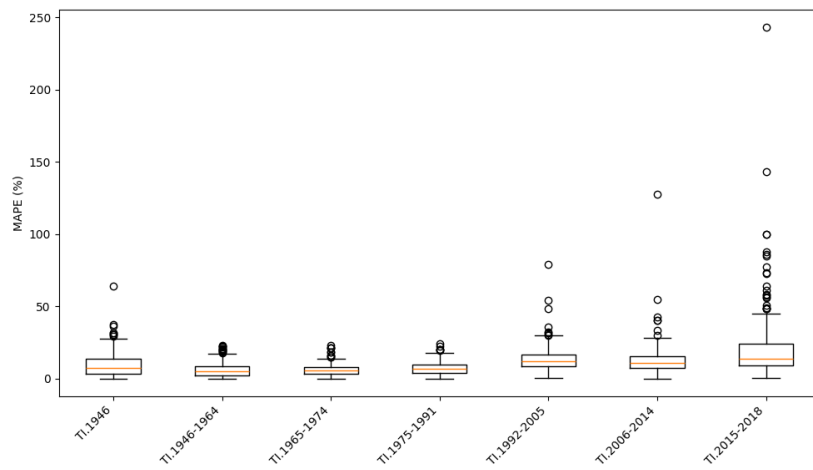


Figure 163: Phase 2 cooling MAPE (%) by archetype: Terraced Intermediate.

